CDF/ANAL/TOP/CDFR/9153
Version 3.0
August 1, 2008

Combined template-based top quark mass measurements in the Lepton+Jets and Dilepton Channels using 2.0 fb^{-1} of data

The Top Mass Template Group[1]

Jahred Adelman, Erik Brubaker, Wojciech Fedorko, Young-Kee Kim, Hyun-Su Lee, Mel Shochet

University of Chicago

Sebastian Carron, Trisha Farooque, Pekka Sinervo

University of Toronto

George Velev

Fermilab

Abstract

We report on a simultaneous measurement of the mass of the top quark (M_{top}) using the template method in both the Lepton+Jets and Dilepton channels. Two-dimensional probability density functions in each channel are derived using kernel density estimation. In the Lepton+Jets channel, the reconstructed top quark mass and the dijet mass from the hadronically decaying W are used to measure M_{top} and to constrain *in situ* the uncertain jet energy scale. In the dilepton channel, the mass from the neutrino weighting algorithm and the H_T in each event are used. The combined likelihood from both channels using 1.9 fb^{-1} of data gives a top quark mass of M_{top}=171.9 $\pm$ 1.7 (stat. + JES) $\pm$ 1.1 (syst.) GeV/c^2 = 171.9 $\pm$ 2.0 GeV/c^2. The Lepton+Jets-only measurement gives M_{top}=171.8 $\pm$ 1.9 (stat. + JES) $\pm$ 1.1 (syst.) GeV/c^2 = 171.8 $\pm$ 2.2 GeV/c^2. The dilepton-only measurement gives M_{top}=171.2 $^{+3.6}_{-3.4}$ (stat.) $\pm$ 3.8 (syst.) GeV/c^2 = 171.2 $^{+5.3}_{-5.1}$ GeV/c^2.

Contents

[1] TopMass_Template@fnal.gov

List of Figures

List of Tables

1 Introduction

This note describes the top mass template group's simulataneous measurement of the top quark mass in the Lepton+Jets and Dileptons channels using kernel density estimation (KDE) to form probability density functions that are both 2d in observables and 2d in parameters. We describe the new pieces of our combined analysis here; those unfamiliar with the separate analyses or looking for more information should read our previous notes. These includes information on template-based Lepton+Jets top mass analyses [1], using dijet masses to constraint the Jet Energy Scale [2], studies of the Lepton+Jets χ^2 efficiency [3], the Lepton+Jets measurement using 680 pb^{-1} of data [4], the Lepton+Jets measurement using 1.7 fb^{-1} of data [9], the dilepton measurement using 1.9 fb $^{-1}$ of data [11], earlier dilepton measurements using neutrino weighting [14, 15], applications of kernel density estimation to top mass template measurements [5], studies of KDE and Lepton+Jets sample division [6], studies of KDE and NWA [17], work on deriving Lepton+Jets Gen6 top-specific corrections for Pythia [7], studies on the choice of bandwidth for local polynomial smoothing [13], our modeling of fake

lepton backgrounds for the dilepton measurement [16], and initial studies on combining the L+J and DIL channels into a single measurement [18].

Our primary measurement is the top quark mass using the combined likelihood from both Dilepton and Lepton+Jets events, but we make measurements and carry out bias checks and evaluation of systematics for two additional analyses: (1) a Lepton+Jets-only measurement that includes the conversion of the overall JES systematic into a statistical uncertainty, and (2) a Dilepton-only measurement that keeps the JES as a systematic. The DIL-only measurement still uses two observables, as the H_T provides additional statistical power compared to a 1d measurement. This measurement could, in principle, convert the JES from a systematic error into a statistical error and have the power to do so by including the Gaussian JES prior in the likelihood. A problem arises, however, when trying to measure residual JES systematics - the prior is typically turned off for such measurements, and since the Dilepton channel has no dijet resonance to constrain the JES, the systematics blow up in such cases. Therefore, we choose not to measure the JES in the DIL-only measurement.

A website that includes links to all the above notes and any questions we get during the blessing process can be found on our TWiki:
`http://www-cdf.fnal.gov/htbin/twiki/bin/view/TopMassTemplate/AnalysisCombined08`

2 Changes since version 1.01 of this note

If you picked up this note prior to the preblessing talk on Jan 31st you might notice that the combined fit and dilepton channel measurements quoted there are different from the ones presented here. This is because we have updated the fake background modelling for the dilepton channel. We have determined that the original and incorrect fake model will cause a sizeable shift in the fitted mass. The size of the effect was estimated using pseudoexperiments to give +1GeV bias for the dilepton fit and +0.2GeV fir the combined fit.

We fitted the data with the updated background model and rerun all the data cross-checks - results are presented here. All bias and systematics studies are not updated from version 1.01 of this note. We are working on redoing the bias check. We will reevaluate the background shape systematics, but do not plan on reevaluating any other systematics as the pseudodata and template were self consistent in that evaluation. Changes to the fake model are discussed in section 16

3 Additional changes since Preblessing on Jan 31st (version 1.10 of this note)

There are several additional changes since preblessing:

- We discovered that the NWA parameters used for reconstruction of the fake model were not compatible with those used for reconstruction of the other models and

data. We refit the data using correctly reconstructed fakes model. A minor change can be seen only in the Dilepton fit where the central value moved by 0.01 GeV/c^2

- We have recalculated the uncertainty on the DIL background prediction and added unmodeled Wγ background to the total prediction for the non-tagged subsample (cf. section 6).

- We have redone the bias check using the new fake model and uppdated DIL bg estimate. We also used the expected number of events at $\sigma_{t\bar{t}}$=6.7pb both for Lepton+Jets and Dilepton subsamples. Previously the estimates were inconsistent in the bias check having the expected number of events based on P11 data for Lepton+Jets and based on the theoretical cross section for Dilepton.

- We added QCD background shape systematic for Lepton+Jets

- We recalculated background shape systematics for Dilepton channel and studied more in depth the fake shape systematic.

- We recalculated the systematic due to background MC statistics for DIL and Combined fits.

4 Changes since the blessing of the preliminary result on Feb 14th

Since the blessing of the preliminary result we have made the the following changes

- The dilepton cross section measurement [19] was blessed. The large change from the results used as input to this analysis are in the fake background model. The normalization of this background component was increased by a factor of $\sim$3 from normalization used in the preliminary measurement. The differences in the fake background models are discussed in Section 16. The measurement presented here uses the DIL cross section fake model. In light of this changes we have:

  - Included the new fake model and rerun the bias checks.
  - Repeated the fit on the data. The central values in the dilepton-only result and the combined fit results do not change however the statistical uncertainty increases by $0.1 - 0.2$ GeV/c^2 in the dilepton only fit.
  - Recalculated all the systematic uncertainties except for the PDF systematic and systematic due to the Lepton+Jets background shapes.

- In addition we update the systematic uncertainties as prescribed by the top mass group.

- The generator systematic is calculated using the large Herwig sample otop1s
- b quark jet energy scale systematic includes effects of changing parameters of the Bowler parametrization, semileptonic branching fraction uncertainties and uncertainties due to calorimeter response to b quark jets [20].
- The pileup uncertainty is recalculated. We find a correction is needed in the dilepton only result due to significant dependence of the result on the number of z vertices in the sample. (Section 20)
- We assign a systematic uncertainty due to systematic shifts of the jet energy scale bein not fully correlated for jets of different transverse momenta. (Section 20)
- Systematic uncertainty due to initial and final state energy is calculated using the otop03 and otop04 samples.

5 Event selection for Lepton+Jets

This measurement uses data through period 12, corresponding to 1-9-2.0 fb^{-1} of data with good silicon. We use the standard Lepton+Jets event selection, which we summarize as follows:

- We use Good run list v18, removing runs with bad beamlines.
- We correct jets using jetCorr12 and categorize them at L5. Tight jets are defined as having $E_T > 20$ GeV/c^2 and $|\eta| < 2.0$. Loose jets are those jets failing the tight jets cut but still having $E_T > 12$ GeV/c^2 and $|\eta| < 2.4$.
- No QCD veto is applied.
- We fix the TSCMIO error in TopNtuple and cut on the muon track reduced χ^2.
- MET is corrected to L5 and is required to be greater than 20 GeV/c^2.
- Based on studies shown in [6] and as in the previous analysis, we use only 2 subsamples for the Lepton+Jets measurement, dropping 0-tag and 1-tagL events. We keep the 2-tag jet cuts as previously defined (at least 3 tight jets and at least a 4th jet than can be either loose or tight), but tighten the 1-tagT requirements - our 1-tagT sample consists of events with exactly 4 tight jets.
- A χ^2 cut at 9.0 is made on all events.

We find the same number of total events as given by MII4U estimates with two caveats:

Table 1: Observed number of Lepton+Jets candidate events in data before χ^2 or boundary cuts

	CEM	CMUP	CMX	Total
1-tag == 4 tight jets	154	90	40	284
2-tag	92	39	21	152
2-tag == 3 tight jets (> 0 loose) jets	23	11	3	37
2-tag == 4 tight jets	53	21	13	87
2-tag > 4 tight jets	16	7	5	28

- We count tags only on the leading 4 jets, whereas the MII4U background estimates and the official selection allow tags on any tight jets. This this is not a problem in the 1-tag subsample, since we ask for exactly 4 tight jets. In the 2-tag sample, it affects only events with more than 4 tight jets. The effect is taken into account by modifying the MII4U background estimates. MII4U finds 31 2-tag events with more than 4 tight jets. We find 28 such events.

- We find the same total number of 2-tag 3.5 jet events, but one fewer 2-tag CEM event and one more CMUP event. This difference was traced to how jets are treated in the MET calculation. In both our analysis framework and MII4U, jets for MET are corrected using nVertex==1 so as not to introduce fake MET. In our framework, we loop over all jets and redefine loose and tight jets to be used for MET correction using nVertex==1. Thus, some jets that are not by default loose or tight jets can pass the loose or tight cuts for the purposes of correcting MET. In the top group's standard event selection, jets are always defined using the default number of vertices, and corrections for MET using nVertex==1 are applied always to this single jet list. The effect of this difference is very small, and discussed in more detail in Section 15.

The total number of Lepton+Jets events observed in data is summarized in Table 1.

6 Event selection for Dilepton

The dilepton channel selection is the standard 'DIL' selection described in detail in [8]. We use data through period 12 removing run sections with bad beamlines. In summary the selection requires:

- CEM, CMUP or CMX tight trigger lepton.

- An additional possibly non-isolated lepton (e or μ) (both leptons with $E_T >$ 20 GeV)

- Two L5 jets with $E_T > 15$ GeV
- $\not\!\!E_T > 25$ GeV
- Z-veto incorporating $\not\!\!E_T$significance cut
- $\not\!\!E_T > 50$ GeV if a lepton is closer than 20° in azimuth to the $\not\!\!E_T$vector
- $H_T > 200$ GeV
- Leptons sign to be opposite.

To improve the sensitivity the data sample is divided into non-tagged and tagged subsets. We allow tags only on the two leading jets in the event.

To obtain the expected event count values in non-tagged and tagged subsamples we use the estimates presented in [10] and fake background estimate from [16] (updated for p12 data) which are not categorized by number of b tags.

For the Diboson and Drell-Yan estimates as well as signal estimate we first obtain a probability of a jet to be tagged for the leading two jets in each event. This is calculated using the mistag matrix if given jet is not matched to a heavy flavour quark. If jet is mached to heavy flavour quark the probability of that jet to be tagged is simply the b-tagging scale factor if jet has a SecVtx tag or 0 if not. Knowing the probability of each of the jets to be tagged we calculate probability of obtaining at least one tag in the event $\mathrm{P_{tagged}}$ and complementary probability of obtaining no tags $\mathrm{P_{non-tagged}}$. The tagged and non-tagged estimates are obtained using equation 6.1

$$N_{type,tagged} = E_{type}\frac{\sum_{process}\frac{\sigma_{process}}{N_{MC,process}}\sum_{i=1}^{N_{MC,process}} C_i s_i r_i P_{tagged,i}}{\sum_{process}\frac{\sigma_{process}}{N_{MC,process}}\sum_{i=1}^{N_{MC,process}} C_i s_i} \tag{6.1}$$

E_{type} is the estimate obtained from [10] and type is $\mathrm{WW, WZ, ZZ, DY(ee, \mu\mu), DY(\tau\tau)}$ and $t\bar{t}$. The first sum in both numerator and denominator runs over all process simulated. For the diboson backgrounds and $t\bar{t}$ signal inclusive Pythia samples were used so there is only one term in that sum. Drell-Yan sample is composed of nearly 60 Alpgen+Pythia subsamples with different parton multiplicities, heavy flavour content and Z mass ranges. Heavy flavour overlap removal was used to remove oversampling of the phase space due to parton showering. $\sigma_{process}$ is the cross section for given process calculated by Alpgen. $N_{MC,process}$ is the number of generated Monte-Carlo events generated for this process. The inner sum in both numerator and denominator runs over all events in that MC sample. If the event is DIL selected the variable s_i is 1, otherwise 0. Similarly if event is NWA-reconstructed and satisfies boundary cuts (*cf.* section 13) r_i is 1 otherwise 0. The variable C_i is a correction factor dependent on the dilepton category of the event (described in detail in section 4 of [8]). The probability $\mathrm{P_{tagged}}$ is calculated as described above.

Estimate for the non tagged sample is obtained in the same manner but $\mathrm{P_{non-tagged}}$ is used.

The estimate for the fake background is simply a sum of fake ratios from events which have one denominator lepton selected from W+jets sample. We separate the sum based on presence of b-tags obtaining the tagged and non-tagged estimate.

The results of the calculation are shown in table 2.

	non-tagged	tagged
WW	6.41 ±1.10	0.23 ±0.04
WZ	1.53 ±0.25	0.03 ±0.00
ZZ	0.97 ±0.76	0.07 ±0.05
Wgamma	0.17 ±0.18	0.00 ±0.00
DYtt	4.81 ±0.93	0.26 ±0.05
DYeemm	11.14 ±1.96	0.61 ±0.11
fakes	19.26 ±5.56	2.72 ±0.95
total background	44.28 ±7.03	3.91 ±0.98
$t\bar{t}$	40.05 ±3.05	55.76 ±4.24

Table 2: Backgrounds and signal estimates for integrated luminosity 2.0 fb^{-1} for the DIL tagged and non-tagged subsamples

The uncertainty is calculated assuming the statistical uncertainties and fakes total uncertainty are not correlated among background components and that the systematic uncertainties are fully correlated among all backgrounds except fakes. Note that we do not model the Wγ background since the expectation is consistent with no events. We add this background to the non-tagged estimate.

7 P12 data validation

To validate the P12 data used in this analysis, kinematic distributions are compared between P12 data and the well studied data prior to P12. Distributions in Figures 1 through 4 show distributions for a W selection derived from our Lepton+Jets selection without any requirements on jets or tagging. Most distributions are similar, with some expected changes: the CMX p_T distributions are different due to changes in the trigger selection (this can be seen from the fact that P12 is the same as the exclusive P11 distribution in Figure 5), the MET distribution is wider and slightly higher in the more recent data, and the number and energy of jets are slightly different as well.

Similar distributions for the DIL selection are showin in Figures 6 to 9. The selection is based on the DIL selection, removing any requirements on the number of jets or tagging.

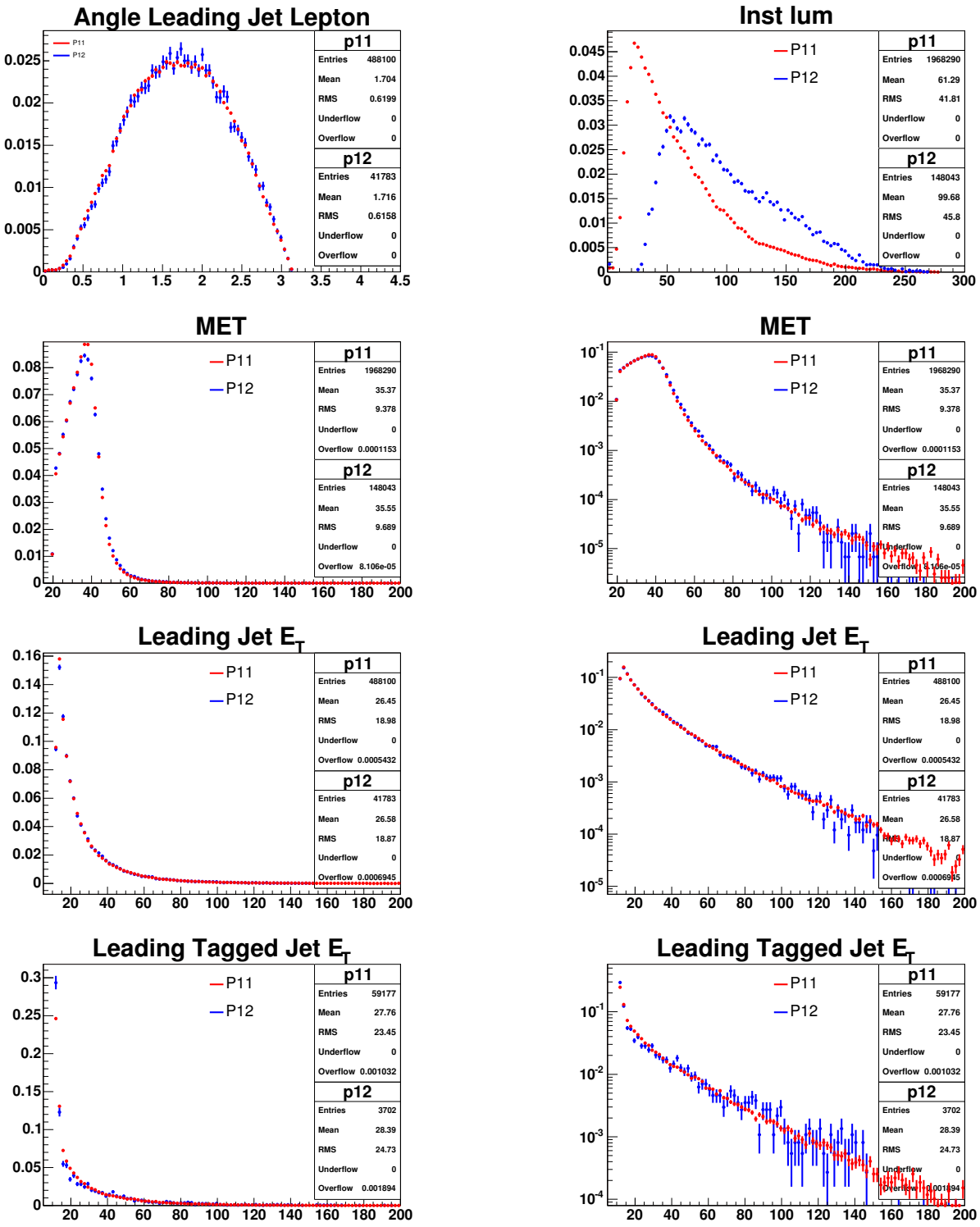

Figure 1: Kinematic distributions for L+J data validation (1)

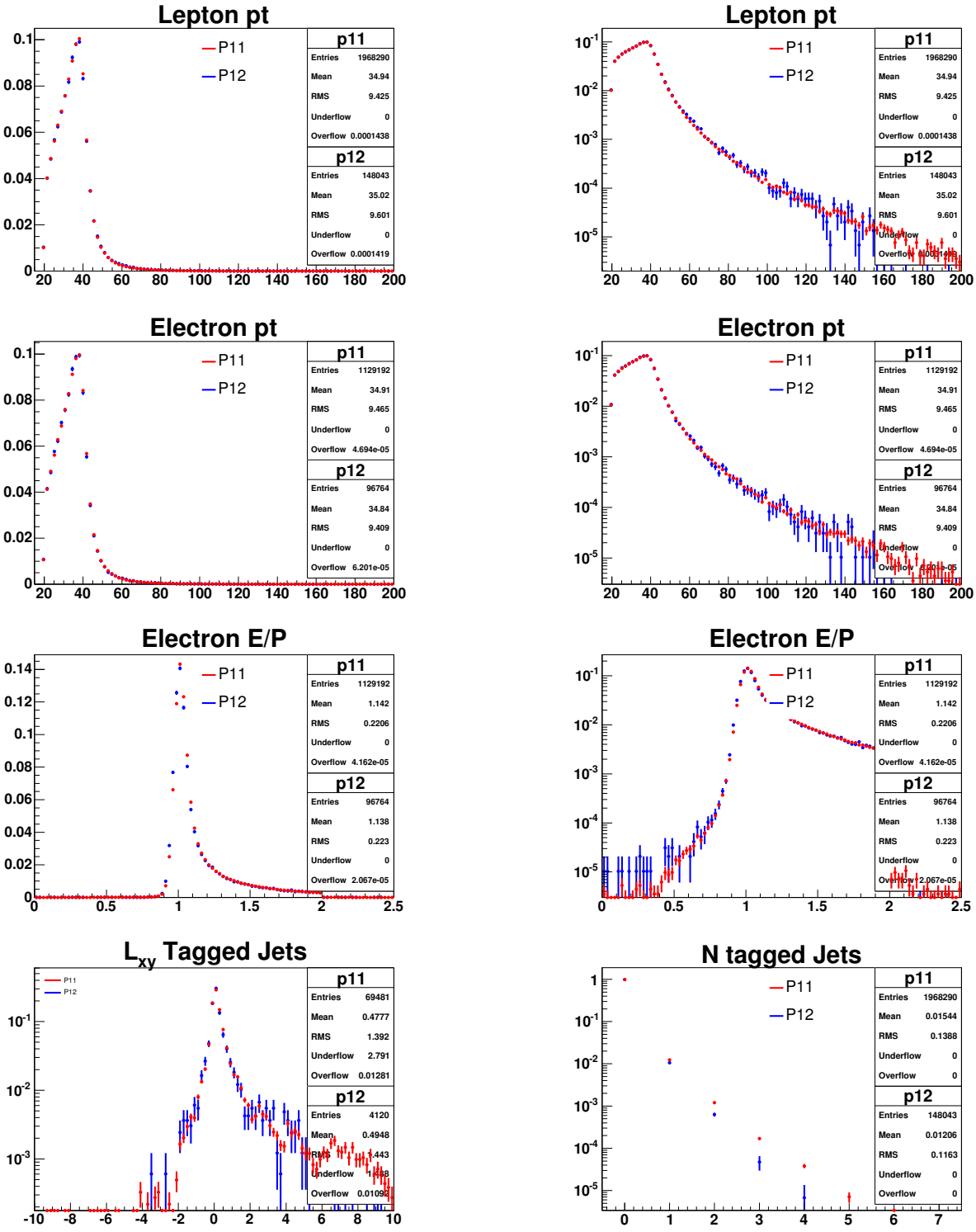

Figure 2: Kinematic distributions for L+J data validation (2)

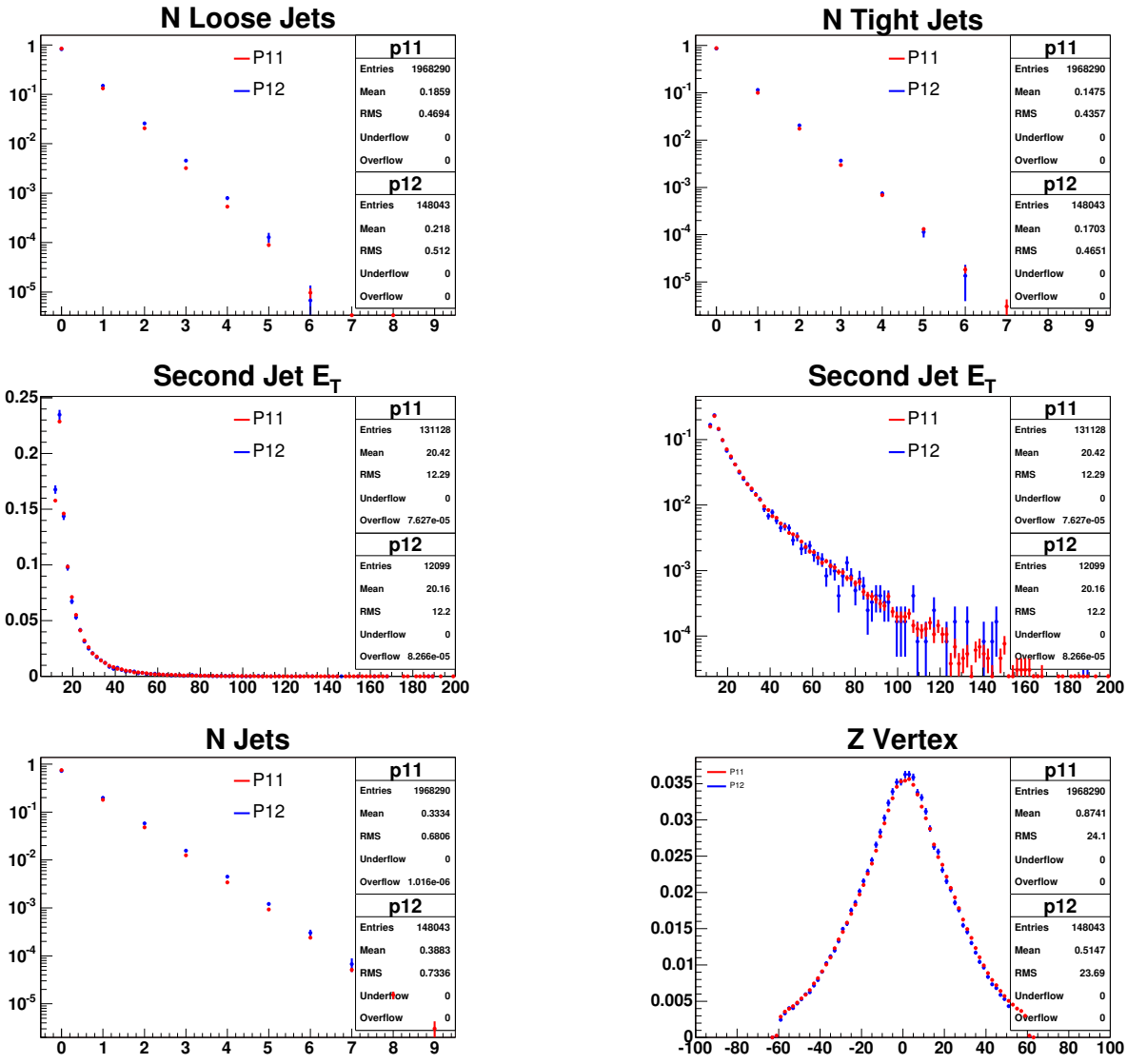

Figure 3: Kinematic distributions for L+J data validation (3)

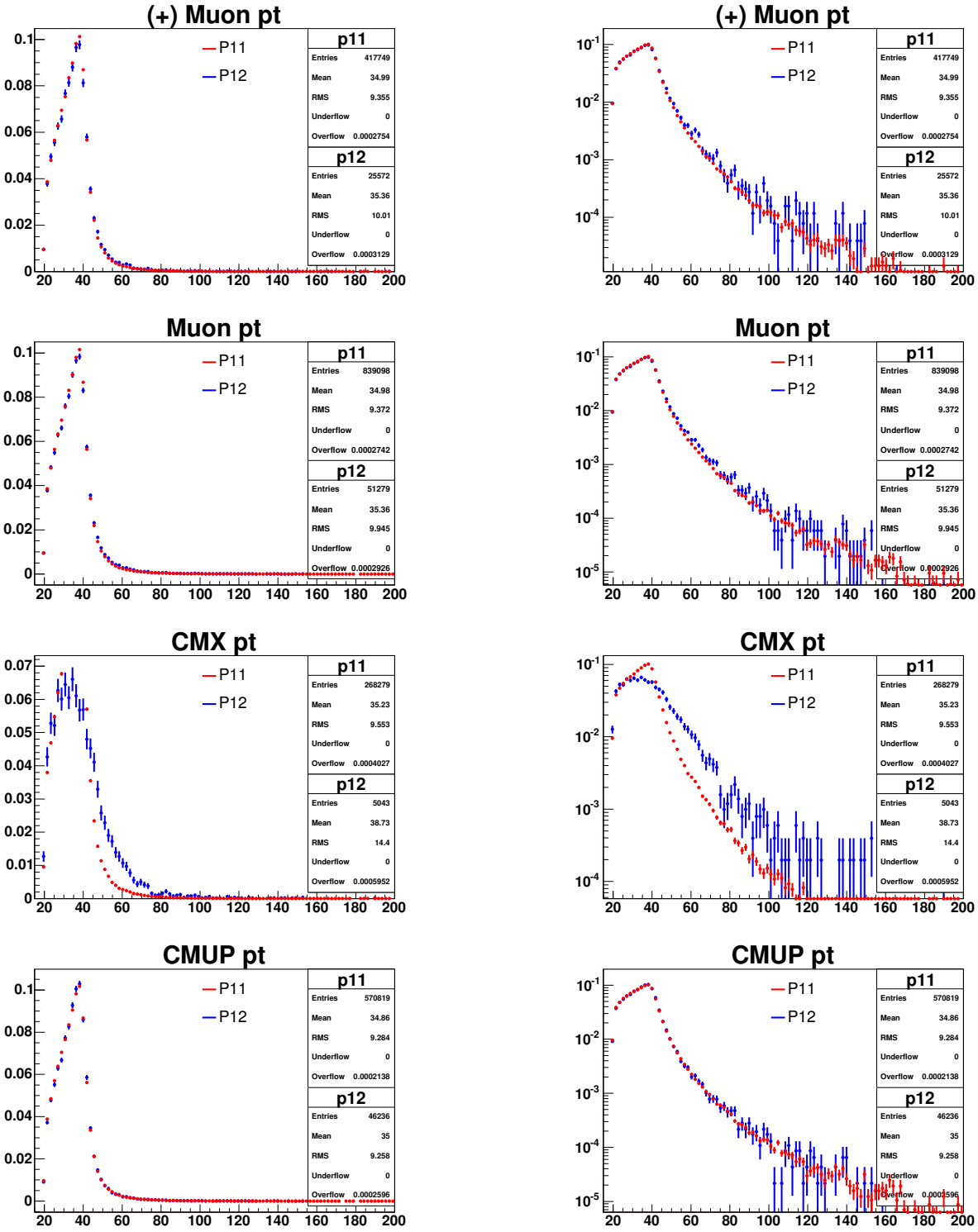

Figure 4: Kinematic distributions for L+J data validation (4)

8 Reconstructed top quark masses for Lepton+Jets

The reconstructed top quark mass ($M_t^{\rm reco}$) in the Lepton+Jets channel is the same variable that has been used since Run I to measure $\rm M_{top}$. The output of a χ^2 minimization for the overconstrained kinematics of the $t\bar{t}$ system, the kinematic fitter gives one number per event ($M_t^{\rm reco}$) that is used as an estimator for $\rm M_{top}$. The fitter also gives a χ^2 that can be used to reject poorly reconstructed events and events not consistent with $t\bar{t}$ production and Lepton+Jets decay. Distributions of $M_t^{\rm reco}$ for 1-tag and 2-tag events are shown in Figure 10.

The χ^2 efficiency for signal events is not explicitly used in the analysis, but is shown in Figures 11 and 12.

9 Dijet mass in Lepton+Jets Channel

The dijet mass from the hadronically decaying W in the Lepton+Jets channel is the same variable as used in the 1.7 $\rm fb^{-1}$ analysis: in 2-tag events, we choose the dijet mass from the 2 nontagged leading jets. In 1-tag events, we select the dijet mass from among the 3 nontagged leading jets that is closest to the W mass. The difference between this analysis and the previous analysis is that we now fully correct jets using the light-flavor TS corrections. Previously, we used jets only at L5. As before, we cut away events failing the χ^2 cut both for $M_t^{\rm reco}$ as well as for $W_{\rm jj}$. This simplifies our likelihood significantly with respect to our previously published result (using 318 $\rm pb^{-1}$), and removes only events with very little power to measure JES near $0\sigma_c$.

Distributions of our dijet variable for 1-tag and 2-tag events are shown in Figure 13.

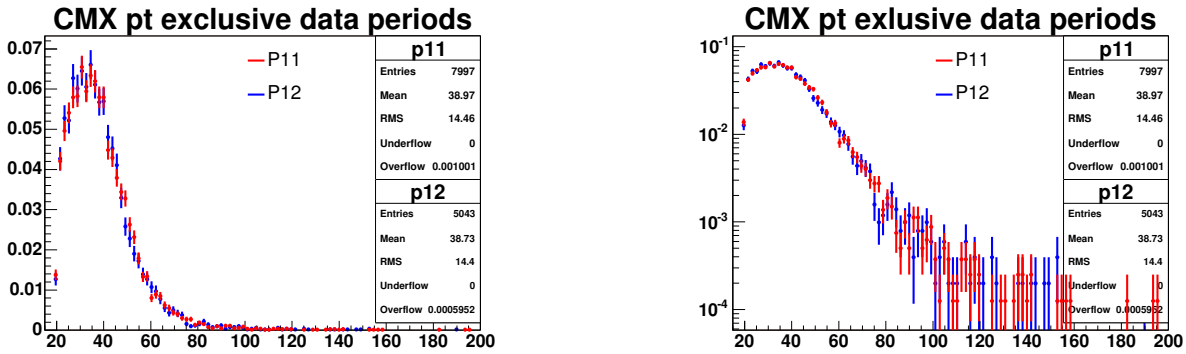

Figure 5: Exclusive P11 to P12 CMX p_T distributions

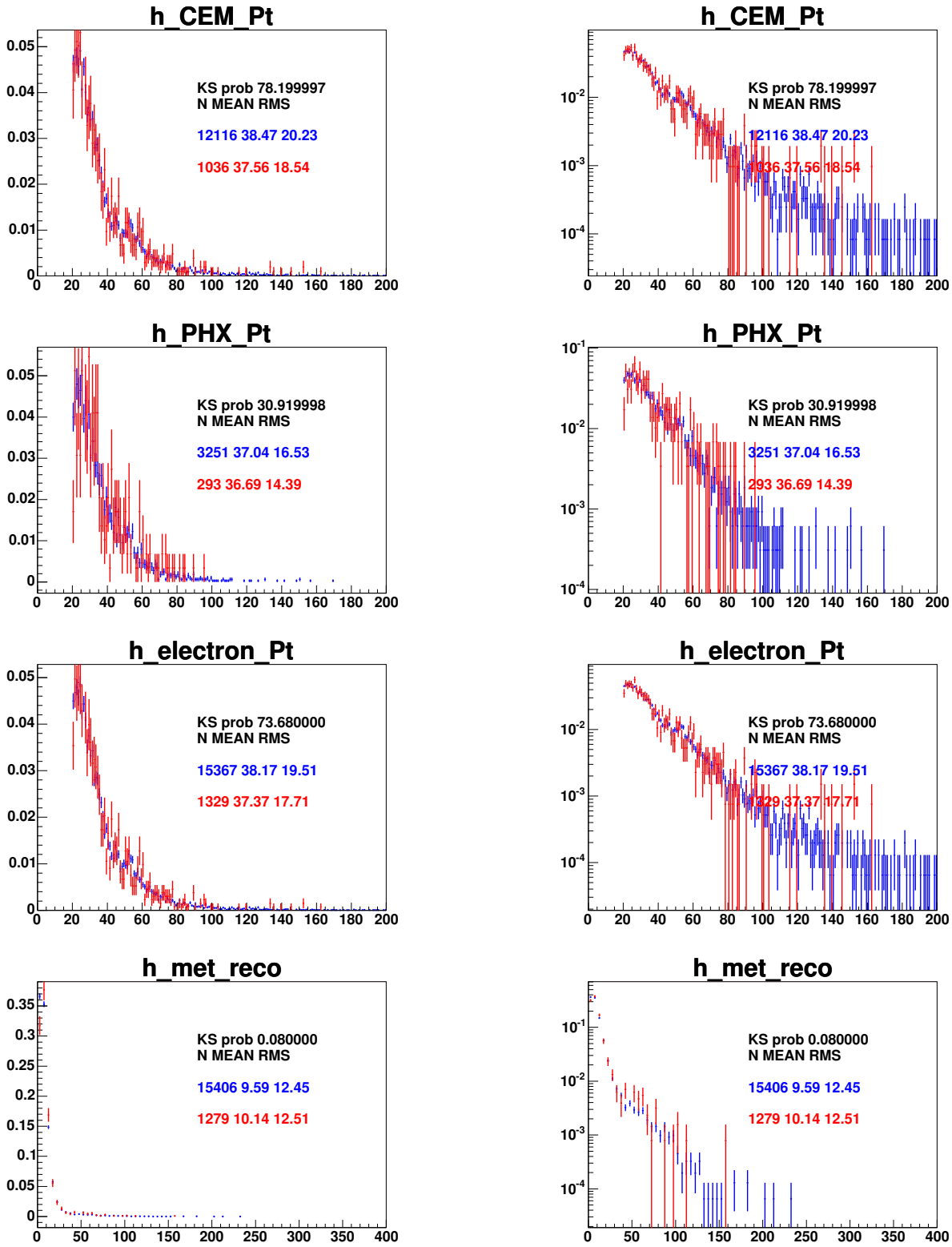

Figure 6: Kinematic distributions for dilepton data (1)

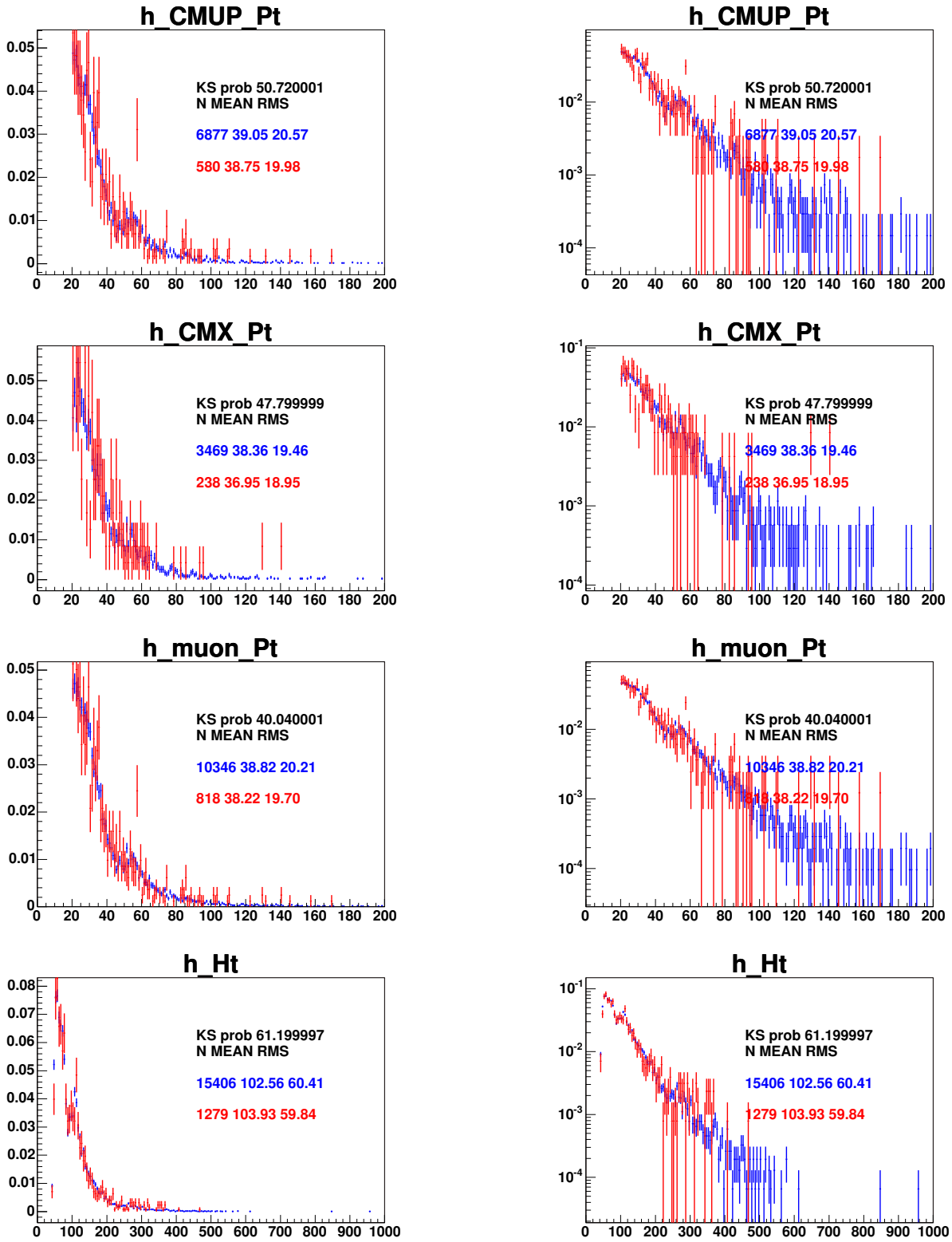

Figure 7: Kinematic distributions for dilepton data (2)

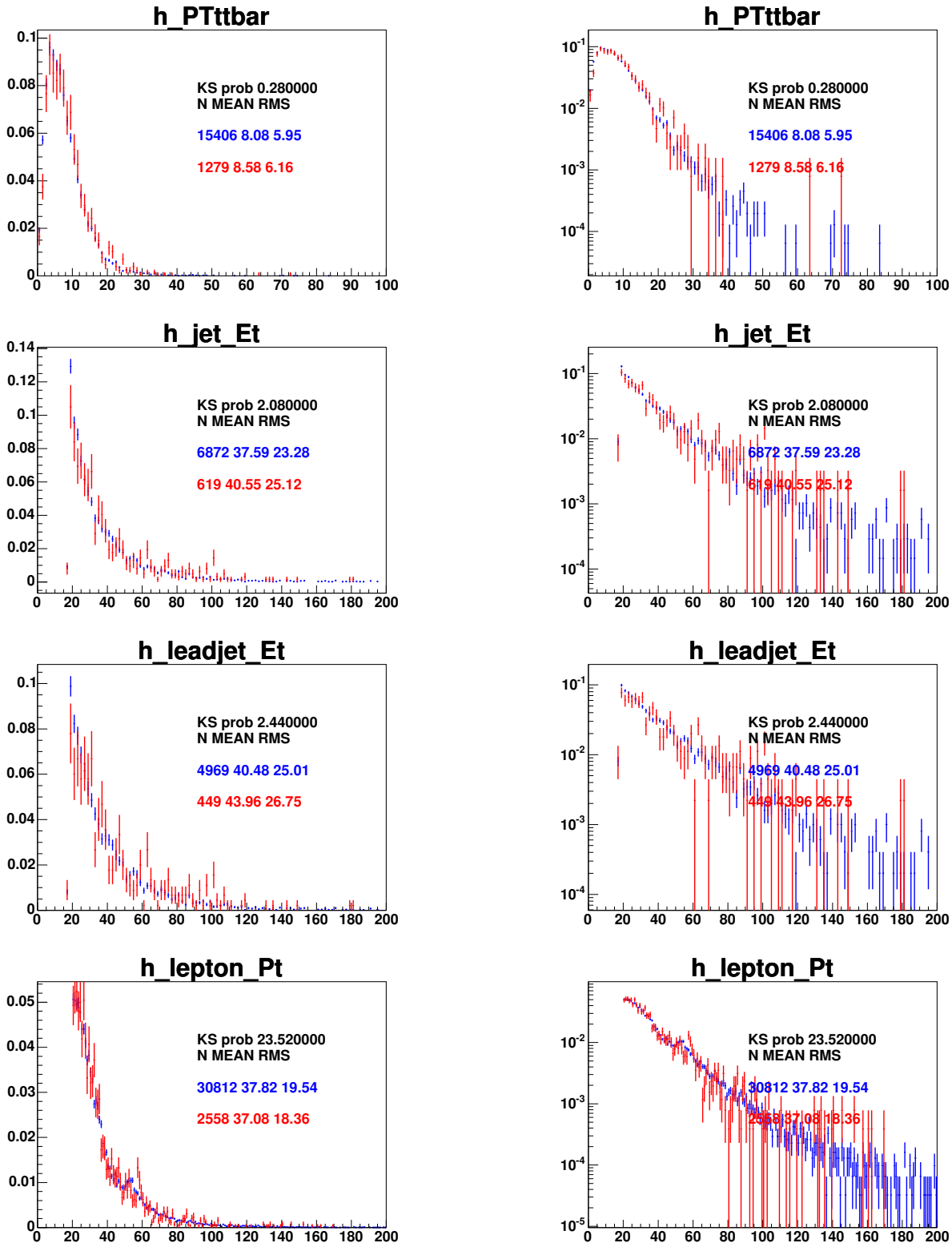

Figure 8: Kinematic distributions for dilepton data (3)

10 Neutrino Weighting Mass

The NWA algorithm is used to form an estimator for the top quark mass in the dilepton channel. We scan a range of top masses. For a given top mass we sum over parton to jet assignments and integrate over η values for each of the two neutrinos allowing us to solve for the transverse momenta of the neutrinos. We compare the solutions to the measured values and pick the top mass which yields highest weight. Algorithm is described in more detail in [11]. Distributions of the NWA mass for non-tagged and tagged events are shown in Figure 14.

11 Second variable for DIL channel

The KDE machinery used to form 2d PDFs is very general. Any second variable in the dilepton channel with less than 100% correlation to the NWA variable should improve the resolution on M_{top} and possibly provide additional signal-to-background separation. Many such variables were studied. In the end, two possible candidates giving similar improvement to the measurement (5-10% in statistical power) were identified: The second M_{top} solution out of NWA, and the total H_T in the event. We decided to

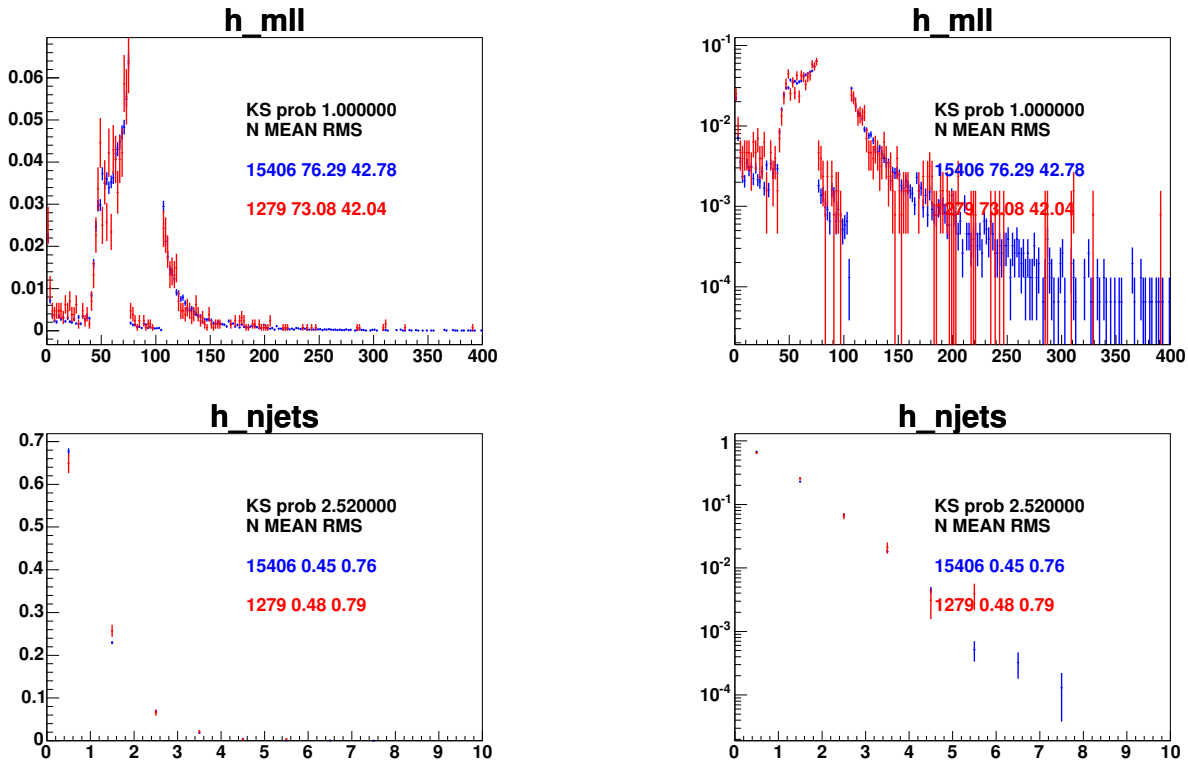

Figure 9: Kinematic distributions for dilepton data (4)

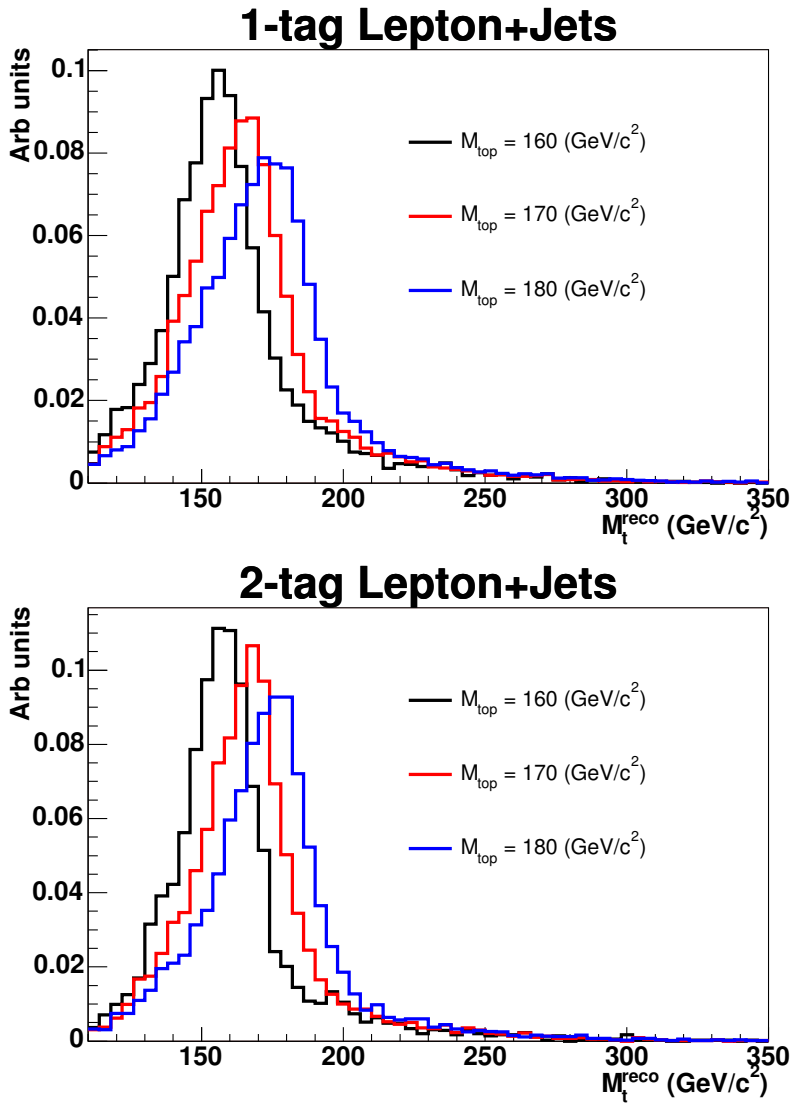

Figure 10: Reconstructed mass distributions from MC for 1-tag(top) and 2-tag(bottom) events.

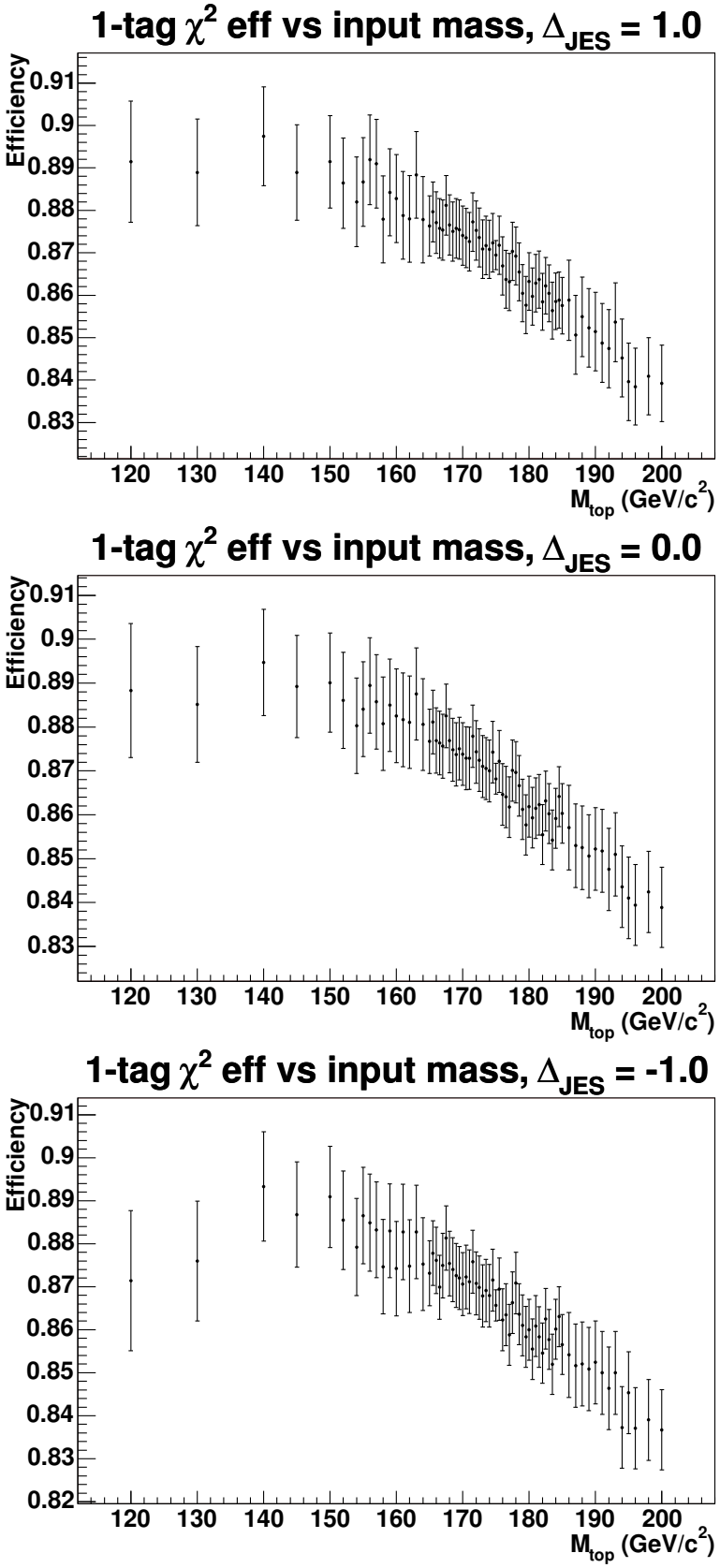

Figure 11: Efficiency to pass the $\chi^2 < 9.0$ cut for 1-tag signal events for $\Delta_{\rm JES} = +$ 1.0 (top), 0.0 (middle) and -1.0 (bottom) $\sigma_{\rm C}$.

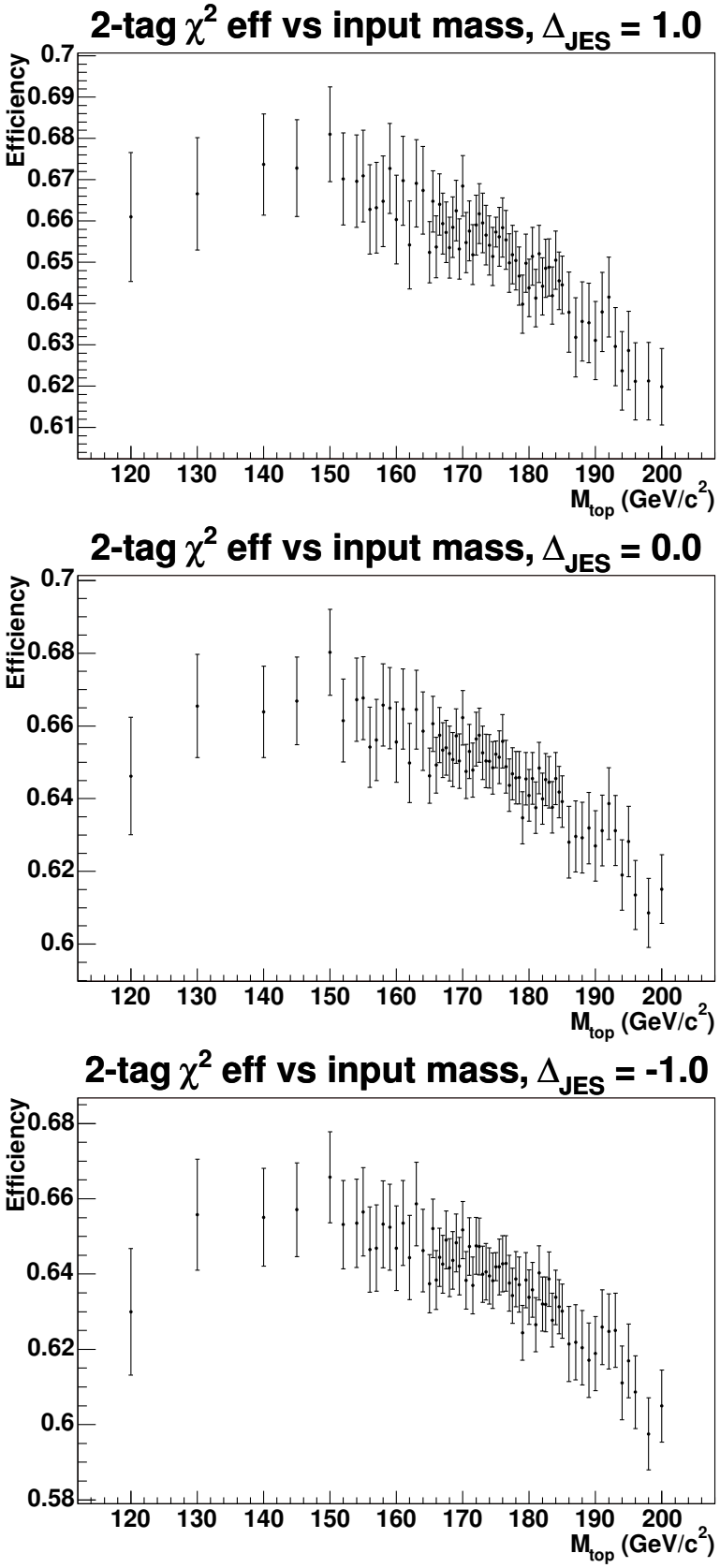

Figure 12: Efficiency to pass the $\chi^2 < 9.0$ cut for 2-tag signal events for $\Delta_{\rm JES} = +$ 1.0 (top), 0.0 (middle) and -1.0 (bottom) $\sigma_{\rm C}$.

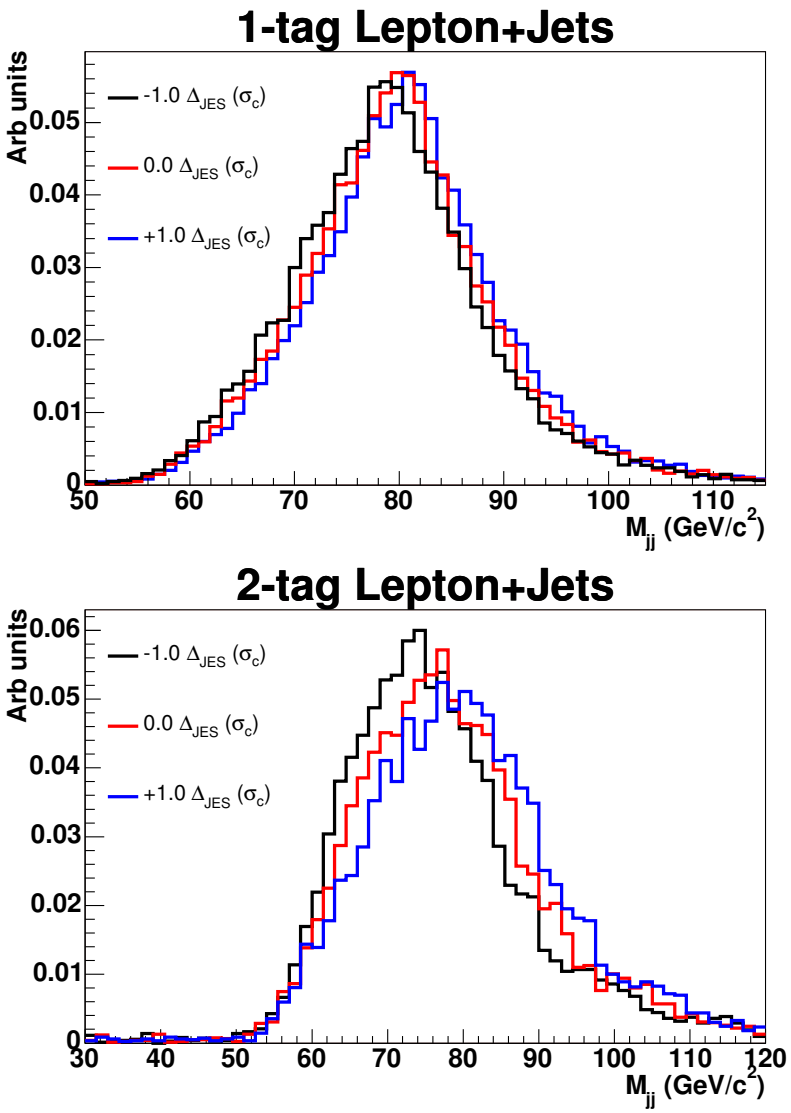

Figure 13: Dijet mass distributions for 1-tag(top) and 2-tag(bottom) events. The input mass is 170 GeV/c^2.

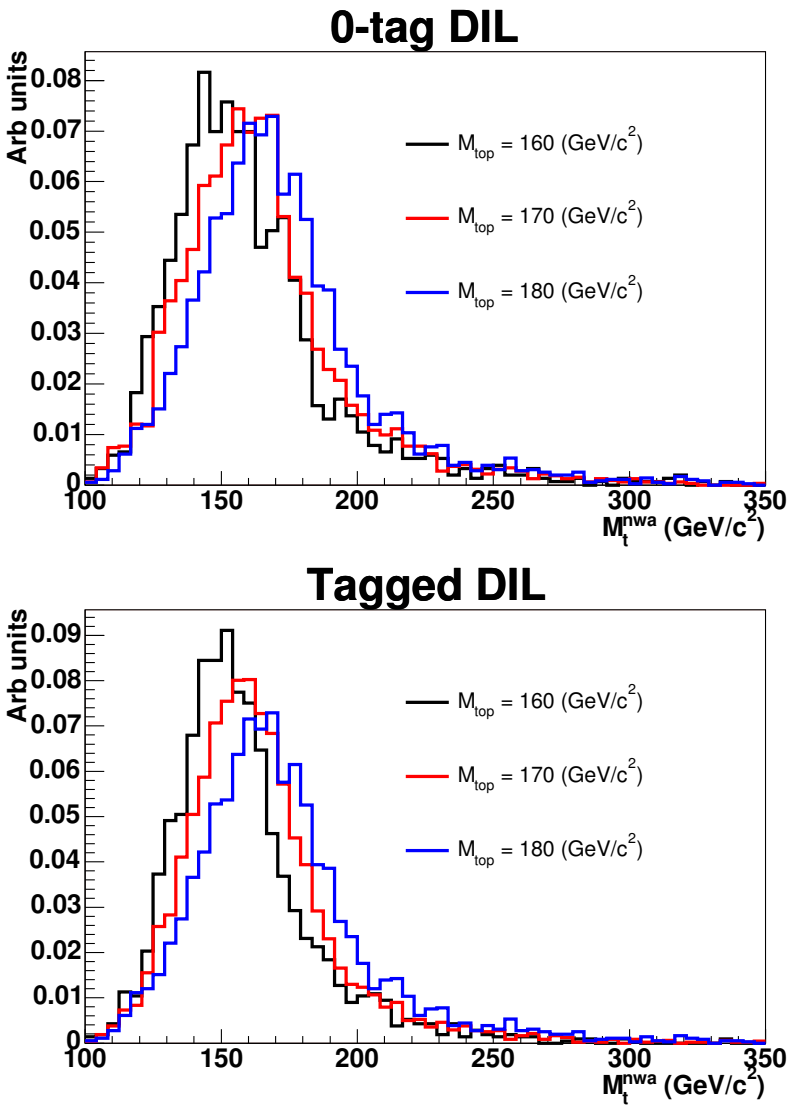

Figure 14: Reconstructed NWA top mass distributions from MC for non-tagged (top) and tagged(bottom) events.

use the H_T, both because the second mass value gave biased results from the machinery, and also because 10% of the time the NWA algorithm does not identify a second solution. The power of H_T to distinguish top quark mass values is not surprising. It is typically a poor variable to use because of its strong dependence on the JES, but the *in situ* calibration from the Lepton+Jets ensures that the JES is kept under control.

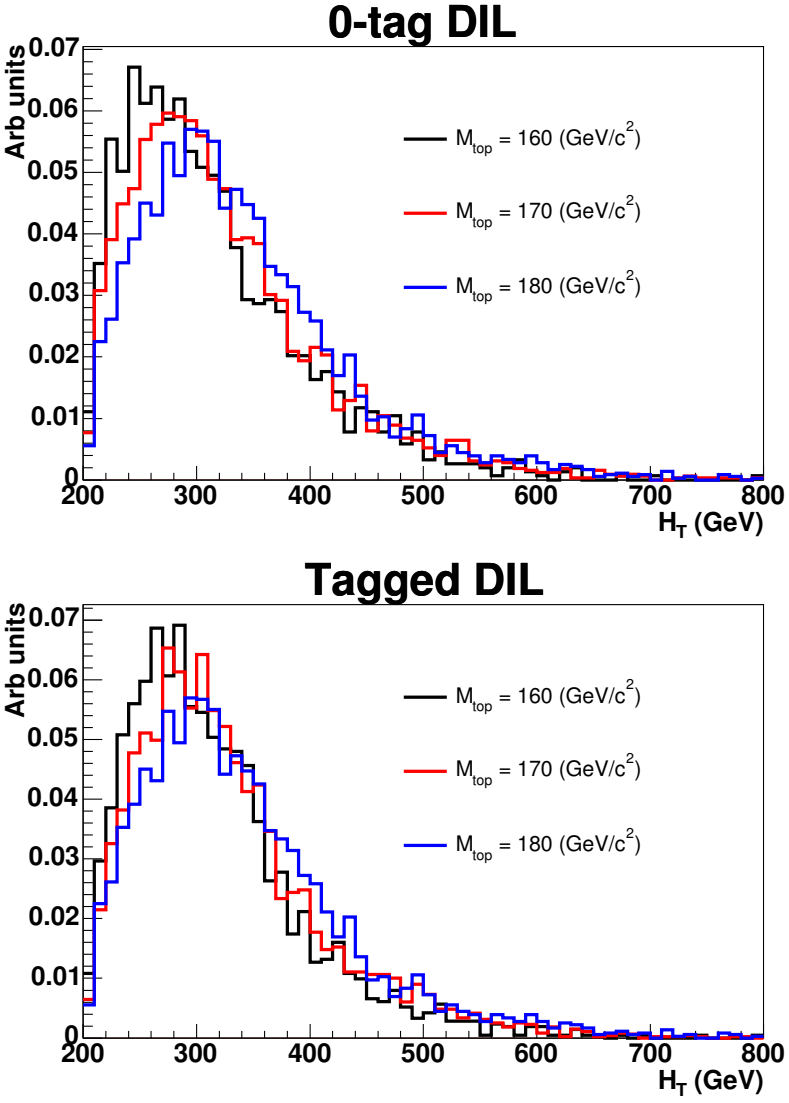

Figure 15: H_T distributions from MC for non-tagged (top) and tagged(bottom) events.

12 Likelihood and LPS

For each subsample we have a likelihood term shown in Eqn. 12.1

$$\mathcal{L}_{\rm shape} = \frac{\exp(-(n_s+n_b))(n_s+n_b)^N}{N!} \times e^{\frac{(n_{b0}-n_b)^2}{2\sigma^2_{n_{b0}}}} \times \prod_{i=1}^{N} \frac{n_s P_s(m_t^{reco}, v_2; {\rm M_{top}}, \Delta_{\rm JES}) + n_b P_b(m_t^{reco}, v_2; \Delta_{\rm JES})}{n_s + n_b} \tag{12.1}$$

where $\rm n_s$ and $\rm n_b$ are signal and background expectations and N is the number of events in the sample, $\rm P_s$ is the signal probability density function and $\rm P_b$ is the background probability density function. The variable $\rm v_2$ is the dijet mass in case of lepton+jets samples and $\rm H_T$ for dilepton samples. The first term in the likelihood is present because this is an extended maximum likelihood, in which the numbers of signal and background events obey Poisson statistics. The second term in the product expresses the Gaussian constraints on the background expectation. We use the *a-priori* estimate $\rm n_{b0}$ and its uncertainty $\sigma_{\rm n_{b0}}$ to improve sensitivity. Shape information is used in the third term where probability density functions are used to discern between signal and background events and to extract mass information. Note that the background probability density function $\rm P_b$ is allowed to vary as a function of $\Delta_{\rm JES}$ which is a new feature for this analysis. We have four terms like this - one for each subsample are multiplied. We also impose a unit Gaussian constraint on $\Delta_{\rm JES}$.

From the KDE method we obtain the values of the probability density functions only at the values of M_{top} and $\Delta_{\rm JES}$ where signal Monte Carlo is available. Similarly background pdf's exist only at discrete values of $\Delta_{\rm JES}$. To obtain signal pdf's which are continuously varying as a function of $\rm M_{top}$and $\Delta_{\rm JES}$ and bacground pdf's which are continuosly varying as a function of $\Delta_{\rm JES}$ we employ local polynomial smoothing [23] [24]. This procedure is valid for any function so we will describe it in general. We will obtain an estimate $\hat{\mu}(x)$ at arbitrary x for the true value of function $\mu(x)$. We have estimates Y_i of the value of this function only at certain points x_i. We assume that the uncertainty for the estimates Y_i is common for all points i.e. $Y_i = \mu(x_i) + \epsilon_i$ where ϵ_i are identically distributed and have zero mean and finite variance. Expanding $\mu(x)$ around x we get equation 12.2

$$\mu(t) = a_0 + a_1(t-x) + \frac{1}{2}a_2(t-x)^2 = \langle a, A(t-x)\rangle \tag{12.2}$$

where $a = (a_0, a_1, a_2)$ and $A(v) = (1, v, \frac{v^2}{2})$. We find $\hat{a}$ that minimizes the criterion

$$\sum_i w_i(x)(Y_i - \langle a, A(x_i - x)\rangle) \tag{12.3}$$

The value $\hat{a_0}$ is the desired estimate $\hat{\mu}(x)$. $w_i(x) = W(\frac{x_i}{h(x)})$ is a weighting function. It assigns more importance to the points close to the desired value x. For the function $W(u)$ we use a 'tricube' function $W(u) = (1-|u|^3)^3$ for $u < 1$. The parameter h controls the width of the smoothing window and can in principle depend on x; we use

constant value. The procedure is naturally extendible to two or more dimensions. We need to replace $A(v)$ with $A(\vec{v}) = \mathcal{B}$ where $\mathcal{B}$ is any basis of second order polynomials in desired number of dimensions. For instance for 2-d smoothing we may pick: $A(\vec{v}) = (1, v_1, v_2, v_1^2, v_2^2, v_1 v2)$. All points are replaced vectors and the weight is evaluated as a function of Euclidian distance in d-dimensional space.

We employ local polynomial smoothing on a per-event basis. This means that for each event in the product term inEqn. 12.1 reconstructed with particular values of m_t^{reco} and v_2 we create a function in $\mathrm{M_{top}}$and Δ_{JES}. We then take a product of these functions during the minimization of negative log likelihood.

For Lepton+Jets events, we use $\mathrm{h}_{Mtop} = 10.0$ GeV/c^2. For DIL events, $\mathrm{h}_{Mtop} = 15.0$ GeV/c^2. For both categories, $\mathrm{h}_{JES} = 0.8\ \sigma_{\mathrm{c}}$. To smooth out background JES, $\mathrm{h}_{JES}^{bkgd} = 3.0\ \sigma_{\mathrm{c}}$.

13 Boundary cuts

As before, we define hard boundary cuts on our templates to keep the probability density functions normalized within the physical region. For the 1-tag Lepton+Jets sample, we cut away events not satisfying: 110 GeV/$c^2 < M_t^{\mathrm{reco}} <$ 350 and 50 GeV/$c^2 < W_{\mathrm{jj}} <$ 115 GeV/c^2. For the 2-tag sample, we loosen the cut on the dijet variable and cut away events not satisfying: 110 GeV/$c^2 < M_t^{\mathrm{reco}} <$ 350 and 50 GeV/$c^2 < W_{\mathrm{jj}} <$ 125 GeV/c^2. Note that the M_t^{reco} cuts are the same as we used for the 1.7 fb$-$1 blessing. For the dijet variable, the 2-tag cut was moved to account for the larger dijet masses after correcting back to the parton level using TS corrections. These boundary cuts are not very efficient as a first cut, but for those events that pass the χ^2, the efficiency is high, even across Δ_{JES} and $\mathrm{M_{top}}$. Table 3 summarizes the boundary cut efficiencies for signal Lepton+Jets events.

For the Dilepton and combined measurements, we make similar boundary cuts on the value of $\mathrm{M_t^{reco}}$and H_T. For both the untagged and tagged samples, we remove any events that does not have 100 GeV/$c^2 < \mathrm{M_{top}}_r^{NWA} <$ 350 GeV/c^2 and 200 GeV/$c^2 < H_T <$ 800 GeV/c^2. The efficiency to pass these cuts is quite good, as shown in Table 4. Note that the boundary cut efficiency for NWA includes the effect of the small NWA non-reconstruction probability.

14 Signal samples

PYTHIA MC is used to model the signal events. Kernel Density Estimation is applied to a grid of MC with $\mathrm{M_{top}}$ varying from $120 - 240$ GeV/c^2 and Δ_{JES} varying from -3.0 to +3.0 σ_{c}. A total of 76 mass points are used, with 29 different Δ_{JES} values at each mass point, corresponding to 2204 total signal points in the grid. Figures 16 and 17 show the 2d PDFs for the Lepton+Jets sample at $\mathrm{M_{top}} = 170$ GeV/c^2 and $\Delta_{\mathrm{JES}} = 0.0\sigma_{\mathrm{c}}$. Figures 18 and 19 show the 2d PDFs for the DIL sample at

Table 3: Efficiencies to pass the boundary cuts for Lepton+Jets signal events.

	1-tag	2-tag
Pre-χ^2 (M_{top}= 170 GeV/c^2, Δ_{JES} = 0.0 σ_c)	0.865	0.650
Post-χ^2 (M_{top}= 170 GeV/c^2, Δ_{JES} = 0.0 σ_c)	0.989	0.981
Pre-χ^2 (M_{top}= 170 GeV/c^2, Δ_{JES} = 3.0 σ_c)	0.861	0.651
Post-χ^2 (M_{top}= 170 GeV/c^2, Δ_{JES} = 3.0 σ_c)	0.989	0.981
Pre-χ^2 (M_{top}= 170 GeV/c^2, Δ_{JES} = -3.0 σ_c)	0.846	0.601
Post-χ^2 (M_{top}= 170 GeV/c^2, Δ_{JES} = -3.0 σ_c)	0.987	0.977
Pre-χ^2 (M_{top}= 150 GeV/c^2, Δ_{JES} = 3.0 σ_c)	0.880	0.671
Post-χ^2 (M_{top}= 150 GeV/c^2, Δ_{JES} = 3.0 σ_c)	0.988	0.980
Pre-χ^2 (M_{top}= 150 GeV/c^2, Δ_{JES} = -3.0 σ_c)	0.860	0.618
Post-χ^2 (M_{top}= 150 GeV/c^2, Δ_{JES} = -3.0 σ_c)	0.980	0.975
Pre-χ^2 (M_{top}= 200 GeV/c^2, Δ_{JES} = 3.0 σ_c)	0.818	0.602
Post-χ^2 (M_{top}= 200 GeV/c^2, Δ_{JES} = 3.0 σ_c)	0.987	0.975
Pre-χ^2 (M_{top}= 200 GeV/c^2, Δ_{JES} = -3.0 σ_c)	0.814	0.562
Post-χ^2 (M_{top}= 200 GeV/c^2, Δ_{JES} = -3.0 σ_c)	0.986	0.979

Table 4: Efficiencies to pass the boundary cuts for Dilepton signal events.

	0-tag	Tagged
M_{top}= 170 GeV/c^2, Δ_{JES} = 0.0 σ_c)	0.994	0.994
M_{top}= 170 GeV/c^2, Δ_{JES} = 3.0 σ_c)	0.992	0.993
M_{top}= 170 GeV/c^2, Δ_{JES} = -3.0 σ_c)	0.996	0.995
M_{top}= 150 GeV/c^2, Δ_{JES} = 3.0 σ_c)	0.989	0.995
M_{top}= 150 GeV/c^2, Δ_{JES} = -3.0 σ_c)	0.997	0.995
M_{top}= 200 GeV/c^2, Δ_{JES} = 3.0 σ_c)	0.990	0.993
M_{top}= 200 GeV/c^2, Δ_{JES} = -3.0 σ_c)	0.994	0.996

$M_{top} = 170$ GeV/c^2 and $\Delta_{JES} = 0.0\sigma_c$.

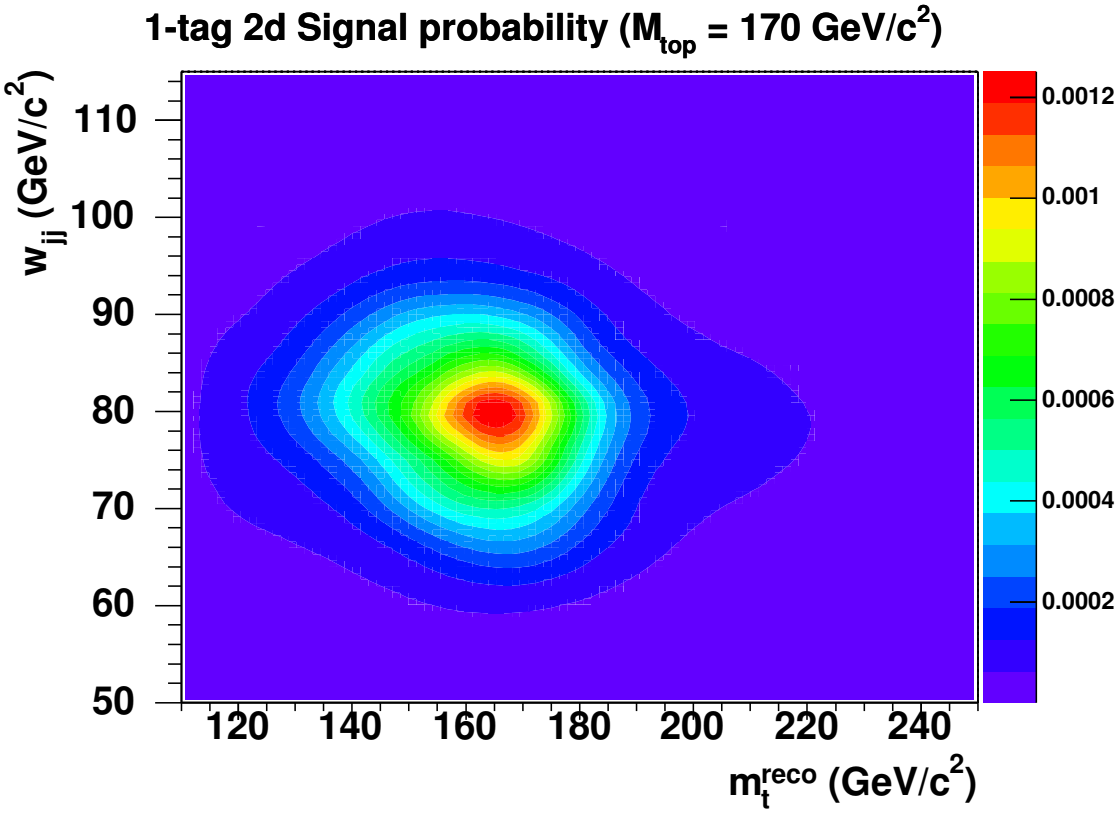

Figure 16: Two-dimensional PDF used for Lepton+Jets 1-tag events at $M_{top} = 170$ GeV/c^2 and $\Delta_{JES} = 0.0\sigma_c$

15 Lepton+Jets backgrounds

For the final background estimates and composition, we take the P12 MII4U results for our 1-tag sample, and numbers including a loose 4th jet cut for the 2-tag sample. We implement jet-based HFOR, and weight events by both their Alpgen weight and their boundary cut efficiencies. Mistag templates are derived from W+LF samples, and use events weighted by their mistag probability from the mistag matrix. We do not double-count events with one real tag and one mistag (since to first order they can have 2 "real" tags in the MC), and derive the 2-mistag background estimate from the W+LF samples. For the mistag templates derived from the inclusive W+$\geq$ 4-parton sample, we use only every 4th event in our output ntuple to keep the number of background pseudodata events at a reasonable level. This still keeps extremely high statistics for

the mistag pseudodata and templates; the probabilities to draw the pseudodata are altered accordingly to keep the W+LF fraction of our background events correct.

There is an additional correction to account for the fact that we don't allow tags on jets beyond the leading 4 jets. This effect is accounted for separately on individual backgrounds, and is typically 3-7% across the W+HF samples, 7-8 % in the H+LF samples (where we ask for the mistag probability on additional jets), 2-3 % for the single-top samples, 5-7 % for the WZ and ZZ samples, and 8 % for the QCD sample.

The different background samples have density estimates derived independently. They are stitched together according to their expected weights. To be conservative and since we know the background constraint does not provide much information, the uncertainties on the number of events across jet bins and lepton categories are added linearly. We also assume 100% correlation across W+jets samples and across the 6% luminosity uncertainty on the MC backgrounds. The uncertainties on the backgrounds are added in quadrature otherwise. We model QCD by using non-isolated leptons (we anti-select on these leptons by requiring isolation > 0.2). Table 5 shows the background

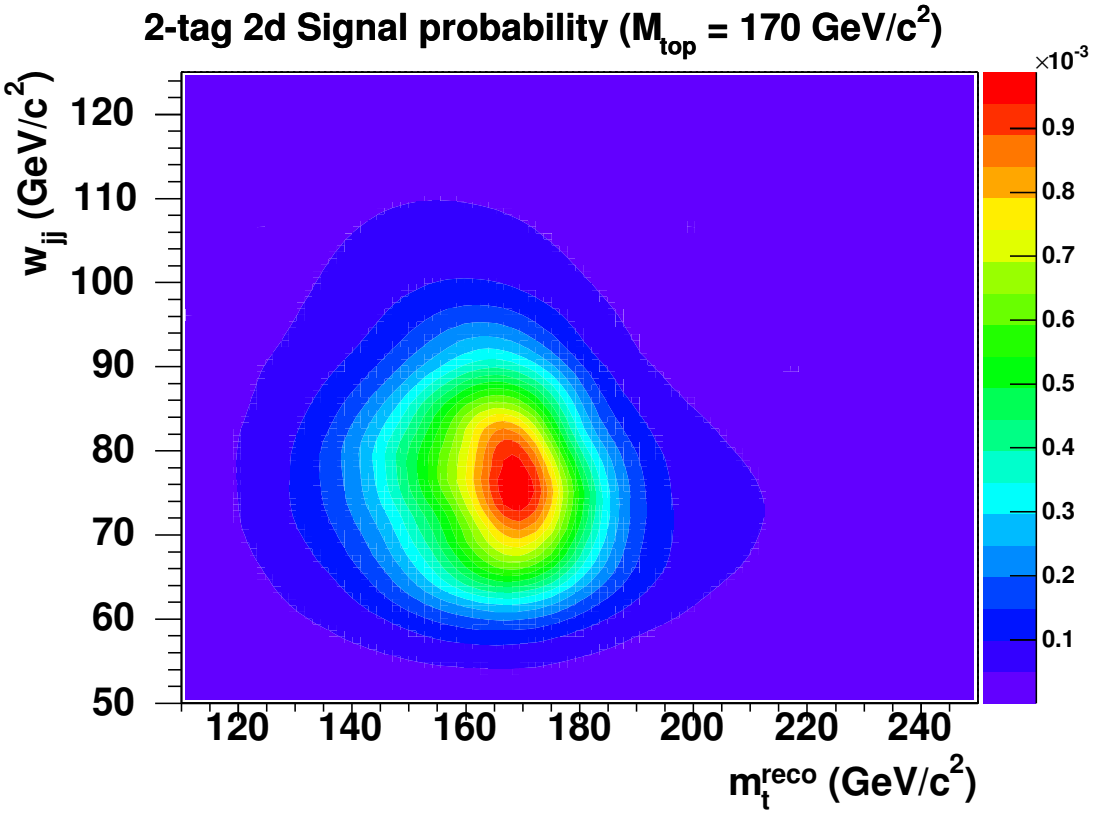

Figure 17: Two-dimensional PDF used for Lepton+Jets 2-tag events at $M_{top} = 170$ GeV/c^2 and $\Delta_{JES} = 0.0\sigma_c$

estimates both before and after the χ^2 cut. Unlike in our previous analysis, when the JES was fixed at 0.0 and the background JES was taken as a systematic, we now shift the JES for the backgrounds in the same grid of 29 $\Delta_{\rm JES}$ values as used for the signal events. The JES is not shifted for the QCD background, which is data-based. Table 6 shows the boundary cut efficiencies for a few of the major Lepton+Jets backgrounds.

Figures 20, 21, 22 and 23 shows the 1d templates derived from KDE for all individual background samples, weighted by their contribution to the entire background sample. Figures 24 and 25 show the combined 2d PDFs used for background events.

As described in Section 5, we have very tiny differences in calculation of MET for event selection with respect to MII4U. As our templates and analysis machinery are self-consistent, this affects us only if the acceptance for backgrounds shift significantly between the two MET calculations. Figures 26 and 27 show templates for the inclusive W+LF and W+bb samples with the two different types of selections. As expected, the size of the effect is small - at or less than the 0.1% level, so the difference should not affect our analyses.

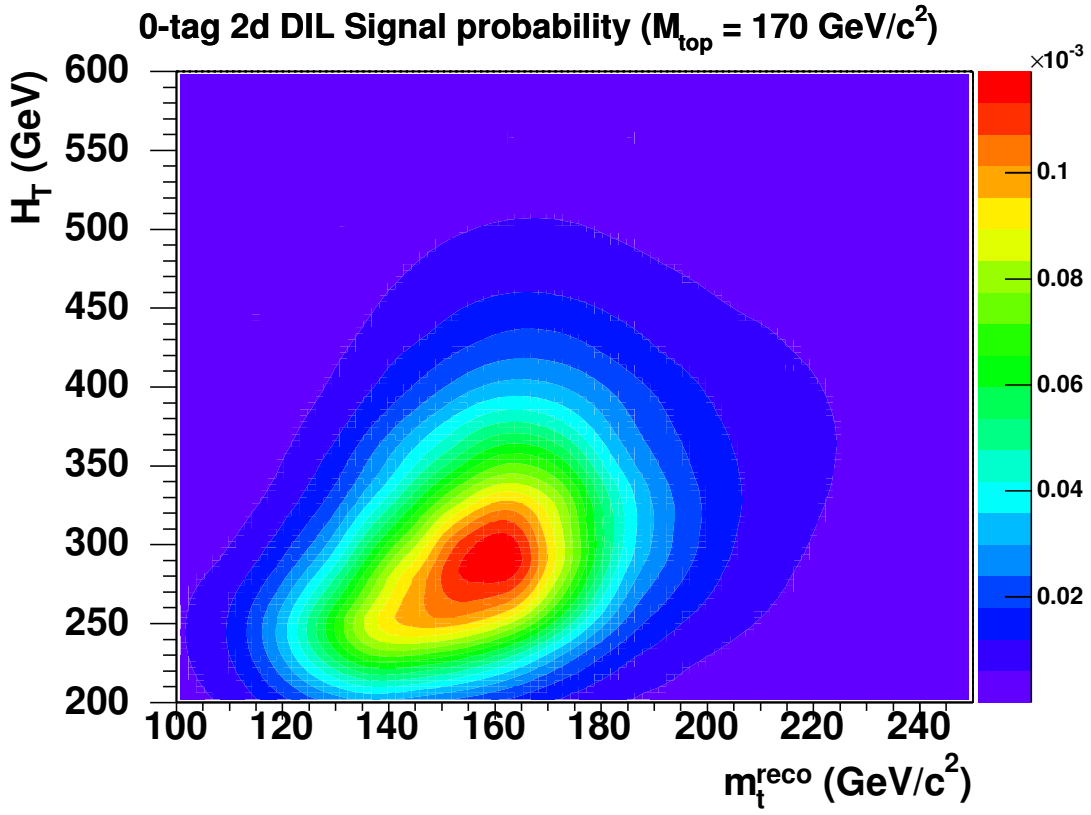

Figure 18: Two-dimensional PDF used for Dilepton 0-tag events at $\mathrm{M_{top}} = 170$ GeV/c^2 and $\Delta_{\rm JES} = 0.0\sigma_{\rm c}$

Table 5: Expected number of Lepton+Jets background events. Both sets of numbers are after the boundary cuts and include correction for tagging only on the leading jets.

	After χ^2 cut		Before χ^2 cut	
	1-tag	2-tag	1-tag	2-tag
W$b\bar{b}$+ ≥2P	7.89	1.41	9.76	2.05
W$b\bar{b}$+1P	0.96	0.65	1.17	0.90
W$b\bar{b}$+0P	0.23	0.06	0.30	0.11
W$c\bar{c}$+ ≥2P	4.37	0.23	5.34	0.33
W$c\bar{c}$+1P	0.5	0.05	0.61	0.08
W$c\bar{c}$+0P	0.08	0.16	0.08	0.16
Wc+ ≥3P	2.49	0.06	3.10	0.10
Wc+2P	0.63	0.01	0.79	0.02
Wc+1P	0.21	0.07	0.23	0.07
W+ ≥4P	8.60	0.14	10.73	0.22
W+3P	1.43	0.06	1.73	0.09
W+2P	0.41	0.01	0.47	0.01
s-channel single top	1.03	0.42	1.26	0.61
t-channel single top	0.95	0.32	1.22	0.42
WW	1.83	0.08	2.14	0.19
WZ	0.56	0.12	0.66	0.17
ZZ	0.05	0.01	0.06	0.02
QCD	10.44	0.33	11.66	0.43
Total	42.68 ± 12.48	4.19 ± 1.88	51.32 ± 15.01	5.97 ± 2.68

Table 6: Efficiencies to pass the boundary cuts for selected Lepton+Jets backgrounds. W+LF mistag background numbers use events weighted by the mistag probability.

	1-tag	2-tag
Pre-χ^2 (Wbb+2P $\Delta_{\rm JES} = 0.0\ \sigma_{\rm C}$)	0.818	0.495
Post-χ^2 (Wbb+2P, $\Delta_{\rm JES} = 0.0\ \sigma_{\rm C}$)	0.950	0.957
Pre-χ^2 (Wbb+1P $\Delta_{\rm JES} = 0.0\ \sigma_{\rm C}$)	0.788	0.417
Post-χ^2 (Wbb+1P, $\Delta_{\rm JES} = 0.0\ \sigma_{\rm C}$)	0.946	0.955
Pre-χ^2 (Wcc+2P $\Delta_{\rm JES} = 0.0\ \sigma_{\rm C}$)	0.824	0.521
Post-χ^2 (Wcc+2P, $\Delta_{\rm JES} = 0.0\ \sigma_{\rm C}$)	0.952	0.962
Pre-χ^2 (W4P $\Delta_{\rm JES} = 0.0\ \sigma_{\rm C}$)	0.804	0.503
Post-χ^2 (W4P, $\Delta_{\rm JES} = 0.0\ \sigma_{\rm C}$)	0.883	0.720

16 DIL backgrounds

The dilepton backgrounds fall into three main categories: Diboson, Drell-Yan and Fakes (or QCD). The Diboson background is modeled by the pythia datasets itopww, itopwz and itopzz. The Drell-Yan backgrounds are described by the 'matched' Alpgen+pythia Monte Carlo datasets. We use full Drell-Yan model except for samples at very low Z mass ($8 - 20$ GeV/c^2). The samples are combined as decribed in Chapter 6.

The rates of jets faking leptons are calculated by the DIL cross section group using the 4 QCD samples 'JET20', 'JET50', 'JET70' and 'JET100'. Number of well identified leptons as well as the number "fakeable" objects are counted in the "JET50" sample. The "fakeable" objects are selected from the lepton collections with some quality cuts such as presence of a stub or Hadronic to Electromagnetic energy invertted. Monte Carlo samples are used to subtract the contribution of leptonically decaying W boson from the lepton and fakeable count. The ratio of those two (W-subtracted) counts is the fake rate. The calculation is performed for different lepton categories and in bins of the lepton E_T. Based on the differences of fake rates calculated using the "JET50"

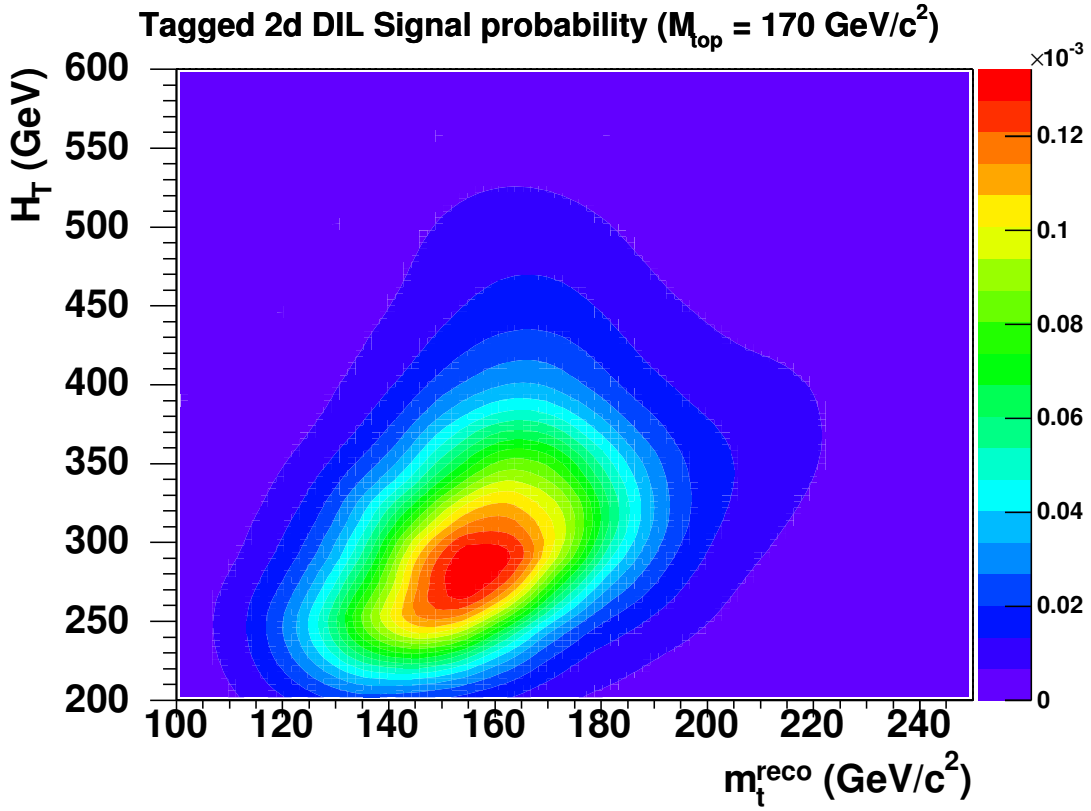

Figure 19: Two-dimensional PDF used for Dilepton tagged events at $M_{top} = 170$ GeV/c^2 and $\Delta_{JES} = 0.0\sigma_c$

sample and other jet samples a 30% uncertainty is assigned on the fake rates.

Data samples collected on the high p_T lepton triggers (the same samples as are used to perform the final fit) are used to obtain the estimate of number of fake events. Events with one lepton and one or more "fakeables" are selected. The fakeable is then interpreted as a lepton. This implies that the missing energy as well as E_T sum will be corrected if the fakeable is a muon. If the fakeable object concerned is to be interpreted as an electron closest jet within cone of 0.4 is removed from the jet collection. The dilepton selection is applied to events prepared this way. We sum the fake rates of the fakeable objects from events passing the dilepton selection to obtain the estimate of total number of events entering our dataset. We also apply Neutrino Weighting Algorithm reconstruction to obtain this background model. Note that a single event can enter the sum multiple times if more than one fakeable objects are present in the event. Details of the procedure as well as fakeable cuts are presented in the cross section blessing note [19]. We have replicated the selection used by the DIL cross section, however we remove the bad beamline runs from the data. In addition we observe several more events than the cross section group - the difference was traced to a minor bug in the cross section group code.

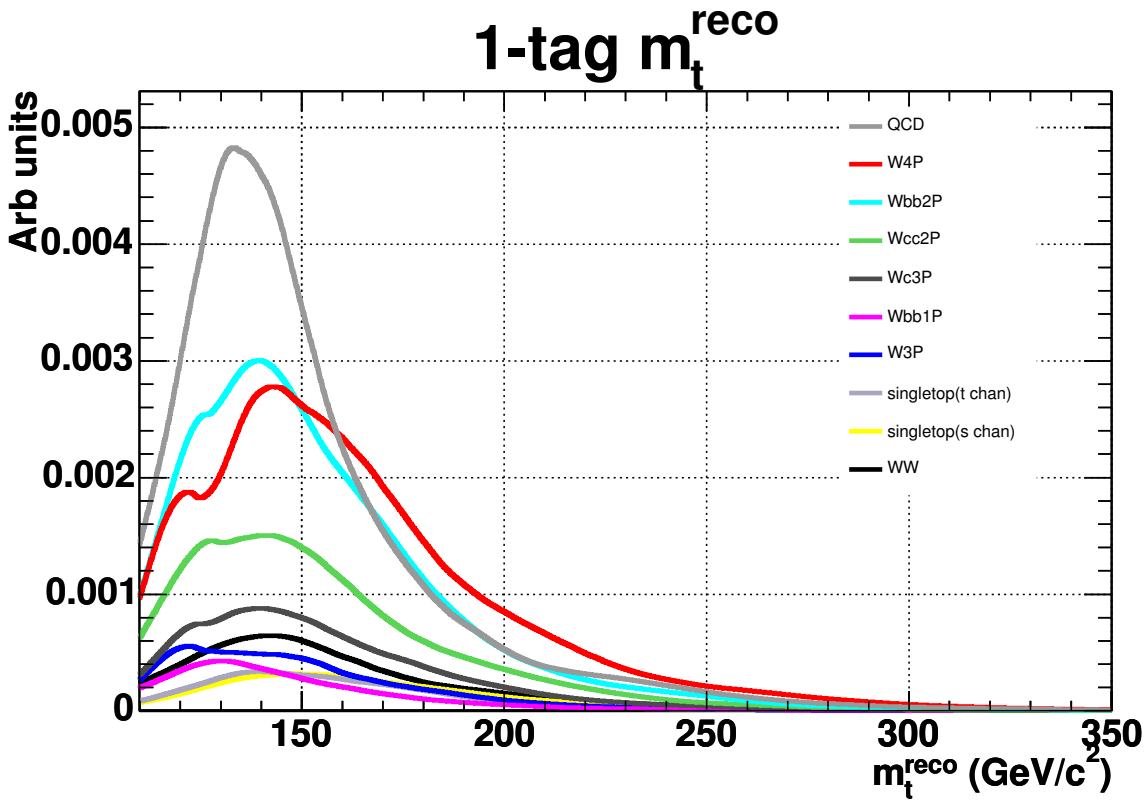

Figure 20: Reconstructed masses for individual 1-tag backgrounds, weighted by the contribution to the entire background sample.

The model used for the preliminary result is described in more detail in version 1.10 of this note. The main differences are:

- Instead of W subtraction from the QCD datasets using Monte Carlo samples cuts on $\not\!\!E_T$ and transverse mass of fakeable and $\not\!\!E_T$ were made- this was found to bias the fake rate.
- Jets matched to fakeable muons were removed from the jet collections when selecting events from the lepton trigger samples.
- Custom (loose) fakeable cuts were used (shown in reference [16])

The second item is understood to be the most important one for changing the fake contribution estimate. The estimate used for the preliminary measurement is 6.1 events in non-tagged sample and 1.2 events in the tagged sample. This compares to 19.3 and 2.7 events respectively expected with the current procedure. Figures 28 and 29 show a comparison of the reconstructed top quark mass and $H_T$in the old and updated fake model.

Figures 30 and 31 show the 2d dilepton backgrounds.

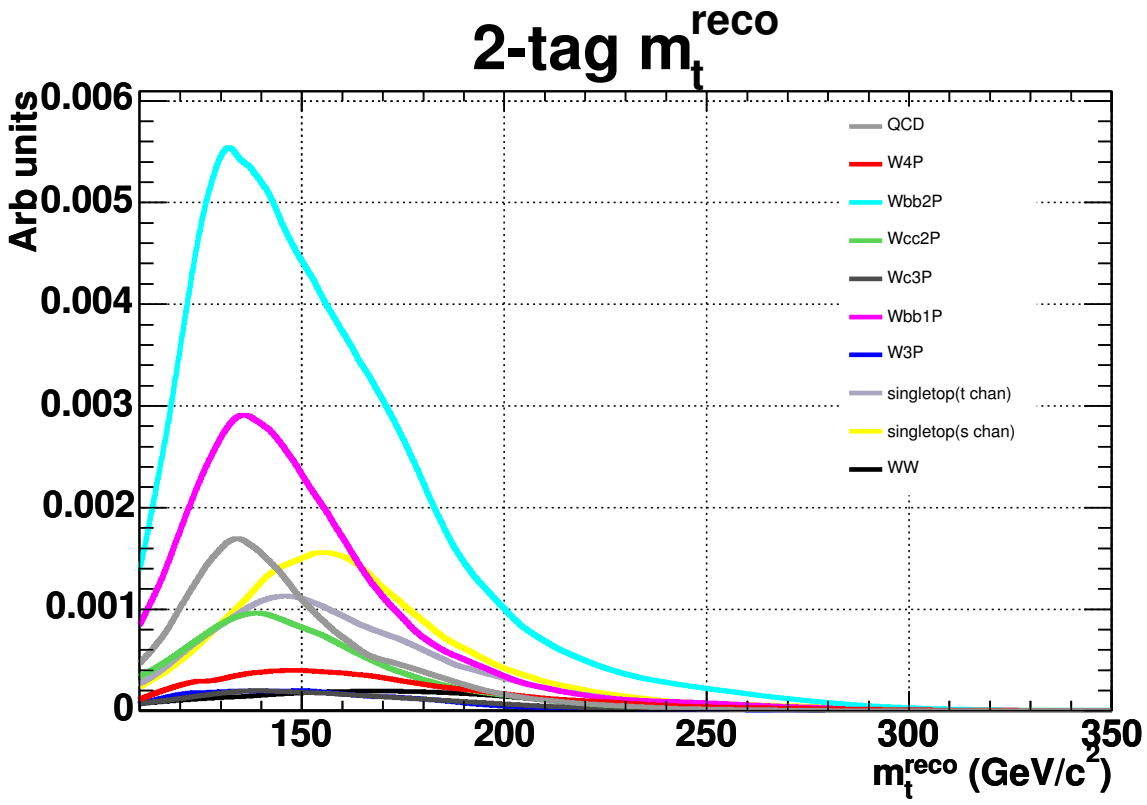

Figure 21: Reconstructed masses for individual 2-tag backgrounds, weighted by the contribution to the entire background sample.

17 Blind samples

Results from the blind tests for the combined fit are shown in Figure 32. The distributions are dominated by the Lepton+Jets fits, which are shown in Figure 33. The Dilepton-only blind results are showin in Figure 34. All PEs use the number of events from P11 event data scaled up by luminosity, with the expected backgrounds given in the above sections. The final fakes model was not ready for the DIL background, so a MC-based approach from the W+4p MC samples was used. Asymmetric MINOS errors were used to create the pull distributions. One of the blind samples had a mass that was too high to be reconstructed accurately by the Dilepton-only fit. This sample was thrown away in the blind results by the top mass conveners.

The residuals all look good and consistent with no bias. The pull widths are shown before any correction, so we don't necessarily expect widths consistent with 1.0, but the obtained values slightly larger than 1.0. There is one sample that seems to give an anomylously high pull width in both the L+J and combined fits. It is not clear whether this is the sample with a high mass that needed removal in the DIL-only fit.

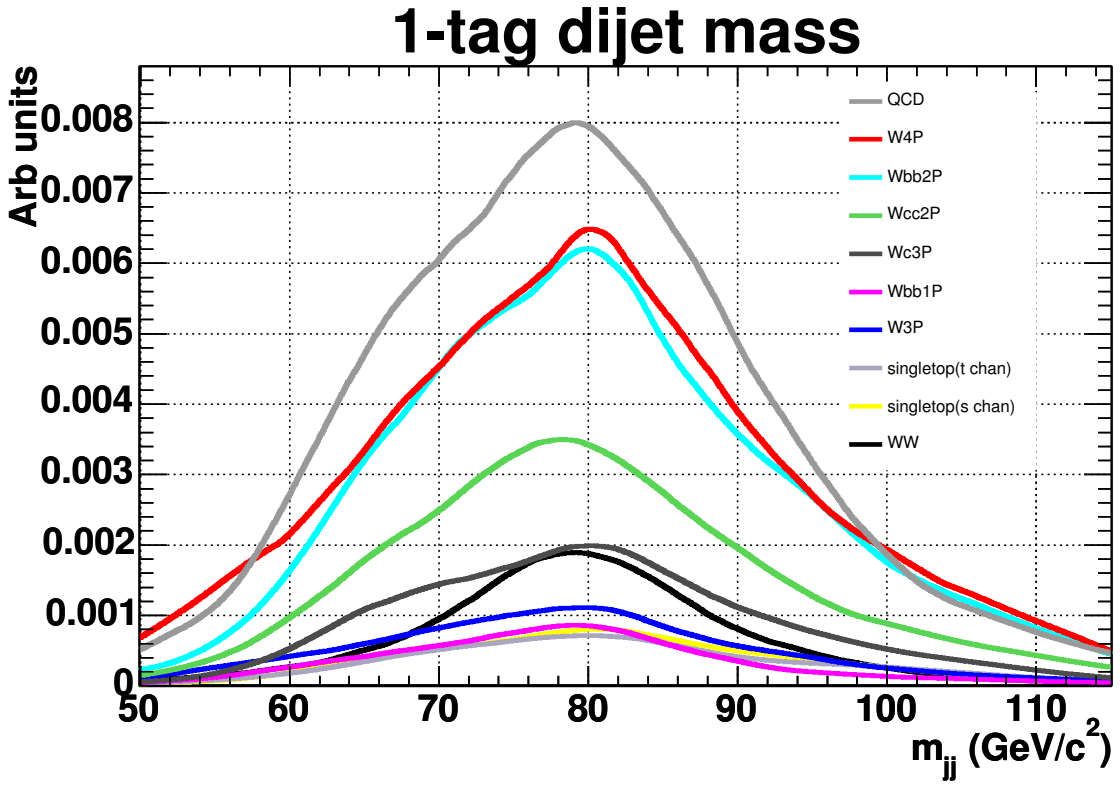

Figure 22: Dijet masses for individual 1-tag backgrounds, weighted by the contribution to the entire background sample.

18 Bias checks

To investigate any possible biases in our method, we run checks at a variety on M_{top} and Δ_{JES} values. For each point, the background pseudodata is drawn with JES having the same value as the signal pseudodata. The number of background events is as described in the above chapters. The number of signal events is obtained using the theoretical cross section at M_{top}=175 GeV/c^2=6.7pb. Errors bars are given by results from the bootstrap method, described in Section 19. The Δ_{JES} values in the plots are given by the color scheme shown in Figure 35. Fits are to points only using Δ_{JES} = 0.0, since points using other Δ_{JES} values are highly correlated to it.

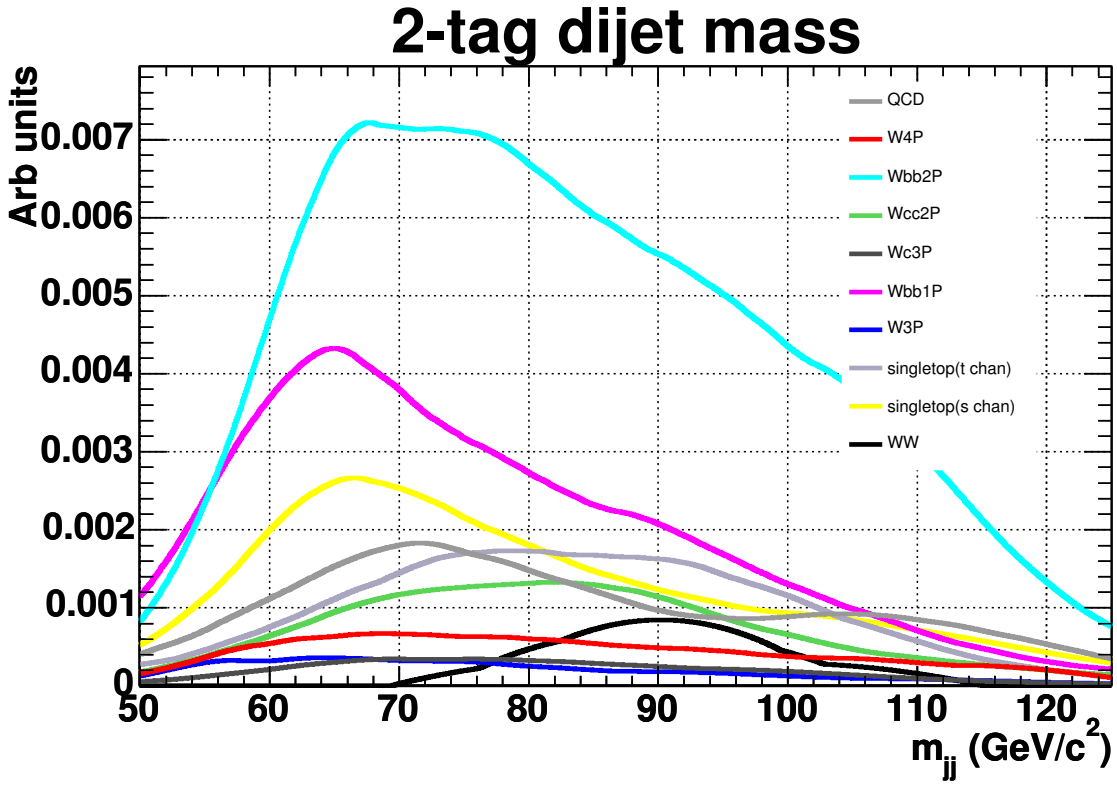

Figure 23: Dijet masses for individual 2-tag backgrounds, weighted by the contribution to the entire background sample.

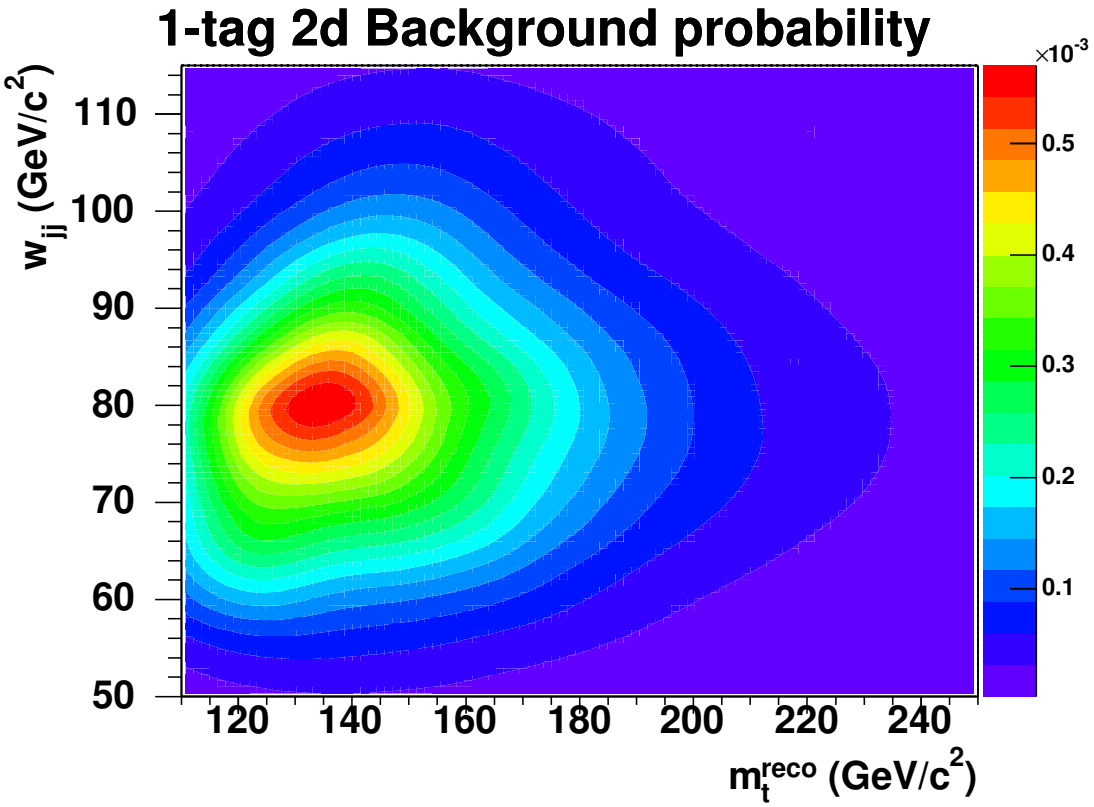

Figure 24: Two-dimensional PDF used for 1-tag Lepton+Jets background events.

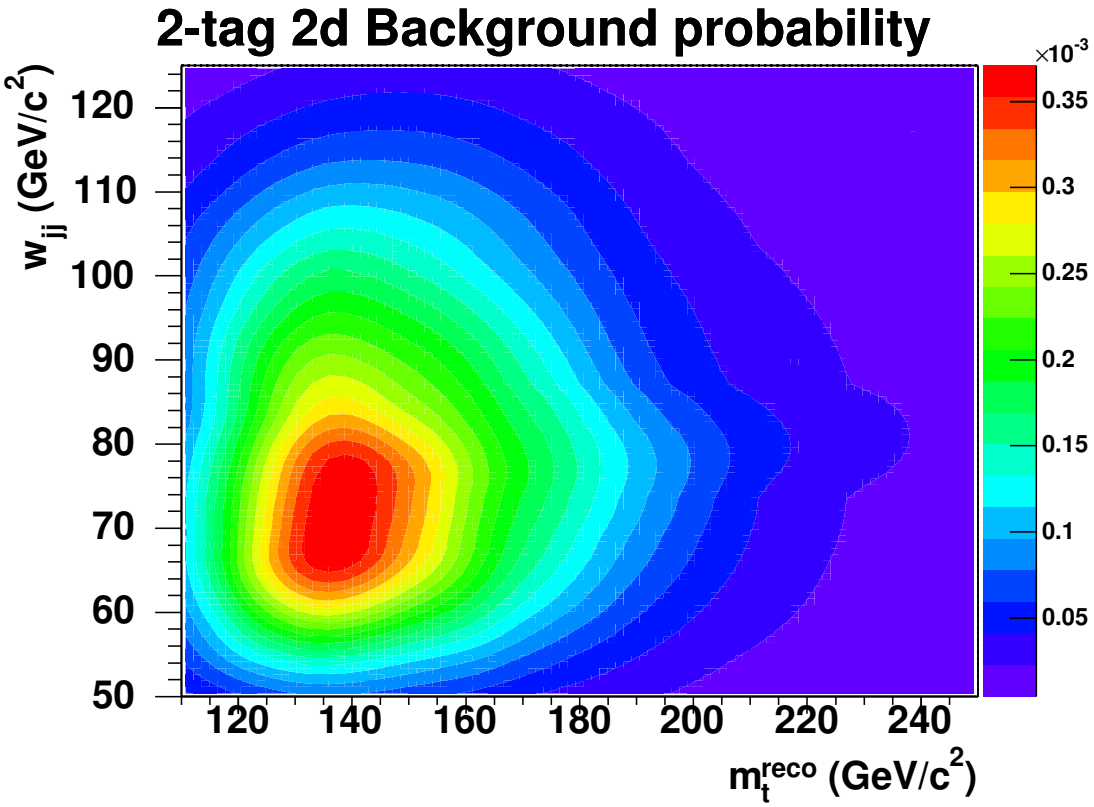

Figure 25: Two-dimensional PDF used for 2-tag Lepton+Jets background events.

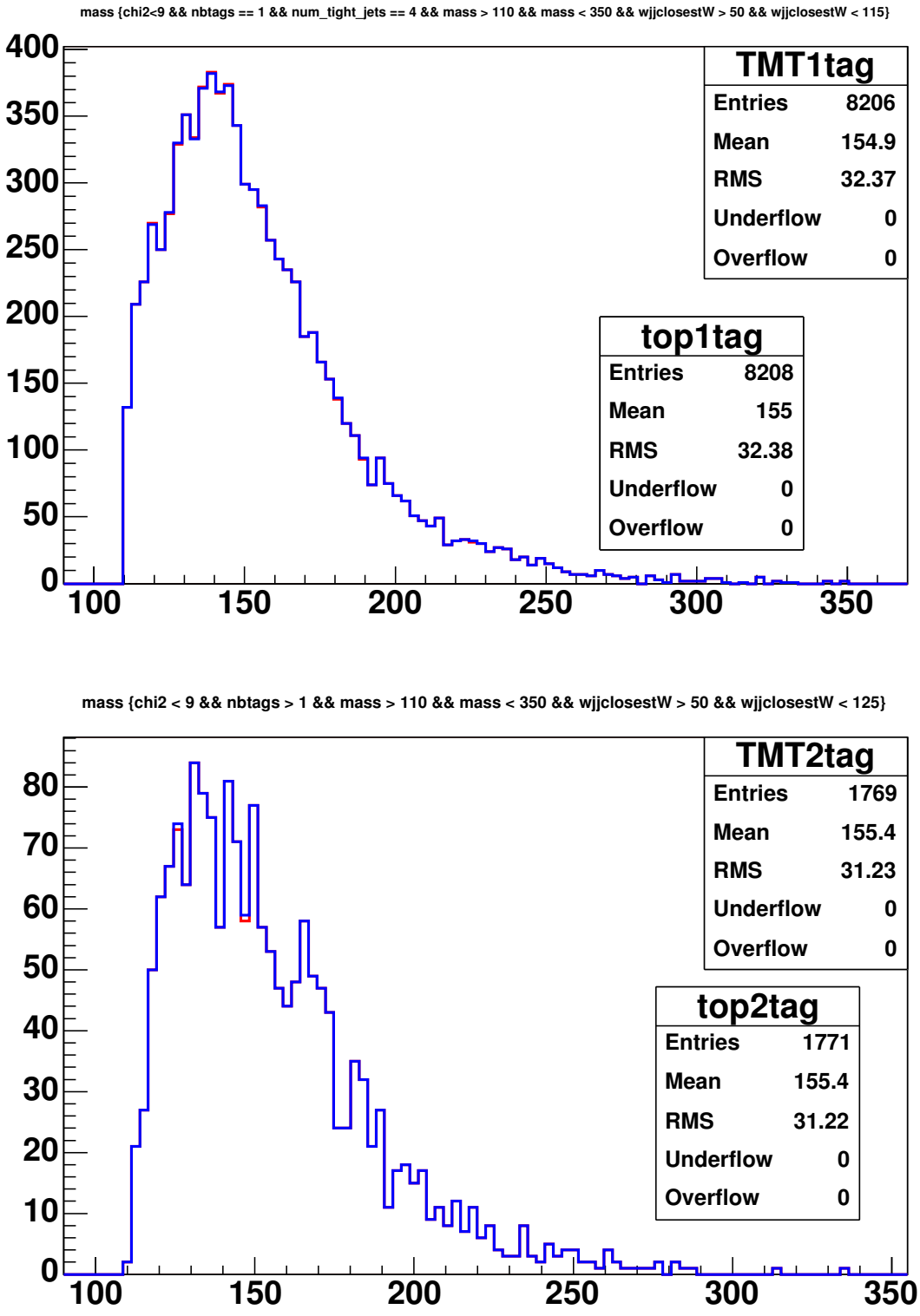

Figure 26: Background templates for 1-tag (top) and 2-tag (bottom) events derived from the Wbb+≥2-parton samples with our event selection(TMT) and MII4U event selection(TMT). Both distributions are included, but are so close together that they overlap almost entirely.

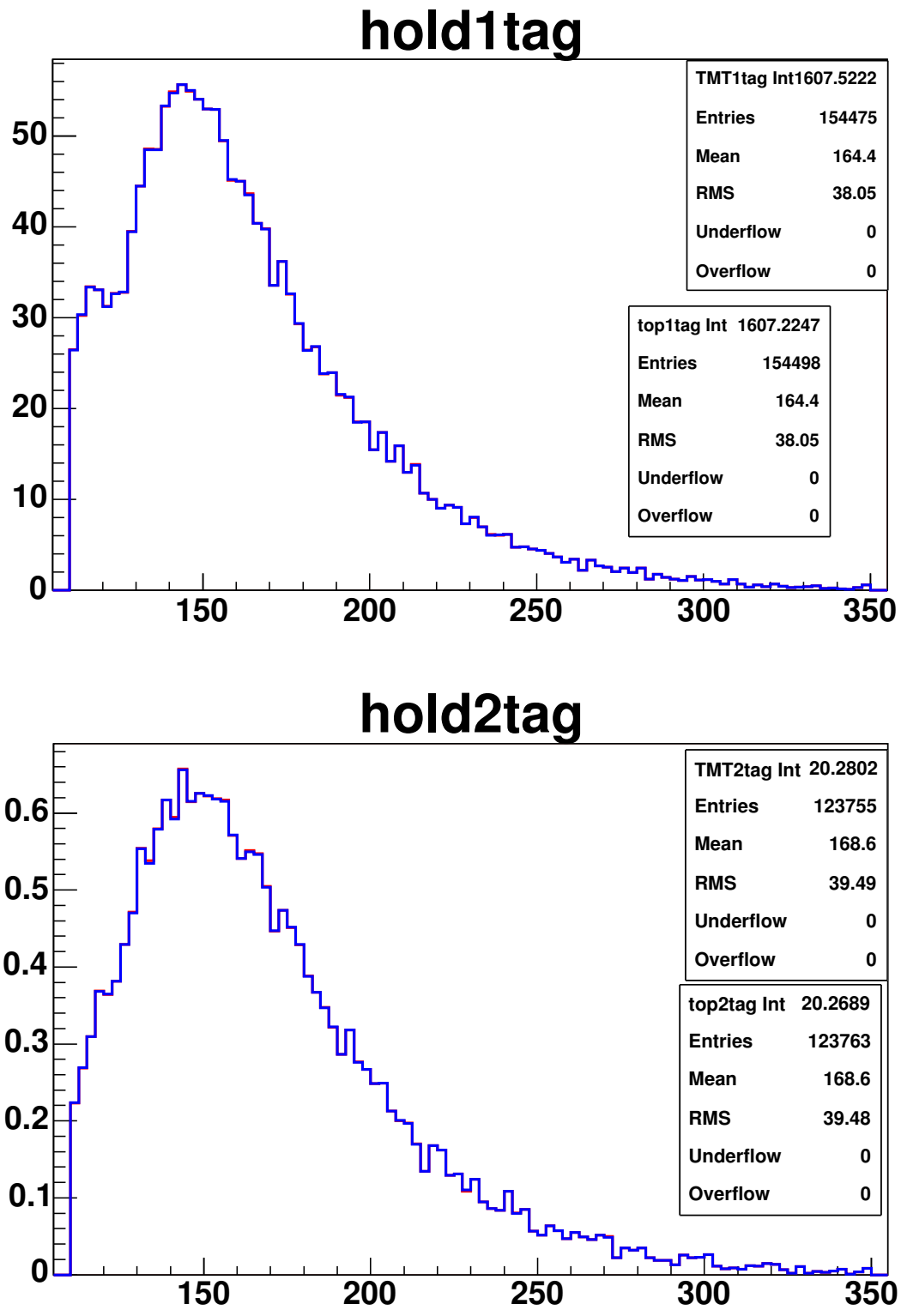

Figure 27: Background templates for 1-tag (top) and 2-tag (bottom) events derived from the W+≥4-LF parton samples with our event selection(TMT) and MII4U event selection(TMT). Events are weighted by their mistag probability, so the figure of merit to compare is the integral of the distributions. Both distributions are plotted, but are so close together that they overlap almost entirely.

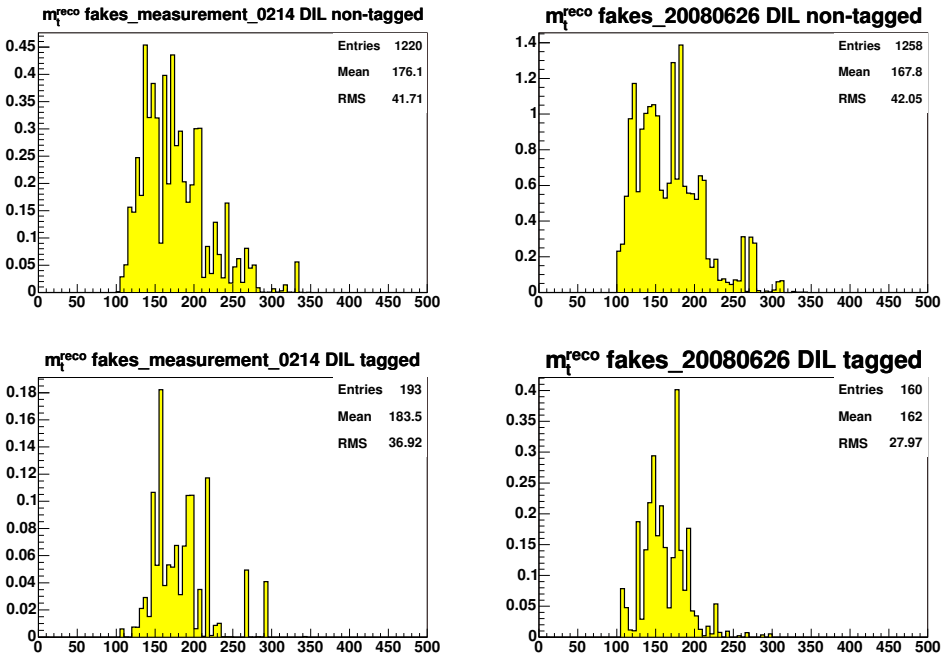

Figure 28: Comparison of M_t^{reco}in the fake model used in the preliminary measurement (left) and the updated model (right), for the non-tagged (top) and tagged (bottom) subsamples

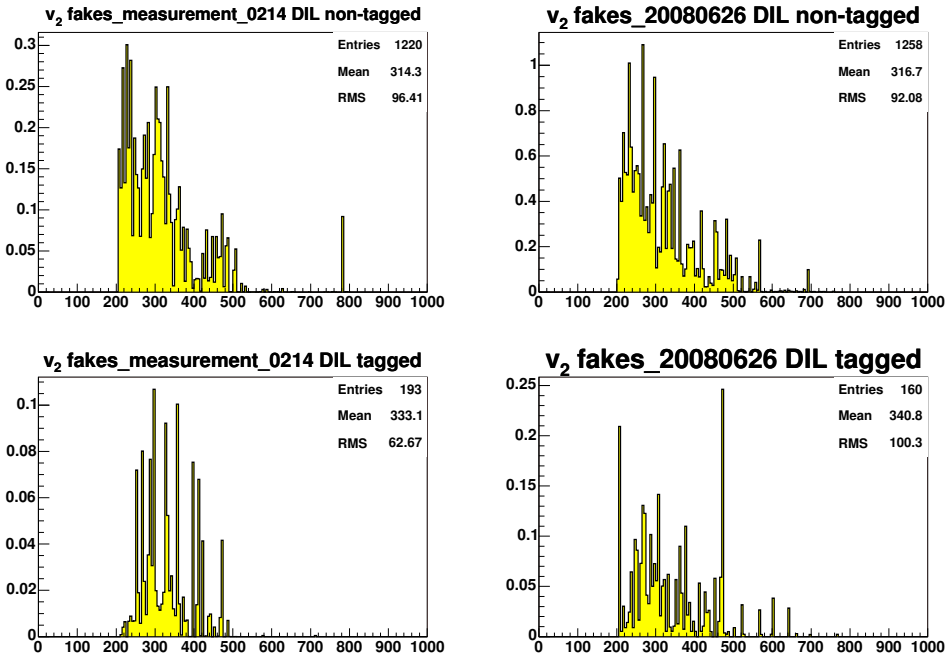

Figure 29: Comparison of $H_T$in the fake model used in the preliminary measurement (left) and the updated model (right), for the non-tagged (top) and tagged (bottom) subsamples

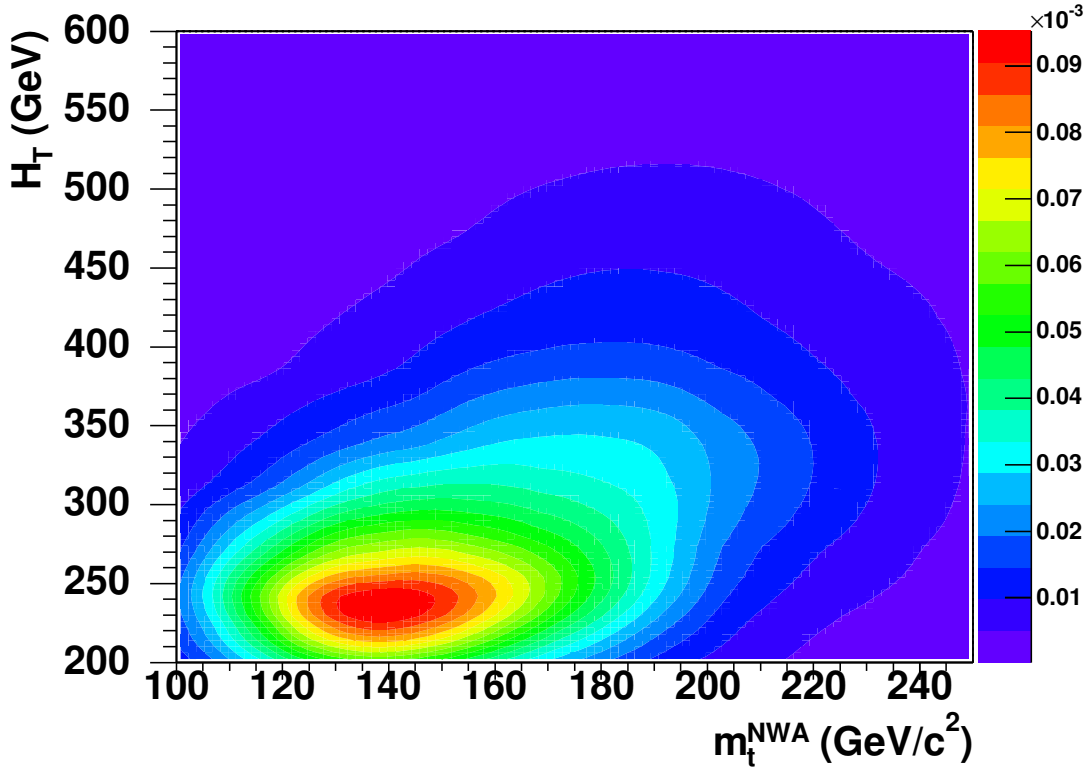

Figure 30: Two-dimensional PDF used for 0-tag Dilepton background events.

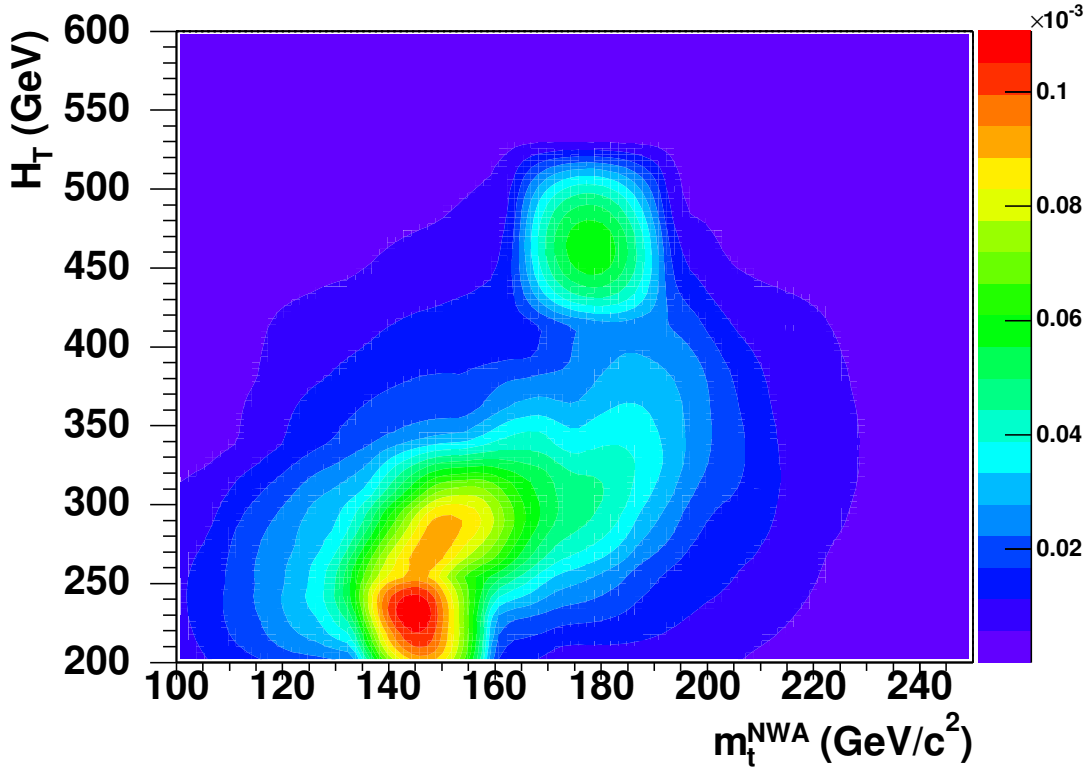

Figure 31: Two-dimensional PDF used for tagged Dilepton background events.

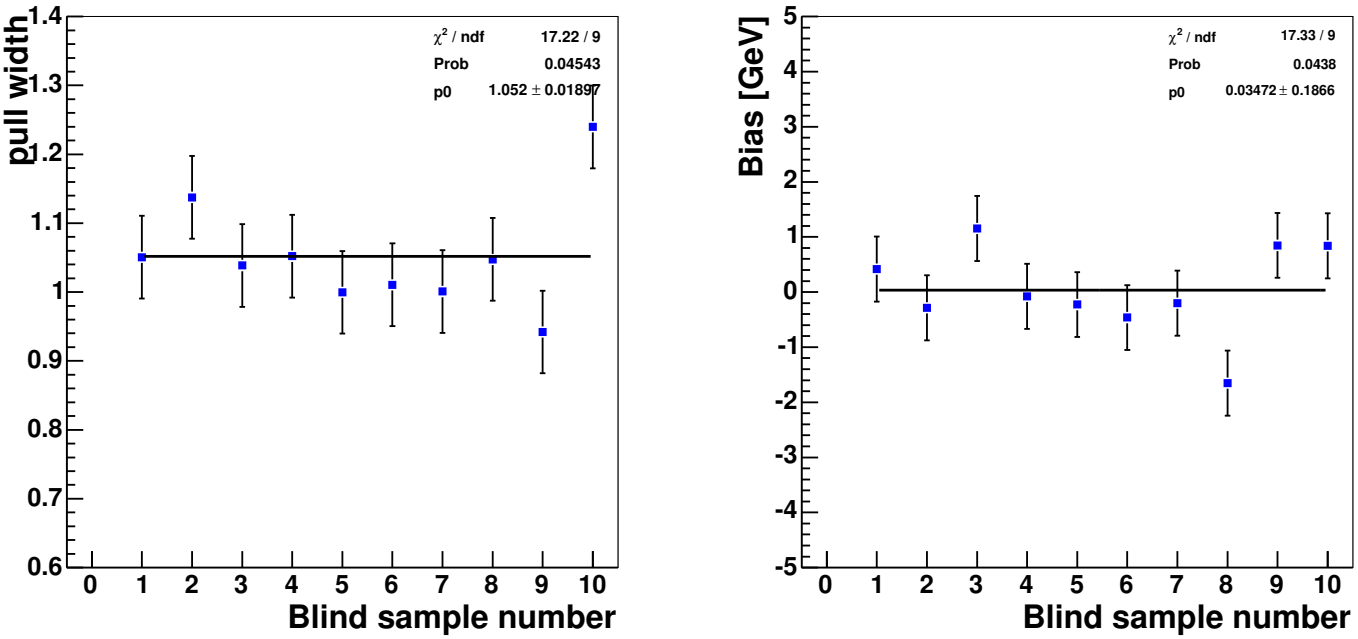

Figure 32: Blind samples pull widths and residuals for the combined fit.

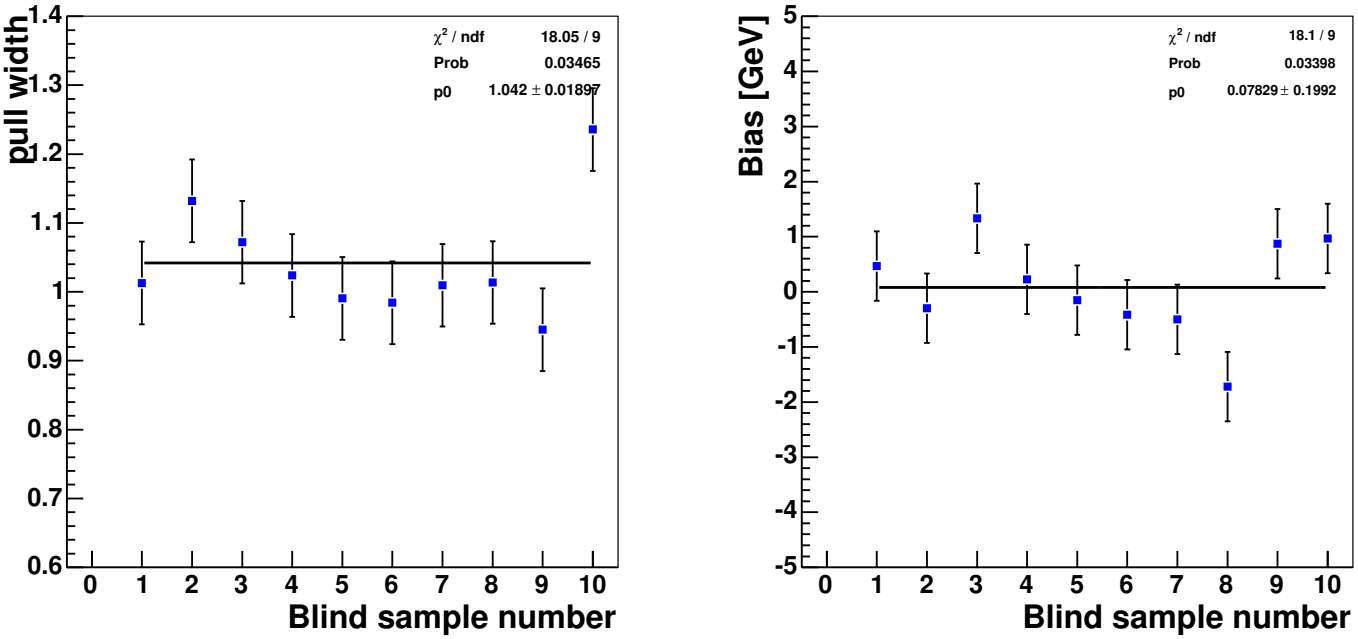

Figure 33: Blind samples pull widths and residuals for the Lepton+Jets-only fit.

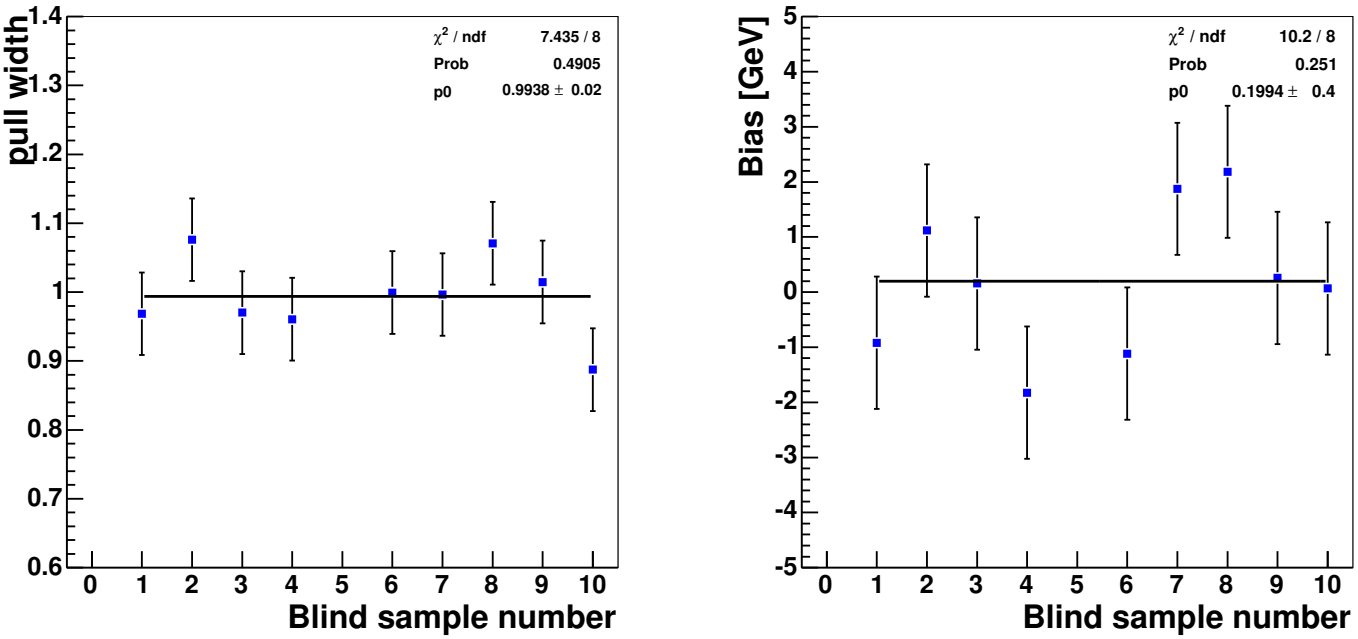

Figure 34: Blind samples pull widths and residuals for the Dilepton-only fit.

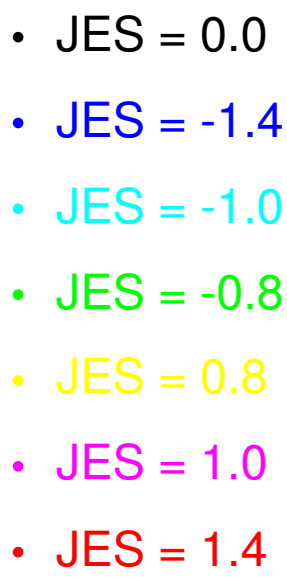

Figure 35: Color JES legend

The most important plots are the bias residuals, shown in Figures 36. Based on the residuals, we conclude that our methods are unbiased. The DIL measurement has an average bias of about 0.26GeV from 0.0. The χ^2 for a line going through residual of 0.0 is 21.42 for the 14 mass points, corresponding to a p-value of 9%. We do not make bias corrections on the measurements. The pull widths are shown in Figure 37. The widths are defined as the RMS of the pull distributions, which use asymmetric errors. As expected, pull widths are near to but slightly larger than unity. We will correct the statistical error of the final measurement by the average pull width. The jet energy scale bias and pull width are shown in Figures 38 and 39. Based on those two figures the uncertainty on fitted Δ_{JES} value needs a small correction. The Figure 40 shows the expected errors from PEs, given by the RMS of the output mass distributions and Figure 41 shows the behavior of median uncertainty. Figure 42 shows RMS for the Lepton+Jets fit and the combined fit.

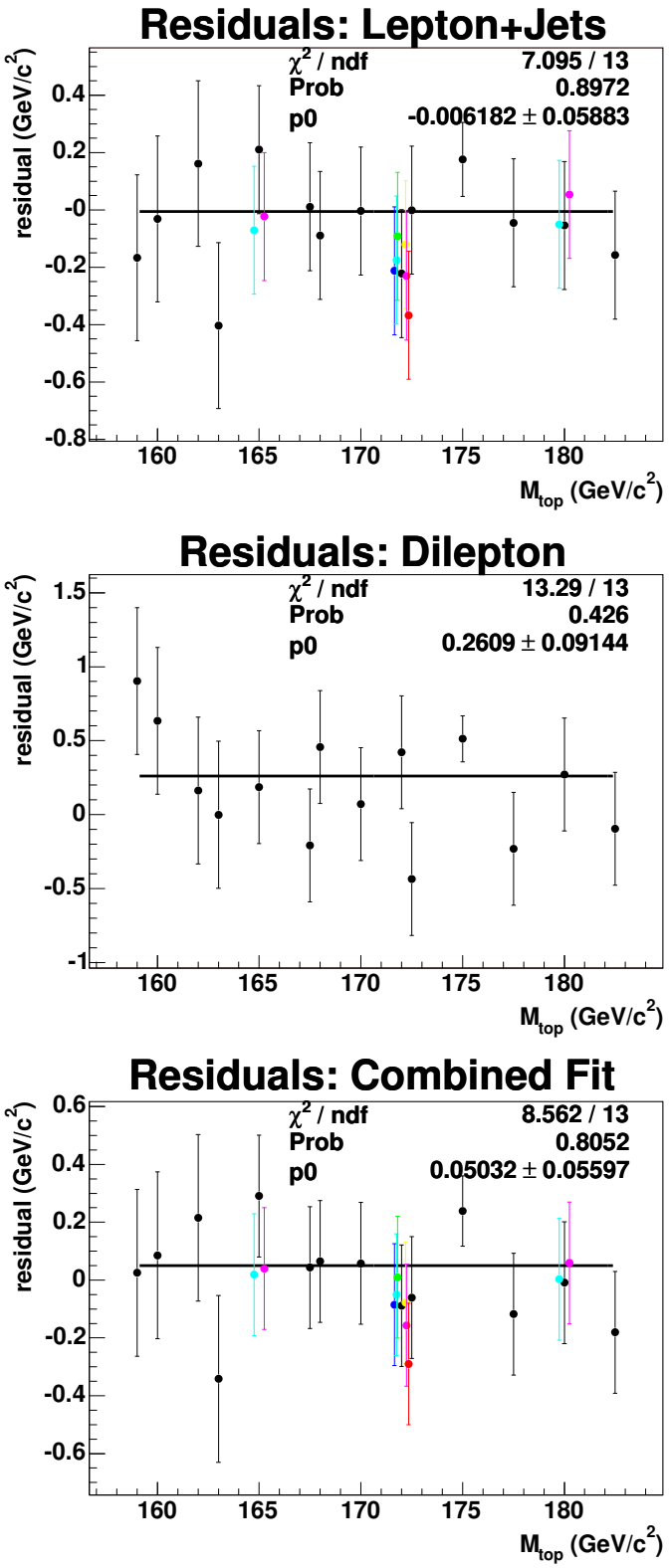

Figure 36: Checks for fitted top mass residual bias for L+J-only PEs (top), DIL-only PEs (middle) and combined PEs (bottom). Straight-line fits are to JES = 0.0 points.

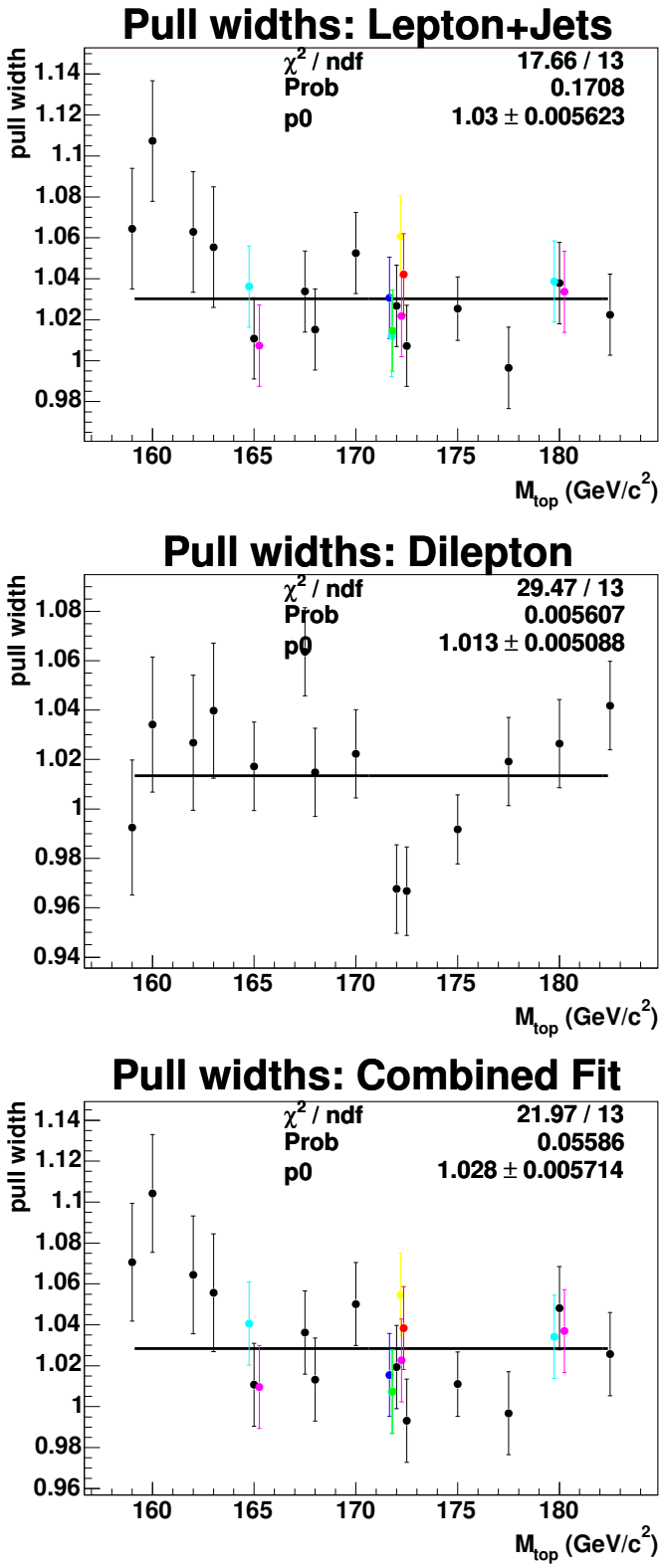

Figure 37: Fitted top mass pull widths for L+J-only PEs (top), DIL-only PEs (middle) and combined PEs (bottom). Straight-line fits are to JES = 0.0 points.

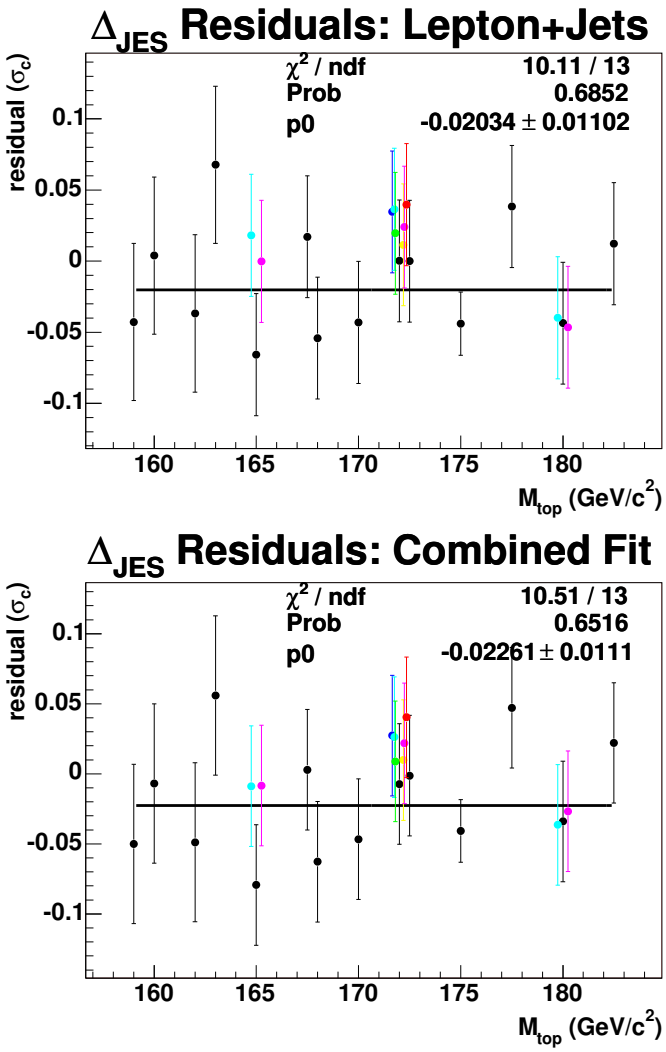

Figure 38: Checks for Δ_{JES} bias for L+J-only PEs (top) and combined PEs (bottom). Straight-line fits are to JES = 0.0 points.

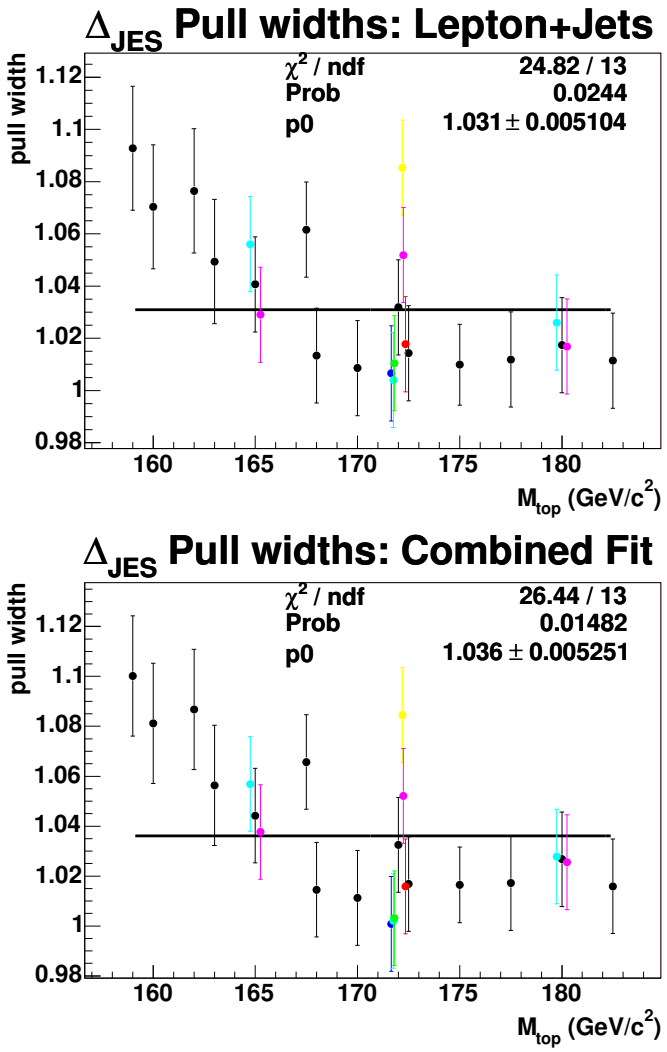

Figure 39: Δ_{JES} pull widths for L+J-only PEs (top) and combined PEs (bottom). Straight-line fits are to JES = 0.0 points.

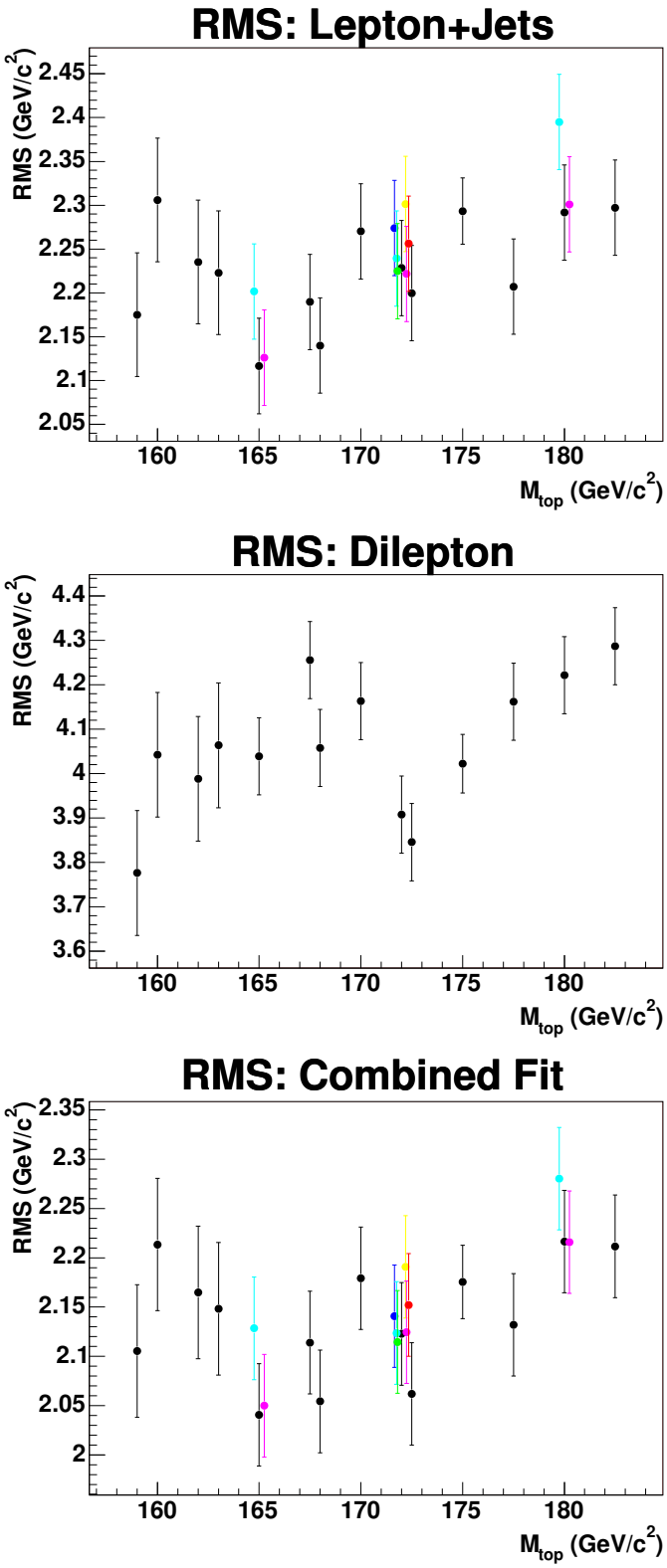

Figure 40: Expected errors for L+J-only PEs (top), DIL-only PEs (middle) and combined PEs (bottom).

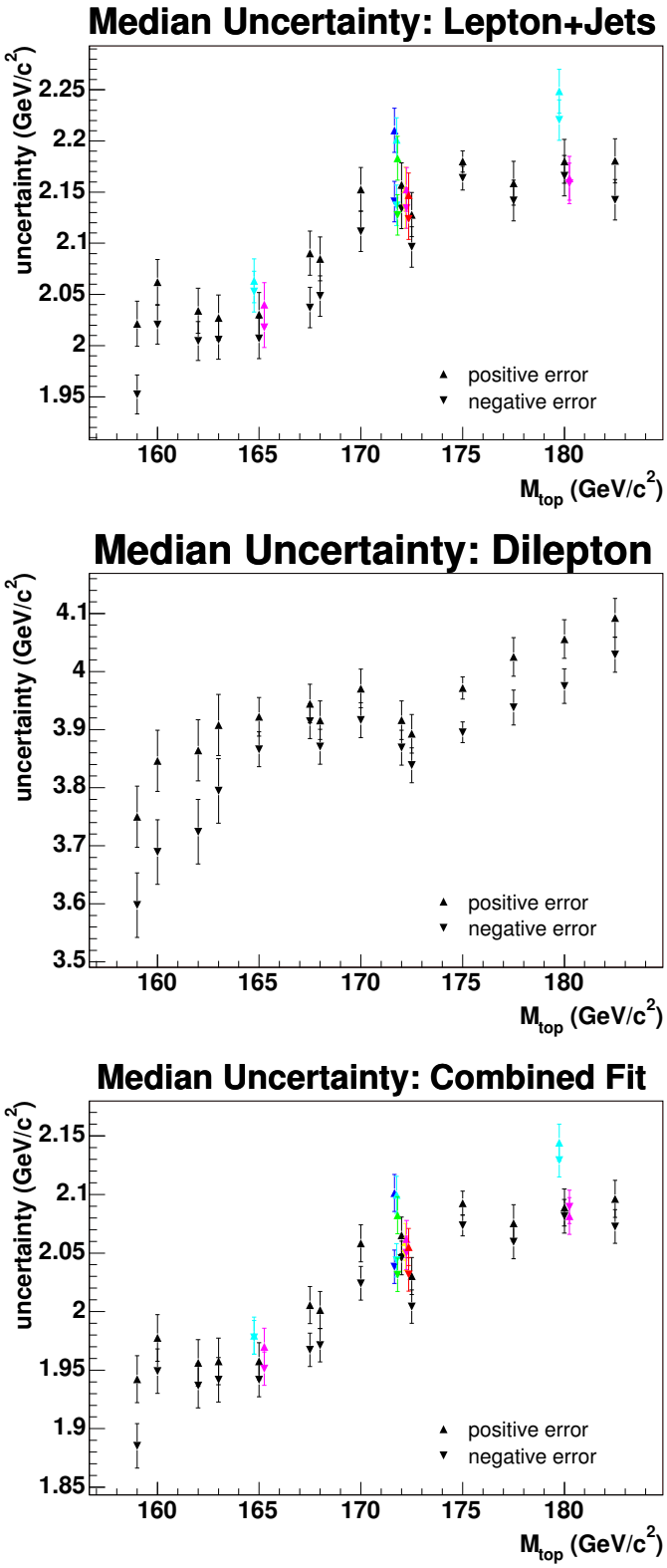

Figure 41: Expected median asymmetric errors for L+J-only PEs (top), DIL-only PEs (middle) and combined PEs (bottom).

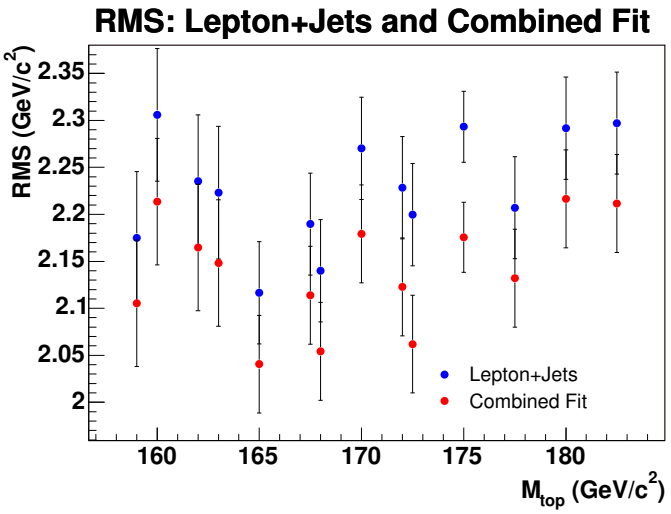

Figure 42: RMS from the L+Jets and Combined fit pseudoexperiments

Figures 43, 44 and 45 show another set of sanity checks: the mass residual, pull width and Δ_{JES} residual for pseudoexperiments with varying Δ_{JES}. We do not put error bars on these plots or fit them, as the points are highly but not completely correlated, but it is good to see that different mass samples seem to have different Δ_{JES} dependence, indicating that the small trends are likely due to statistical fluctuations.

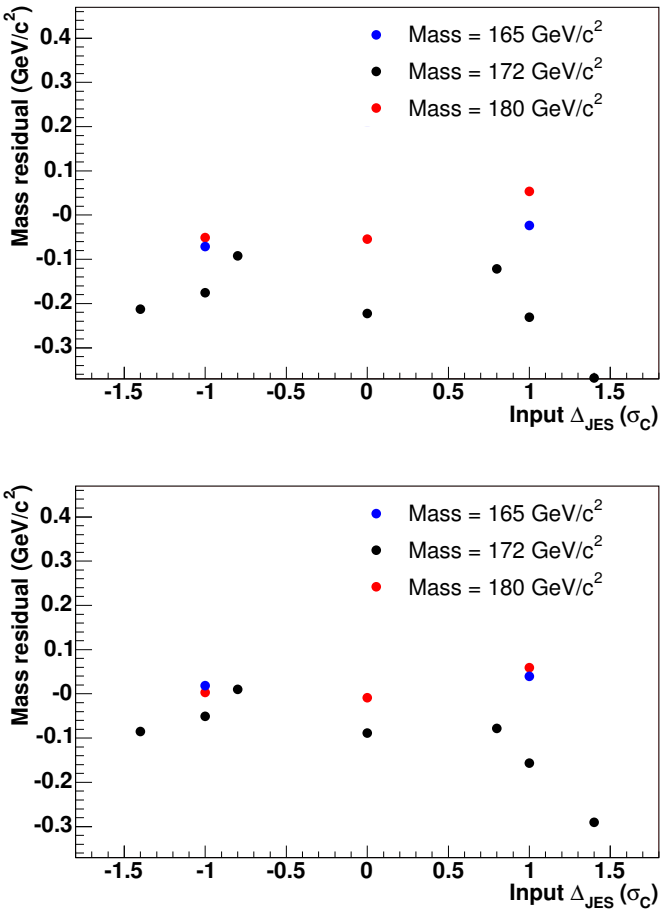

Figure 43: Mass residual as a function of Δ_{JES} for Lepton+Jets fits (top) and combined fits (bottom).

19 Bootstrap

The error bars on our bias checks and for systematics that are statistics limited come from the bootstrap method. For more information on the method, see note [12]. We bootstrap ttkt70 ttkt75 and ttkt60 each 60 times, giving us an estimate for the uncertainty on quantities due to limited MC signal statistics. We use the RMS of quantities

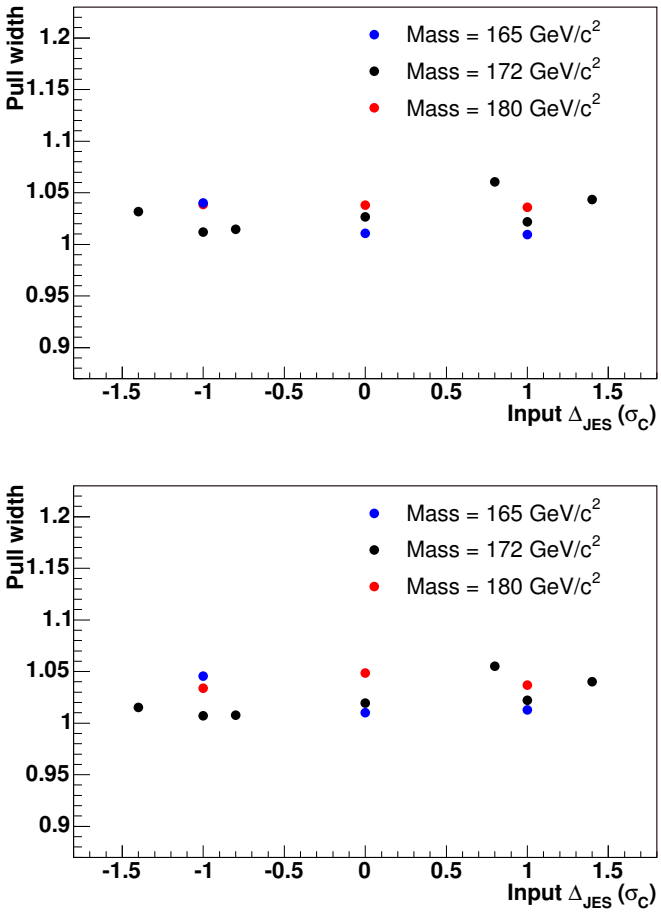

Figure 44: Pull width as a function of Δ_{JES} for Lepton+Jets fits (top) and combined fits (bottom).

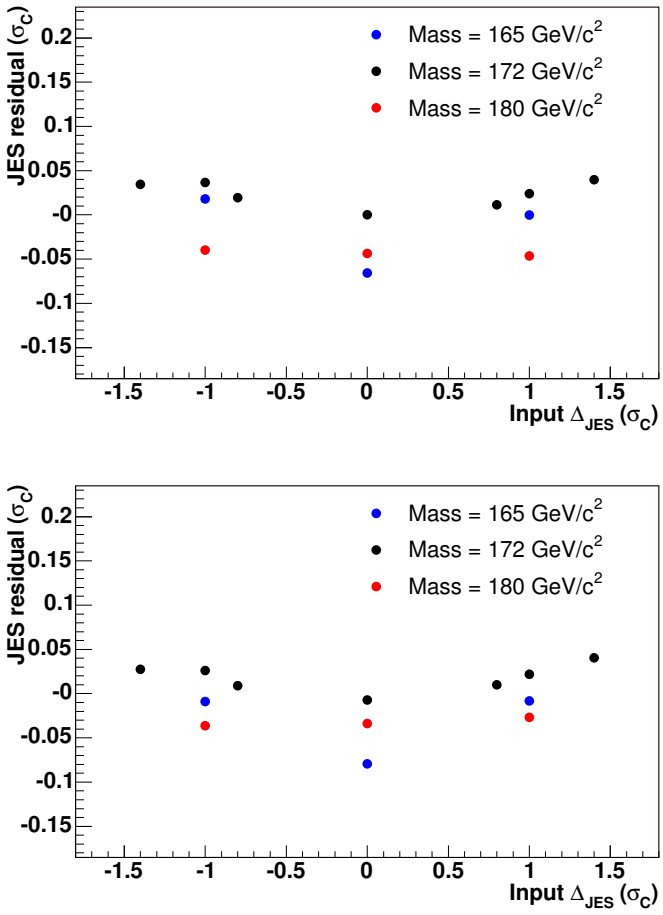

Figure 45: Δ_{JES} residual as a function of Δ_{JES} for Lepton+Jets fits (top) and combined fits (bottom).

from the bootstraped samples as the estimators for uncertainties. The result of the bootstrap run using the ttop70 sample are used to plot errors on the bias plots for most of the mass points. Results from ttkt75 and ttop60 are used for the 4.4M event and 0.6 event samples.

Bootstrapped output masses for the ttkt70 bootstrap set are shown in Figure 46. Bootstrapped pull widths are shown in Figure 47, and bootstrapped mass RMS values are shown in Figure 48.

We also bootstrap the background samples in order to evaluate the effect of limited statistics in the background pseudodata. Bootstrap is performed without taking into account the event and subsample relative weights so that each event has equal chance to enter the bootstrap set. When pseudoexperiments are performed using this background bootstrap the event weights are used to construct pseudodata for a particular pseudoexperiment. The mean fitted mass distributions from background bootstraps run using ttop70 signal sample are shown in Figure 49. We take the RMS of these distribution as the systematic uncerainty due to the background MC statistics. We obtain 0.05 GeV/c^2 for L+J fit, 0.47 GeV/c^2 for the DIL fit and 0.08 GeV/c^2 for the combined fit.

20 Systematics

We study a variety of possible systematics as prescribed by the top mass group. We run pseudoexperiments using the same number of events as for our bias checks. To be conservative, when we find a systematic with uncertainties that are larger than the systematic itself, we take the uncertainty, as defined by the bootstrap method, as the systematic. When comparing variations that go in the same direction from the nominal sample, we take half the largest difference from the nominal sample as the systematic. When comparing highly correlated samples (such as residual JES or reweighted gg-fraction), we do not use the statistical uncertainties.

Detailed results from the study of systematics common to all 3 analyses are decsribed in Tables 10 and 11. Our systematics are summarized in Table 12.

For a systematic on the Generator, we compare Herwig (otop1s) and Pythia with input values of M_{top} = 175.0 GeV/c^2, We find large differences 0.75 GeV/c^2 for the LJ-only fit, 1.33 GeV/c^2 for the DIL-only fit, and 0.67 GeV/c^2 for the combined fit..

The next to leading order prediction for the fraction of $t\bar{t}$ pair production coming from gluon fusion rather than quark anihilation is 15±5%. However the signal Monte Carlo samples used have this fraction set at 5.6%. We reweight the events in Monte Carlo sample generated at 175 GeV/c^2 so that events coming from the gluon fusion constitute 20% of pseudodata and take the difference in the mean fitted mass from pseudoexperiments as a systematic uncertainty. We obtain 0.16 GeV/c^2 for the combined fit, 0.19 GeV/c^2 for the Lepton + Jets only fit and 0.17 GeV/c^2 for the Dilepton only fit.

The amount of initial and final state radiation has been studied in the Drell-Yan

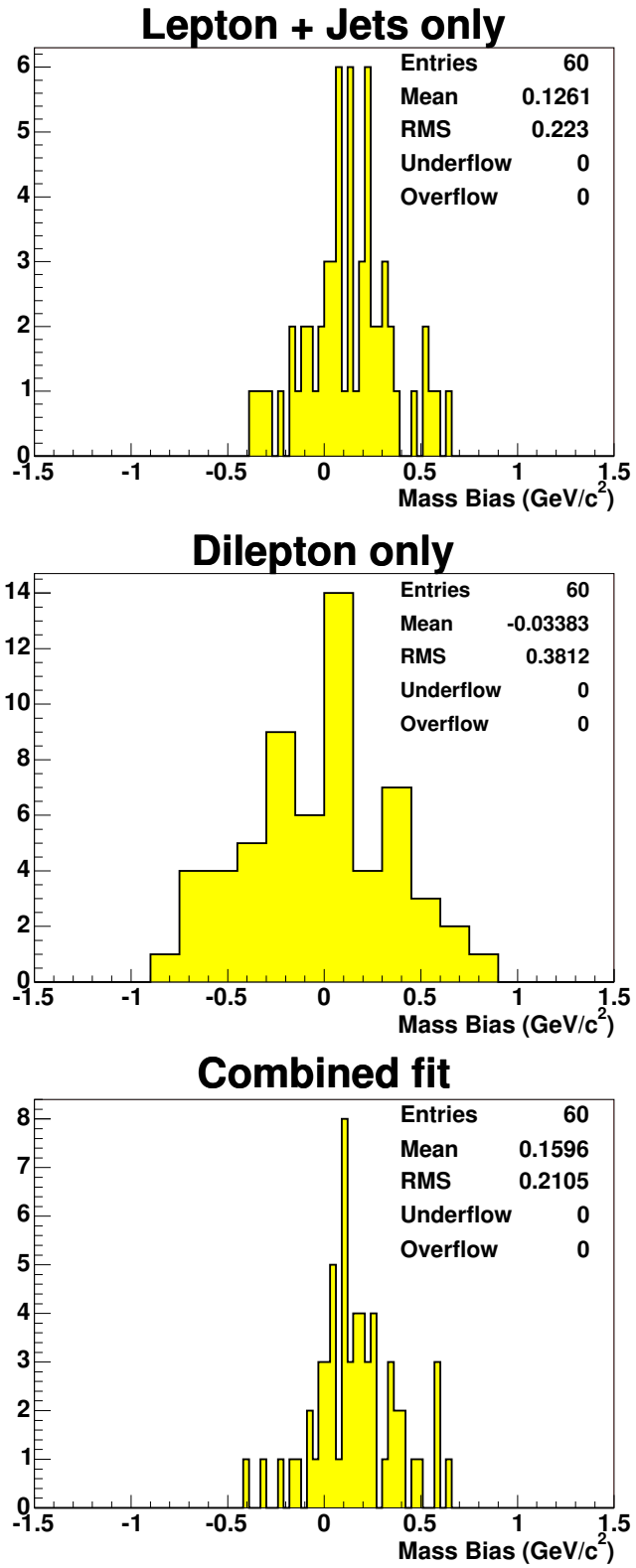

Figure 46: Output masses for bootstrapped samples for L+J-only PEs (top), DIL-only PEs (middle) and combined PEs (bottom).

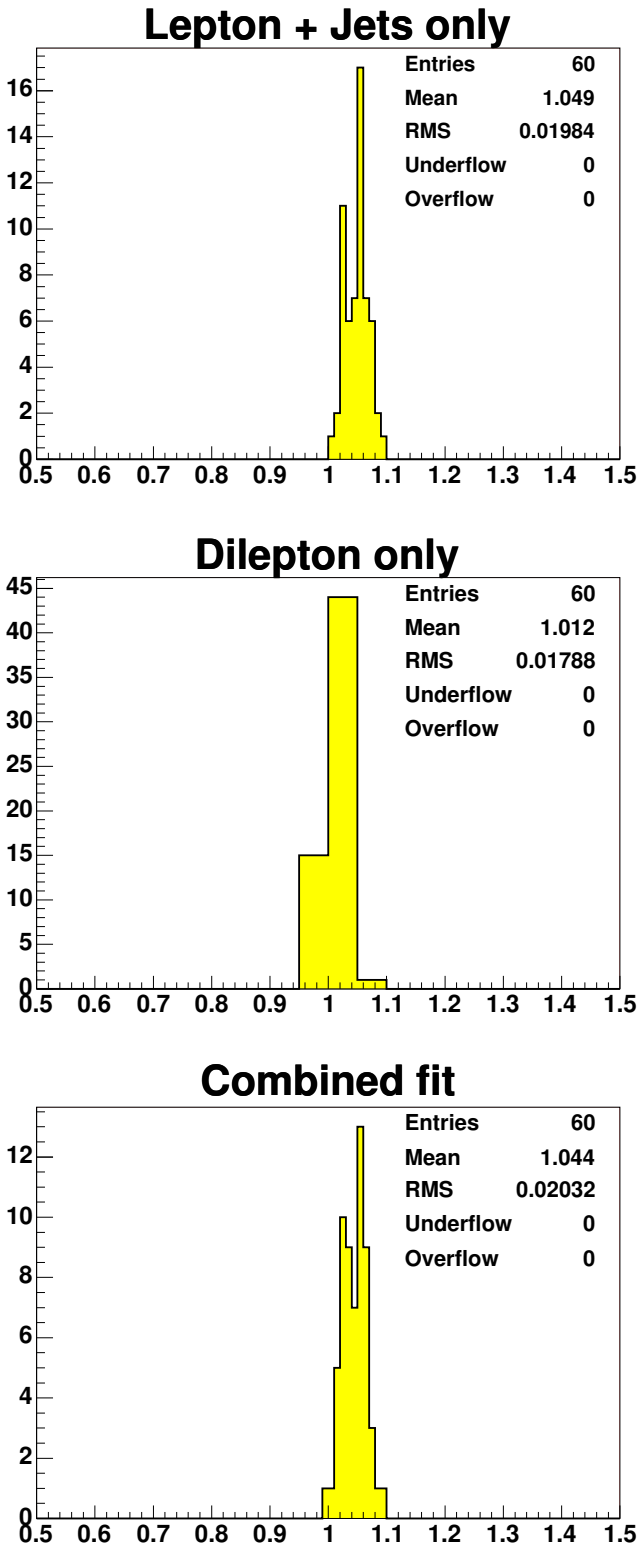

Figure 47: Pull widths for bootstrapped samples for L+J-only PEs (top), DIL-only PEs (middle) and combined PEs (bottom).

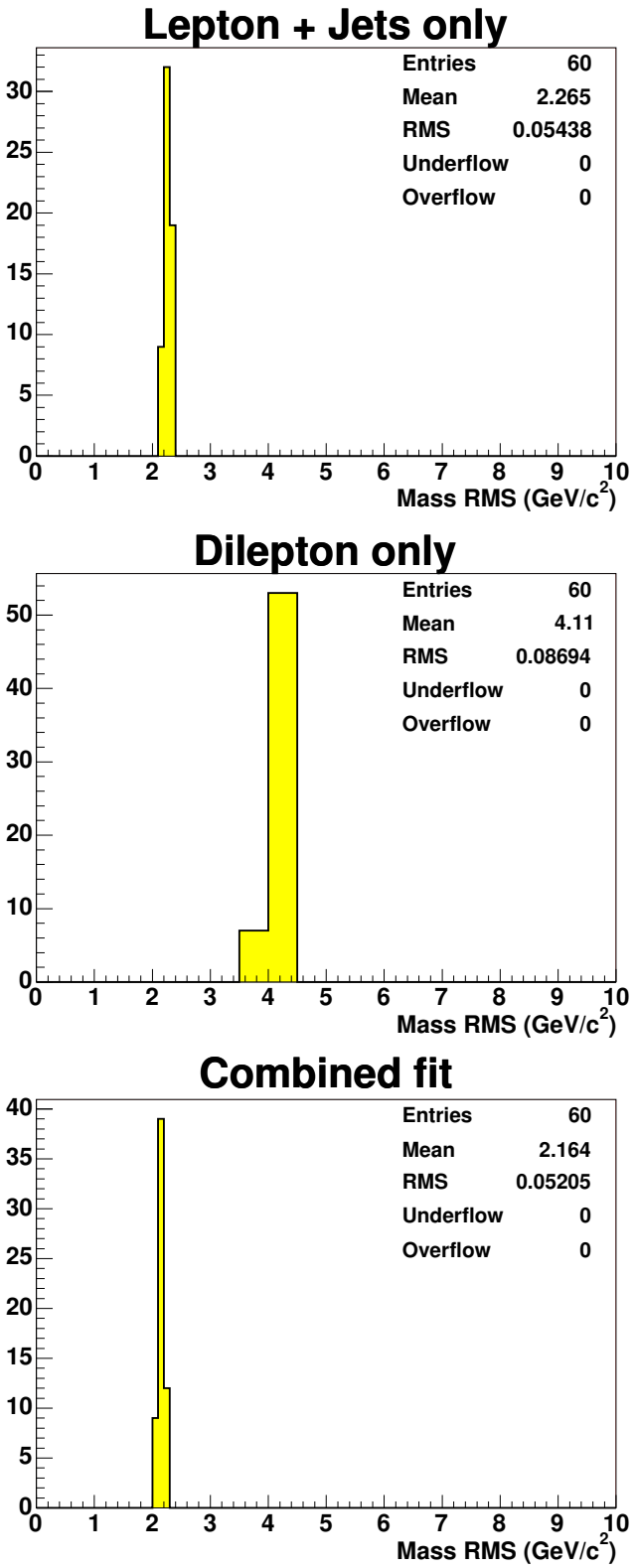

Figure 48: Output mass RMS values for bootstrapped samples for L+J-only PEs (top), DIL-only PEs (middle) and combined PEs (bottom).

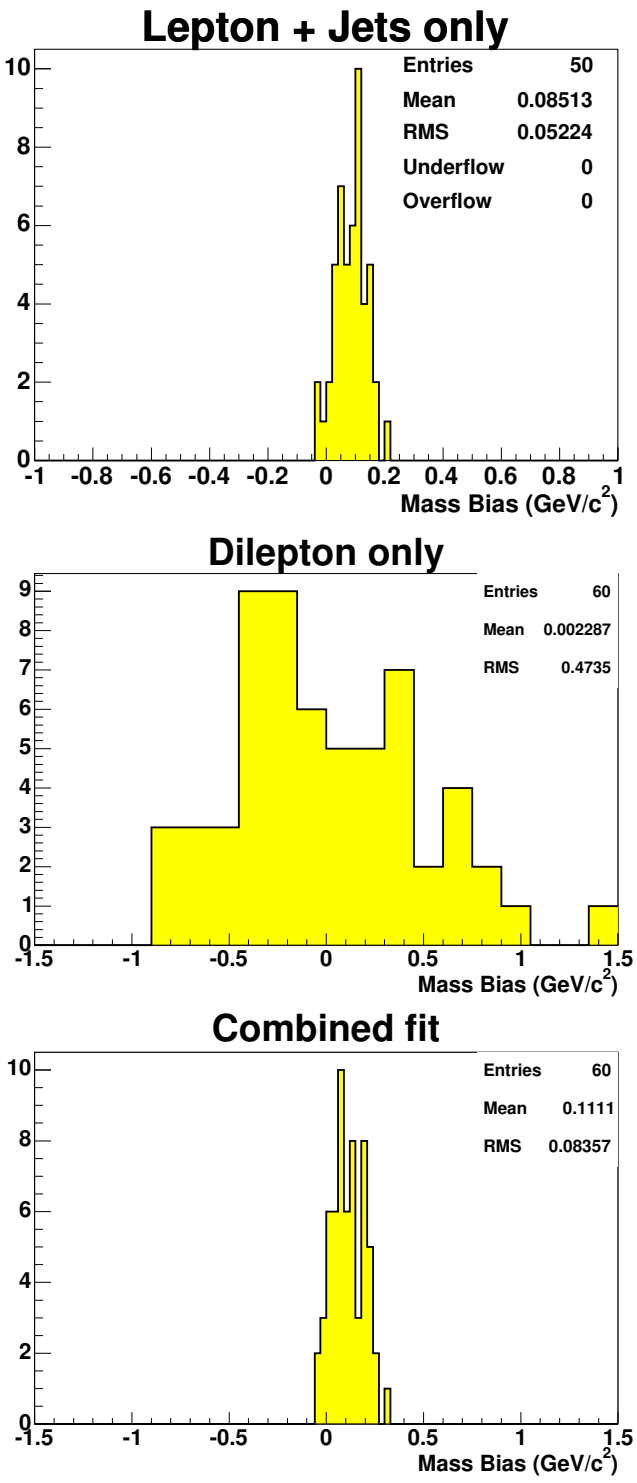

Figure 49: Output masses for background bootstrapped samples for L+J-only PEs (top), DIL-only PEs (middle) and combined PEs (bottom).

system. Those studies are used to constrain parameters in the Pythia Monte Carlo generator that control amount of gluon radiation. We run pseudoexperiments where the data has been drawn from samples in which the amount of gluon radiation from the initial and final state have been coherently varied within these constraints (otop03, otop04). Resulting half difference gives 0.15 GeV/c^2 uncertainty in the Lepton + Jets channel. Both up and down shifts result in a change in the same direction in the Dilepton fit therefore half difference (0.20 GeV/c^2) to the nominal result is taken as a systematic. In the Combined fit the statistical uncertainty on the half difference (0.13 GeV/c^2) is greater than the half difference itself (0.10 GeV/c^2) and is taken as a systematic.

The uncertainty on muon and electron energy reconstruction is estimated to be 1% at the CDF detector. Since measurement of muon energy is based on the track curvature and measurement of electron energy is calorimeter-based we vary the electron and muon response independently. The scaling is performed prior to selection and $\not\!\!E_T$ calculation. In Lepton + Jets only fit and Combined fit up and down electron energy scale adjustment both result in lower than the nominal pseudoexperiment average. We take half difference to the nominal result obtaining 0.03 GeV/c^2 and 0.04 GeV/c^2 systematics for the Lepton + Jets and combined fits. The electron energy scale systematic in the Dilepton fit is 0.23 GeV/c^2. The muon energy scale systematic is 0.09 GeV/c^2, 0.18 GeV/c^2 and 0.06 GeV/c^2 in the Lepton + Jets only, Dilepton only and combined fits respectively.

We evaluate the normal systematics related to the parton distribution functions by reweighting the ttkt75 sample. We compare different groups (CTEQ5L vs MRST72) and take the absolute difference as a systematics. We also compare Λ_{QCD} (MRST72 vs MRST75) and again take the absolute difference as a systematic. Finally, we compare the 20 +/- eigenvectors from CTEQ6M, taking half of the difference between the +1 σ and -1σ shifts for each eigenvector pair. For the LJ measurement, we find systematics of 0.10 GeV/c^2 for the different groups, 0.09 GeV/c^2 for the different QCD scales, and 0.22 GeV/c^2 for the different eigenvectors, giving a total systematic on PDFs of 0.25 GeV/c^2. For the DIL measurement, the numbers are 0.10 GeV/c^2 for the groups, 0.39 GeV/c^2 for the QCD scales and 0.36 GeV/c^2 for the eigenvectors, giving a total PDF systematic of 0.54 GeV/c^2. For the combined measurement, we find systematics of 0.08 GeV/c^2 for the groups, 0.11 GeV/c^2 for the QCD scales, and 0.22 GeV/c^2 for the different eigenvectors, resulting in a combined systematic of 0.25 GeV/c^2. Summary plots for the PDF studies are shown in Figure 56.

To examine possible systematics due to how we combine the Lepton+Jets backgrounds (and because the background weights relative to one another have uncertainties associated with them), we run pseudoexperiments drawing only from certain types of backgrounds for the Lepton+Jets events. We run PEs drawing only from: W$b\bar{b}$, W$c\bar{c}$, Wc, and W+light jets, single top, QCD and the diboson samples. When we draw from a particular type of background, we use the various n-parton samples, keeping the relative weights between them (as given by acceptance and cross-sections) constant. For single top, we draw from both s-channel and t-channel. For diboson, we draw from

WW, WZ and ZZ samples. The largest shifts from the nominal values came from PEs drawing only from the W$b\bar{b}$ sample in the Lepton+Jets only fit and mistag (W+light flavor jets) sample in the combined fit. We assign these shifts (0.17 GeV/c^2 for LJ and and 0.11 GeV/c^2 for the combined measurement) as background composition systematics.

To study possible mismodeling of the background, we run pseudoexperiments drawing from only W$b\bar{b}$ samples that have Q^2 changed by factor of 2^2 and 0.5^2. When drawing from these backgrounds, we reweight the relative ratio of the samples by the cross sections given by ALPGEN. We find shifts of 0.09 GeV/c^2 for the Lepton+Jets measurement and 0.10 GeV/c^2 for the combined measurement, which we add to Lepton + Jets background shape systematics.

We also study possible mismodeling of the Lepton+Jets QCD background. We tried changing the isolation cut from > 0.2 to 0.15 and 0.3, but found only extremely tiny differences in the templates. Perhaps this is a sign that the method is robust, but other models of jets faking leptons are also available; we choose to run over the antielectron sample, giving us a few hundred events. Only a handful of these events are tagged, so we use the mistag matrix on this data, and run pseudoexperiments where we replace the nonisolated lepton pseudodata with antielectron events (weighted by the associated mistag probabilities). We see small shifts of 0.02 GeV/c^2 in the Lepton+Jets measurement and 0.05 GeV/c^2 in the combined measurement, which we take as Lepton+Jets QCD systematics. The differences between the two types of templates are shown in Figures 50 and 51. The dijet masses are fairly similar, and though $M_t^{\rm reco}$ peaks at a similar location for both selections, the antielectron samples have significantly longer tails.

To study the effect of the dilepton background sample composition on the DIL fit and on the combined fit we perform six sets of pseudoexperiments where we vary given type of background (DY, diboson and fakes) up or down by uncertainty on it's estimate while holding the total number of background constant. We take half the differnce from each of the shifts and sum in quadrature. We obtain 0.11 GeV/c^2 uncertainty for the DIL fit and 0.06 GeV/c^2 for the combined fit. The results of the pseudoexperiments are shown in Table 7.

Table 7: Results of pseudoexperiments when DIL background composition is shifted. Masses are in units of GeV/c^2 and $\Delta_{\rm JES}$ are in units of $\sigma_{\rm c}$.

Shift	DIL $M_{\rm top}$	Comb $M_{\rm top}$	Comb $\Delta_{\rm JES}$
$+\sigma_{D-Y}$	175.59	175.24	-0.03
$-\sigma_{D-Y}$	175.41	175.19	-0.02
$+\sigma_{Diboson}$	175.43	175.22	-0.02
$-\sigma_{Diboson}$	175.54	175.15	-0.01
$+\sigma_{Fakes}$	175.51	175.26	-0.04
$-\sigma_{Fakes}$	175.45	175.17	-0.02

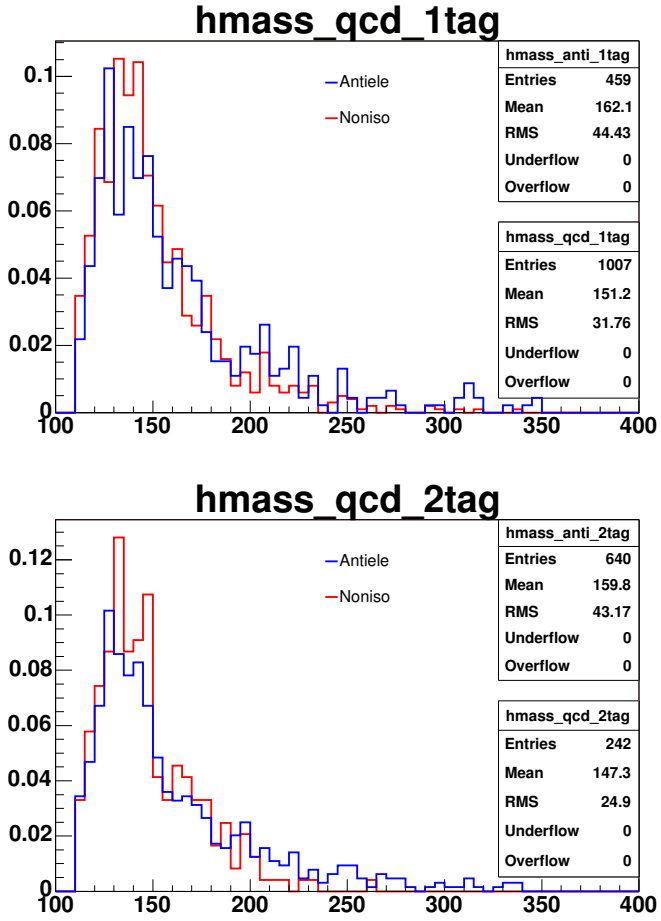

Figure 50: Comparison of M_t^{reco} for the nonisolated lepton sample (with real tags) and antielectrons (with the mistag matrix) for 1-tag (top) and 2-tag (bottom) events

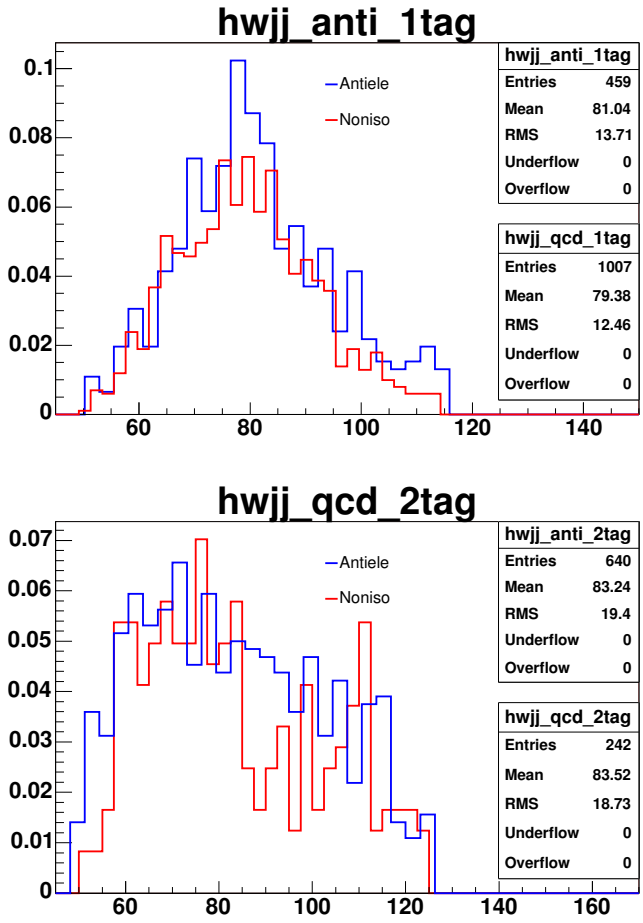

Figure 51: Comparison of W_{jj} for the nonisolated lepton sample (with real tags) and antielectrons (with the mistag matrix) for 1-tag (top) and 2-tag (bottom) events

The 30% uncerainty on the electron and muon fake rates are obtained by measuring the difference in the calculated fake ratio in a given E_T bin between different QCD samples. The origin of the large discrepancy in the fake ratios is not known, however the cause must be related to the energy available in the event and therefore will be correlated to the E_T of the fakable object. We examine the impact of this effect on the dilepton and combined fits by reweighting the dilepton fake template according to:

$$w_{\pm} = w_0 \pm \frac{1}{5}(2i_{E_T} - 7)\sigma_w \tag{20.1}$$

where w_0 is the unshifted event weight, σ_w is the uncertainty on the weight, and i_{E_T} denotes the $E_T$bin. Therefore we will have linear E_T-dependent shifts in the event weights. Results of pseudoexperiments are shown in table 8 Such scaling results in

Table 8: Results of pseudoexperiments when DIL fake template is reweighted

Shift	DIL M_{top}	Comb M_{top}	Comb Δ_{JES}
+ve linear shift	175.67	175.17	-0.03
-ve linear shift	175.42	175.17	-0.03

0.12 GeV/c^2 effect for the Dilepton only fit. In the Combined fit we take the half difference to the maximum shift and obtain 0.04 GeV/c^2 systematic.

Drell-Yan events appear in the dilepton channel signal region due to mismeasurement of $\not\!\!E_T$. Accurately modelling the $\not\!\!E_T$ distribution is very difficult as it relies on correct handling of jet simulation as well as accurate detector model. We examine the effect of inaccurate modelling of $\not\!\!E_T$ on the DIL Drell-Yan shape by reweighting $\not\!\!E_T$ distribution in the template using data-MC comparison. We select events in W+jets data satisfying the same dilepton cuts as regular DIL selection and we require that:

- leptons form electron-positron pair or muon-anti-muon pair.
- Dilepton mass falls within 15 GeV/c^2 from the Z boson mass
- two or more 15 GeV jets are present

Thus we select DY+2jets sample. We compare $\not\!\!E_T$ distribution in data to the one obtained from full DY model. The comparison is shown in Figure 52. We obtain $\not\!\!E_T$ dependent weights from this comparison (table 9). The reweighted template is used in pseudoexperiments yielding mean fitted $M_{top}$of 175.74 GeV/c^2 for the dilepton channel and 175.21 GeV/c^2 for the combined fit. This results in 0.23 GeV/c^2 systematic effect on the DIL fit and 0.03 GeV systematic on the combined fit.

The method of using the W resonance to calibrate the jet energy scale depends on two assumptions. First we assume that different effects contribute to the unknown systematic shift in such a way that jets of different momenta and pseudorapidities are all shifted by common fraction of σ_C. We also assume that shifts are 100% correlated as

Table 9: $\not\!\!E_T$ dependent weights for DY shape shift.

$\not\!\!E_T$ bin	scale factor
25-30	1.11
30-35	0.78
35-40	0.81
40-45	1.10
45-50	0.96
>50	2.09

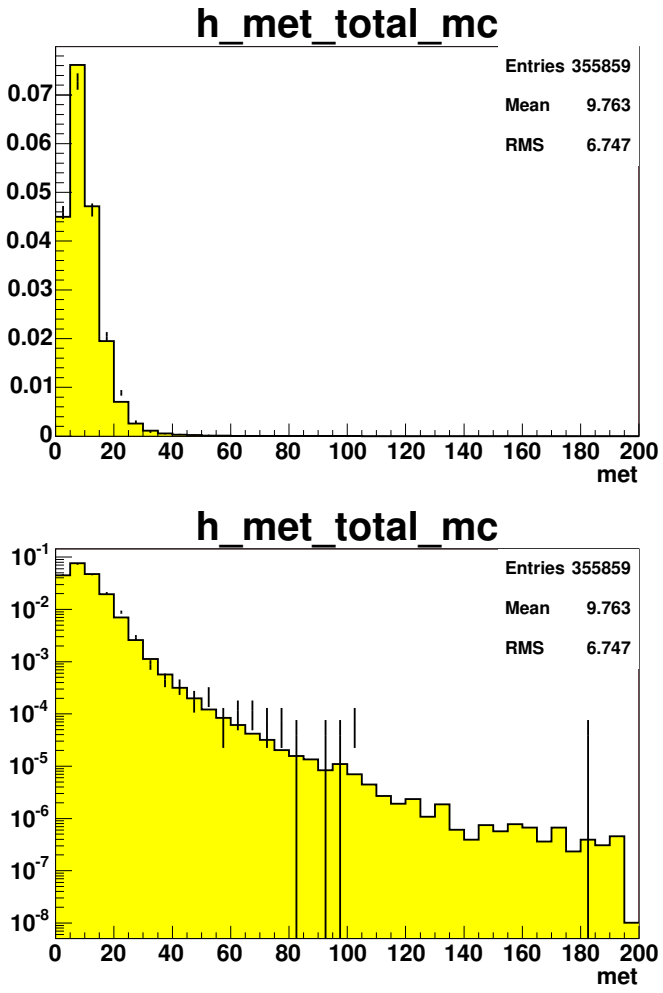

Figure 52: Data - Monte Carlo comparison of the $\not\!\!E_T$ distribution. Linear and log scale. Points are data

a function of the jet p_T. That is we assume that all information about the systematic miscalibration of b quark jets (generaly high in p_T) is contained in the shift of the W daughter jets (at medium and low p_T). We test how the measurement behaves when these assumptions are broken and compute the residual JES uncertainty. We prepare two sets of of pseudodata. In the first set we increase and decrease the size of each jet energy scale effect up and down by 1 σ. This breaks the first assumption as the separate JES contributions will not have the same effect on jet energies as a function of p_T and η as their sum in quadrature.

The effect of systematic shifts being not fully correlated is expected to be the most important for the out-of-cone energy flow. The uncertainty on jet momentum due to this effect is of the order of 10% for low p_T jets, has a falling exponential shape until it becomes constant at p_T of 70 GeV/c. This imples that we can be artificially strongly constraining jets at high momenta using the jets at low momenta even if shifts at high and low momenta are decorrelated by only a small amount. In addition the uncertainty on the out-of-cone energy flow is derived using differences in data and Monte Carlo samples and not by estimating some set of parameters describing modeling of the jets, therefore there is no *a-priori* reason to believe that the out-of-cone jet energy scale shifts are correlated. On the other hand the main effect impacting the out-of-cone energy flow is understood to be modelling of gluon radiation. This implies that the systematic shifts in jet energies due to out-of-cone energy flow are highly correlated between jets of different p_T in high momentum range. At high momenta jets are collimated and therefore the uncertainty is on the radiation at similar angle to the jet axis (or at similar momentum in the direction perpendicular to the jet axis). However in the low momentum region jets of different momenta will occupy different portion of the jet cone therefore in this region the shifts in jet energies are not neceserily correlated. Exact study of these correlations is not possible and we are forced to assume a reasonable form for these correlations. Let us denote by $s_{ooc}(p_T)$ a relative systematic shift for a jet o momentum p_T (at parton level). We assume that the correlation between shifts at different momenta has the following form:

$$\rho(s_{ooc}(p_{T1}), s_{ooc}(p_{T2})) = k(p_{T1})^{(p_{T2}-p_{T1})}. \tag{20.2}$$

In the equation above p_{T1} is taken to be smaller of the two momenta. The coefficient k is a linear function of p_{T1} in the range $0-50$ GeV/c and becomes constant for $p_{T1} >$ 50 GeV/c. We choose k so that $\rho(s_{ooc}(0), s_{ooc}(100)) = 0.5$ and $\rho(s_{ooc}(50), s_{ooc}(150)) =$ 0.8. Since the jet momentum spectrum is continuous we have infinite number of random variables $s_{ooc}(p_T)$. The correlation is nearly 100% for separation of 1 GeV/c and varies little for separation of several GeV/c therefore we will consider a finite set of random variables - the shifts s_i at integer transverse momenta in the range $8-300$ GeV/c. Lowest energy jets used in this analysis have particle level momenta of 8 GeV/c and there will be essentially no jets above 300 GeV/c in p_T. Having this finite set of random variables, their standard deviations given by the size of out-of-cone uncertainty, and correlations given by Equation 20.2 we write a covariance matrix for them. Next we apply so called Princpal Component Analysis procedure. We find 293 eigenvalues λ_j

of the covariance matrix and a set of 293 orthonormal eigenvectors v_j. We order the eigenvalues from largest to smallest and form a new set of random variables given by:

$$q_j = \sum_{i=1}^{293} v_{j,i} * s_i \tag{20.3}$$

The covariance matrix for such defined random variables q is a diagonal matrix consisting of the eigenvalues λ, therefore the variables q are not correlated. This means that we can study the effect of decorrelations of jet shifts at different momenta by constructing pseudodata with variables q shifted up and down by unit of their uncertainty. Variable q_j taking on a value of it's uncertainty $\sqrt{\lambda_j}$ is equivalent to variables s_i taking on values $s_i = \sqrt{\lambda_j} v_{j,i}$. Figure 53 shows relative shift in jet momentum induced by 1 σ variation in the out-of-cone energy flow in black curve. The colored curves show relative shifts induced by 1 σ shifts in successive q_j variables. Sum in quadrature of the shifts induced by first five variables q_j is drawn in a red dashed curve showing that the first five q_j are sufficient to cover the out-of-cone systematic. Values of the shifts for non-integer momenta are obtained by linearly interpolating between the integer momenta. We therefore generate 10 additional pseudodata samples (both signal and

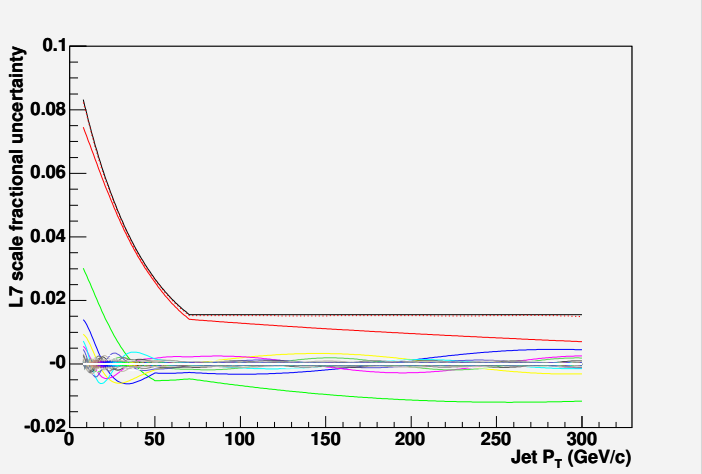

Figure 53: Relative shift on jet momentum induced by 1 σ variation in out-of-cone energy flow (black solid line); Relative shifts induced by 1 σ variations of variables q_j (colored solid lines); Sum in quadrature of the shifts induced by first five variables q_j (red dashed line)

background) where the first five variables q_j have been shifted up and down by unit of their uncertainty. Note that these pseudodata samples as well as the pseudodata samples where separate JES contributions vere varied are constructed at selection level, taking into account possible threshold effects due to events with low energy jets entering and leaving the samples. Pseudoexperiments are run using both sets of pseudodata.

In the Lepton + Jets fit and the combined fit the jet energy prior is turned off. If the prior remained it would force the variation in the fitted top mass to be artificially high.

The residual jet energy scale systematic for the combined and Lepton + Jets only fits is constructed by adding in quadrature half differences of pseudoexperiment results where the absolute, relative, underlying energy and splash out energy scales as well as the q_j variables have been increased and decreased by 1 σ. For the Dilepton-only measurement which has no *in situ* JES calibration we use half difference between pseudoexperiment results where the out-of-cone energy scale has been varied instead of the q_j variables. In all fits the pseudoexperiments generated with increased and decreased pileup energy scale fit slightly lower than nominal therefore the base pileup uncertainty is taken to be half of the largest shift from the nominal. The total residual JES uncertainty in the combined fit is 0.68 GeV/c^2, 0.69 GeV/c^2 in Lepton + Jets only fit and 3.49 GeV/c^2 in the Dilepton only fit.

We study possible effects due to ancient Monte Carlo luminosity profile. Figures 54and 55 show dependence of the fitted top quark mass and fitted $\Delta_{\rm JES}$ as a function of z vertices. We used ttop75 to obtain results for the 1,2, and 3 z vertices bins and otop1r for the >=4 vertices bin. In that bin results are plotted at the average number of vertices on the abscissa. Uncertainties on the points are obtained by scaling the relevant bootstrap results by a a square root of the fraction of events in a given bin. A clear trend is observed in the Dilepton result. Based on the difference in average number of z verices in data and ttop75 Monte Carlo sample we calculate that 0.40 GeV/c^2 needs to be subtracted from the Dilepton only result obtained in data. The top mass result does not need to be corrected for the combined and Lepton + Jets only fit however the quoted value of djes will be shifted low by 0.04 $\sigma_{\rm C}$. We scale the base pileup systematic (level 4) by 2.3*($< N_{zvertex}(data) > -1$)/($< N_{zvertex}(ttop75) > -1$)=2.3*(1.93-1)/(1.50)=4.28. This results in a larger uncertainty than the uncertainty due to the error on the slope of correction line. The resulting pileup systematic is 0.10 GeV/c^2, 0.11 GeV/c^2 and 0.07 GeV/c^2 for the Lepton + Jets, Dilepton and combined fits respectively.

Differences in modelling the b quark jets and light flavour jets are a source uncertainty [20]. Three components of this uncertainty are considered: the b fragmentation, semi-leptonic decay branching fractions and differences in the calorimeter response.

The first component is estimated by taking the differences from the nominal ttkt75 sample results with sample reweighted with Bowler parameters estimated by SLD and ADO. Pseudoexperiments using the ADO reweighted sample have largest shift from nominal for all fits and this difference is taken as a systematic due to b fragmentation: 0.13 GeV/c^2 for the Lepton + Jets only fit, 0.08 GeV/c^2 for the Dilepton only fit and 0.14 GeV/c^2 for the combined fit. We reweight the signal sample so that the branching fractions for b and c quarks are shifted coherently up or down. We take half difference of the result and obtain 0.06 GeV/c^2 uncertainty for Lepton + Jets only fit, 0.17 GeV/c^2 uncertainty for Dilepton only fit and 0.07 GeV/c^2 uncertainty for the combined fit.

The uncertainty due to calorimeter response to a b quark jet is estimated by tak-

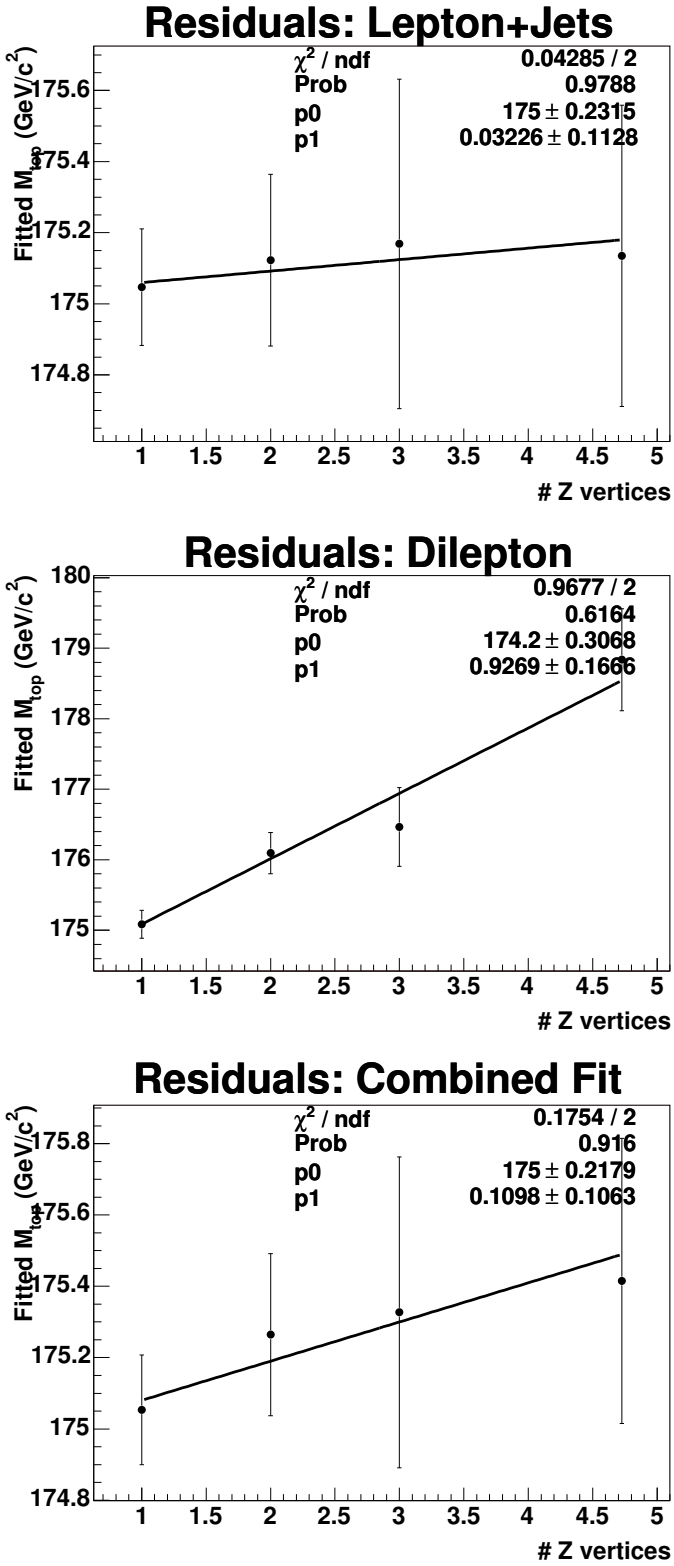

Figure 54: Dependence of the fitted top mass on the number of z vertices. L+J-only PEs (top), DIL-only PEs (middle) and combined PEs (bottom).

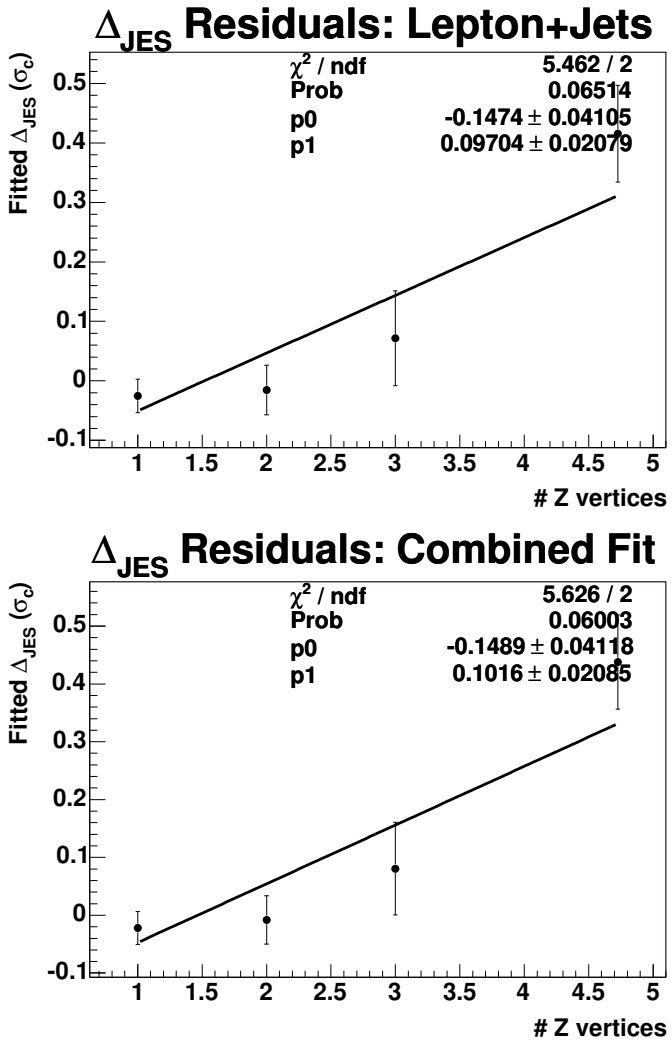

Figure 55: Dependence of the fitted Δ_{JES} mass on the number of z vertices. L+J-only PEs (top), DIL-only PEs (middle) and combined PEs (bottom).

ing 0.2 of the half difference between the pseudoexperiments where the energies of jets matched to b quarks were shifted up and down by 1%. This procedure gives us 0.11 GeV/c^2 systematic for the Lepton + Jets only fit, 0.14 GeV/c^2 for the Dilepton only fit and 0.18 GeV/c^2 for the combined fit. Combining three components we obtain the total b jet energy scale systematic of 0.18 GeV/c^2 for the Lepton + Jets fit, 0.24 GeV/c^2 for the Dilepton fit and 0.19 GeV/c^2 for the combined fit.

We quote the uncertainty on our bias checks as a systematic due to limited statistics of the signal Monte Carlo samples, yielding 0.06 GeV/c^2 for Lepton+Jets and the combined measurement and 0.09 GeV/c^2 for the DIL-only measurement.

We also examine Alpgen pseudodata derived from the exclusive $t\bar{t}$ 0-parton sample in combination with the inclusive $t\bar{t} \geq$ 1-parton sample. The samples are weighted according to the acceptance and cross sections. We keep this as a cross-check, but do not use it to evaluate any additional systematics. As another check on NLO effects, we run pseudoexperiments generated with MC@NLO. One such sample (mtop75) uses MRST02, and another such sample (ctop75) uses CTEQ5M. These samples have events that are given negative weights. When drawing from histograms it is easy to use the negative weights for such events, but when drawing full events from an ntuple, that is not so trivial. To estimate the effect that the events with negative weights might have, we run PEs using those events in pseudodata (as if they had positive weights), and PEs where we simply remove the events (as if they have zero weights). The size of the effect seem sto be roughly 100-200 MeV. We show the results as cross checks, but it is not clear how or if we should use these samples to quote systematics.

21 Data and fit

The number of Lepton+Jets events in data after the χ^2 and boundary cuts is summarized in Table 13. The number of DIL events is summarized in Table 14.

We open the box and measure:

$$\mathrm{M_{top}} = 171.87 \pm 1.68 \text{ GeV}/c^2 \text{ (combined)}$$
$$\Delta_{\mathrm{JES}} = -0.12 \pm 0.34\sigma_{\mathrm{c}}$$

$$\mathrm{M_{top}} = 171.76^{+1.80}_{-1.83} \text{ GeV}/c^2 \text{ (Lepton+Jets-only)}$$
$$\Delta_{\mathrm{JES}} = -0.09 \pm 0.36\sigma_{\mathrm{c}}$$

$$\mathrm{M_{top}} = 171.59^{+3.53}_{-3.34} \text{ GeV}/c^2 \text{ (Dilepton-only)}$$

The likelihood contours for the combined measurement and Lepton+Jets-only measurement are shown in Figures 57 and 58. The likelihood profile for the Dilepton-only fit is shown in Figure 59. A likelihood contour in a wider range for the combined fit

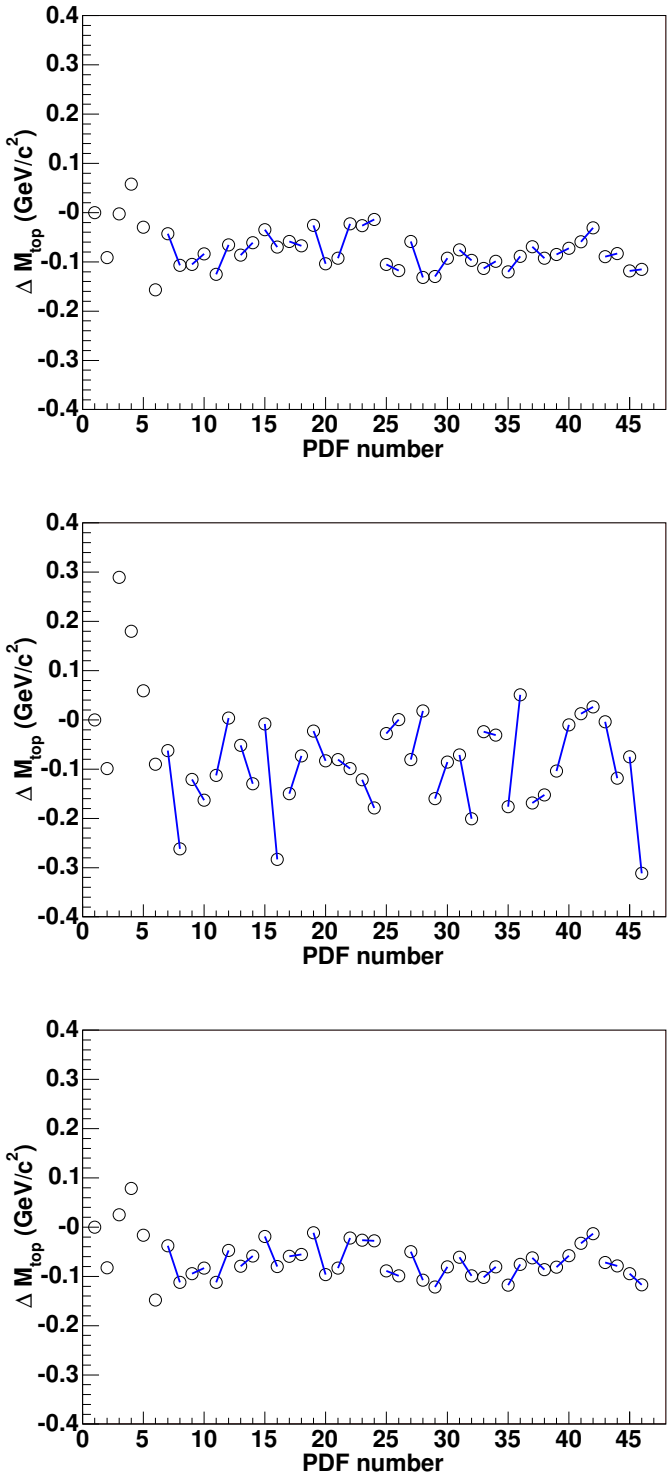

Figure 56: Results from reweighting ttkt75 for PDF systematics for L+J-only PEs (top), DIL-only PEs (middle) and combined PEs (bottom).

Table 10: Samples used to evaluate systematics (part 1). Masses are in units of GeV/c^2 and $\Delta_{\rm JES}$ are in units of $\sigma_{\rm c}$. The background model has not been updated in the asterisked results. The nominal result for Dilepton only fit before update is 175.49 GeV/c^2 and 175.15 GeV/c^2 for the combined fit with $\Delta_{\rm JES}$ of -0.02 $\sigma_{\rm c}$. The fake model used there is as of v1.01 of this note.

Sample	LJ $M_{\rm top}$	LJ $\Delta_{\rm JES}$	DIL $M_{\rm top}$	Comb $M_{\rm top}$	Comb $\Delta_{\rm JES}$
Pythia $M_{\rm top}$= 175.0 (ttkt75)	175.18	-0.04	175.51	175.24	-0.04
Herwig $M_{\rm top}$= 175.0 (otop1s)	174.43	0.32	176.84	174.57	0.33
Pythia $M_{\rm top}$= 170.0 (ttkt70)	170.00	-0.04	170.072	170.06	-0.05
Pythia $M_{\rm top}$= 170.0 (ttkt70) (*)	170.10	-0.07	169.95	170.12	-0.07
Herwig $M_{\rm top}$= 170.0 (htop70) (*)	169.88	0.31	171.72	169.99	0.30
ttkt75 ggfrac weighting	174.99	0.02	175.68	175.08	0.03
ttkt75 Bowler parameters ADO weighting	175.05	-0.01	175.44	175.10	0.00
ttkt75 Bowler parameters SLD weighting	175.08	-0.01	175.55	175.13	0.00
ttkt75 b and c semileptonic fractions -1σ	175.21	-0.02	175.72	175.29	-0.02
ttkt75 b and c semileptonic fractions +1σ	175.10	-0.05	175.37	175.16	-0.04
ttkt75 b jet $E_T \times 0.99$	174.63	-0.04	174.69	174.65	-0.04
ttkt75 b jet $E_T \times 1.01$	175.72	-0.02	176.14	175.77	-0.01
ttkt75 electron $E_T \times 0.99$	175.14	-0.02	175.22	175.15	-0.02
ttkt75 electron $E_T \times 1.01$	175.12	-0.03	175.68	175.20	-0.02
ttkt75 muon $E_T \times 0.99$	175.28	-0.05	175.34	175.30	-0.04
ttkt75 muon $E_T \times 1.01$	175.10	-0.02	175.70	175.18	-0.01
otop03 IFSR up	175.31	0.12	175.91	175.32	0.13
otop04 IFSR down	175.00	0.02	175.90	175.13	0.03
ttkt75 W$b\bar{b}$ for LJ bkgd (*)	175.01	-0.01	–	175.06	-0.01
ttkt75 W$c\bar{c}$ for LJ bkgd (*)	175.02	-0.04	–	175.07	-0.03
ttkt75 Wc for LJ bkgd (*)	175.23	-0.03	–	175.26	-0.02
ttkt75 W+light for LJ bkgd (*)	175.26	0.00	–	175.26	0.01
ttkt75 single top for LJ bkgd (*)	175.21	0.04	–	175.21	0.04
ttkt75 QCD for LJ bkgd (*)	175.07	-0.09	–	175.15	-0.09
ttkt75 diboson for LJ bkgd (*)	175.24	-0.02	–	175.25	-0.01
ttkt75 W$b\bar{b}$ Qfact=2.0 for LJ bkgd (*)	174.95	0.00	–	175.00	0.00
ttkt75 W$b\bar{b}$ Qfact=0.5 for LJ bkgd (*)	175.04	-0.01	–	175.10	-0.01
ttkt75 anti-ele for LJ QCD (*)	175.16	-0.01	–	175.20	-0.01
ttkt75 CTEQ5L (*)	175.27	0.01	173.72	175.11	0.00
ttkt75 MRST72 (*)	175.18	0.01	173.62	175.03	0.00
ttkt75 MRST75 (*)	175.26	0.02	174.01	175.14	0.02
Alpgen $t\bar{t}$ 0p + $t\bar{t} \geq$ 1P (*)	175.46	0.27	176.49	175.46	0.27
MC@NLO-MRST02 remove neg wts (*)	173.36	0.30	175.17	173.44	0.30
MC@NLO-MRST02 use all (*)	173.32	0.30	174.97	173.40	0.30
MC@NLO-CTEQ5M remove neg wts (*)	173.96	0.17	174.64	173.97	0.17
MC@NLO-CTEQ5M us all (*)	173.77	0.18	173.73	173.71	0.17

Table 11: Samples used to evaluate systematics (part 2). Masses are in units of GeV/c^2 and $\Delta_{\rm JES}$ are in units of $\sigma_{\rm c}$.

Sample	LJ $M_{\rm top}$	LJ $\Delta_{\rm JES}$	DIL $M_{\rm top}$	Comb $M_{\rm top}$	Comb $\Delta_{\rm JES}$
Pythia $M_{\rm top}$= 175.0 (ttkt75)	175.18	-0.04	175.51	175.24	-0.04
ttkt75 Residual JES +L1	175.18	0.16	176.05	175.21	0.17
ttkt75 Residual JES -L1	175.16	-0.21	174.77	175.21	-0.21
ttkt75 Residual JES +L5	175.54	0.51	177.77	175.56	0.53
ttkt75 Residual JES -L5	174.61	-0.52	173.26	174.68	-0.52
ttkt75 Residual JES +L7	174.83	0.76	178.03	174.88	0.77
ttkt75 Residual JES -L7	175.38	-0.78	172.95	175.41	-0.78
ttkt75 Residual JES +L4	175.13	-0.01	175.48	175.16	0.00
ttkt75 Residual JES -L4	175.14	-0.05	175.46	175.21	-0.04
ttkt75 Residual JES +L6	175.13	0.05	175.79	175.18	0.06
ttkt75 Residual JES -L6	175.24	-0.13	175.1	175.28	-0.12
ttkt75 Residual JES +L8	175.07	0.11	175.84	175.09	0.12
ttkt75 Residual JES -L8	175.22	-0.16	175.16	175.29	-0.16
ttkt75 $+q_1$	174.76	0.7	177.73	174.80	0.72
ttkt75 $-q_1$	175.54	-0.75	173.33	175.60	-0.75
ttkt75 $+q_2$	174.89	-0.09	174.89	174.93	-0.09
ttkt75 $-q_2$	175.43	0.05	176.00	175.48	0.06
ttkt75 $+q_3$	175.17	-0.14	175.08	175.22	-0.14
ttkt75 $-q_3$	175.21	0.06	175.73	175.24	0.07
ttkt75 $+q_4$	175.36	-0.12	175.35	175.38	-0.11
ttkt75 $-q_4$	175.05	0.02	175.57	175.10	0.03
ttkt75 $+q_5$	175.23	-0.01	175.64	175.29	0.00
ttkt75 $-q_5$	175.08	-0.05	175.35	175.14	-0.05

Table 12: Summary of systematics. All numbers have units of GeV/c^2.

Systematic	LJ	DIL	Combination
Residual JES	0.70	3.49	0.68
Generator:	0.75	1.33	0.67
PDFs	0.25	0.54	0.25
b jet energy	0.18	0.24	0.19
Background shape	0.19	0.28	0.17
gg fraction	0.19	0.17	0.16
Radiation	0.15	0.20	0.13
MC statistics	0.08	0.48	0.10
Lepton energy	0.09	0.29	0.07
Pileup	0.10	0.11	0.07
Total systematic	1.12	3.84	1.05

Table 13: Observed number of Lepton+Jets candidate events in data before χ^2 cut, after χ^2 cut, and after both χ^2 cut and boundary cut.

	1-tag	2-tag
Pre-χ^2, pre-boundary cuts	284	152
Post-χ^2, pre-boundary cuts	237	101
Post-χ^2, post-boundary cuts	233	99

Table 14: Observed number of Dilepton candidate events in data before and after the boundary cuts.

	0-tag	Tagged
Pre-boundary cuts	83	61
Post-boundary cuts	83	61

is shown in Figure 60, and separately for the LJ 1-tag and 2-tag fits (with JES and background constraints removed) in Figure 61.

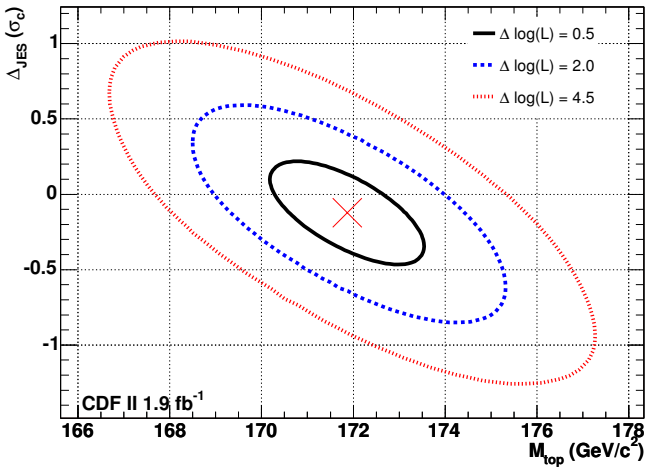

Figure 57: Likelihood contours for the combined fit.

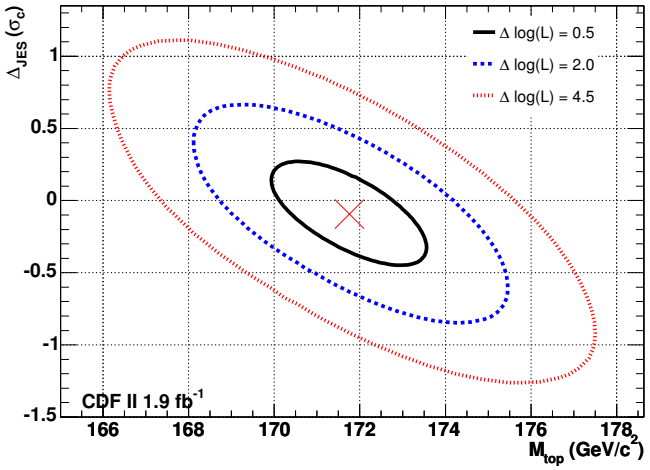

Figure 58: Likelihood contours for the Lepton+Jets-only fit.

22 Cross checks

We run a variety of cross-checks on our measurement. Results are shown in Tables 15, 16, 17, 19 and 18. All errors are uncorrected for pull widths. As in our previous

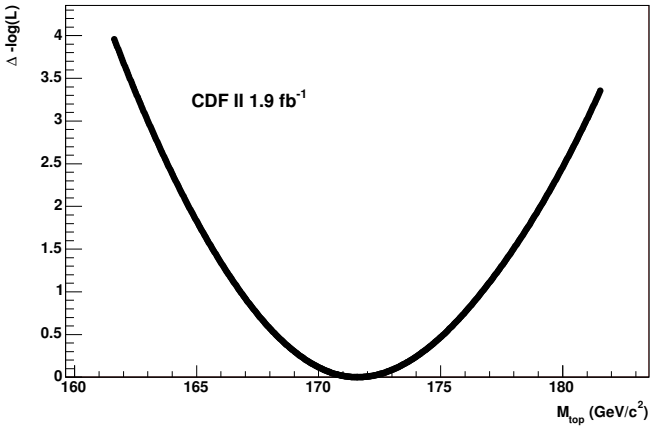

Figure 59: Likelihood profile for the Dilepton-only fit

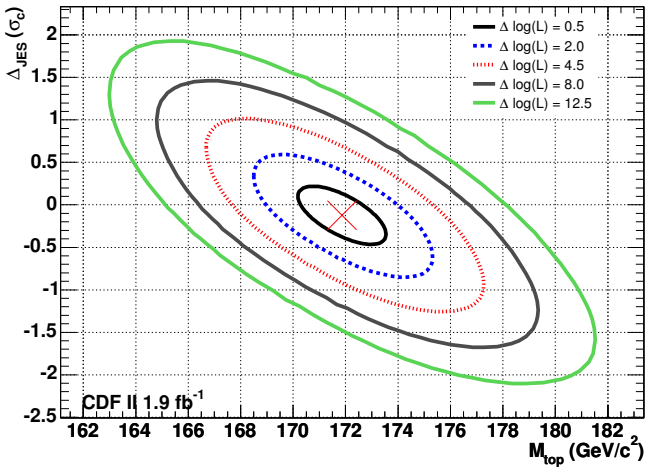

Figure 60: Likelihood contours for the combined fit out to the equivalent Δ log L of 5 σ

.

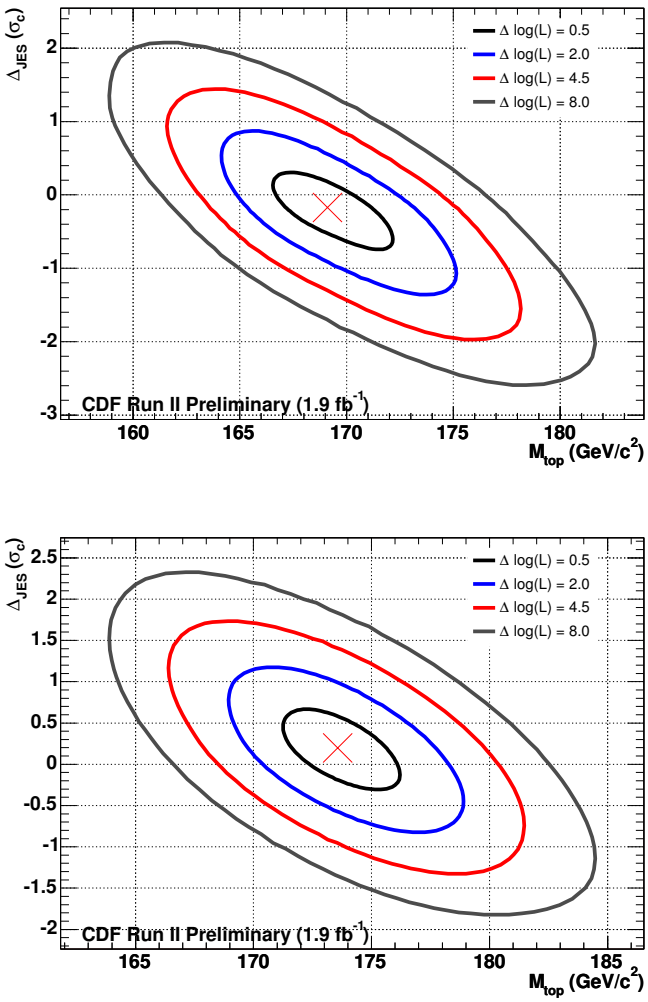

Figure 61: Likelihood contours for the Lepton+Jets 1-tag-only fit (top) and 2-tag-only fit (bottom). No JES constraint or background constraints were used.

LJ measurement, removing the JES prior does not significantly affect our results (the prior does not play a role in the DIL-only measurement). Removing the background constraint also does not change the central value significantly, though as in the previous analysis, the 1-tag LJ measurement prefers more background than expected and the 2-tag LJ measurement prefers no background. The DIL measurements prefers slightly less background than expected from the prior in the non-tagged sample and slightly more in the tagged sample. Note that the 0.0 error indicates that data shape does not have enough power to constrain the background component within the physical region.

We examine the luck (ie p-value) of our data fits by comparing the measured symmetrized errors with those expected from pseudoexperiments. Results are shown in Figure 62. We use PEs with M_{top}= 172 GeV/c^2 and Δ_{JES} = 0.0 σ_c.

Figure 63, 64 and 65 shows distributions out of the kinematic L+J fitter, comparing data to the sum of the fitted number of signal and background expectations using the full background model. There is a wide range of agreement (or disagreement) from the very good to the very bad, with the p_T of the $t\bar{t}$ system and the p_T of the b jets having very poor KS test probablities. The signal model used in these plots is Pythia MC at M_{top}=172 GeV/c^2. The mass dependence is weak, as seen in the comparisons to Figures 66, 67, 68 (Pythia at M_{top}=175 GeV/c^2), and Figures 69, 70 71 (Pythia at M_{top}=170 GeV/c^2). Comparisons to Herwig with M_{top}=170 GeV/c^2 are shown in Figures 72, 73 74. Copmarisons to Algpen ($t\bar{t}$+0partons + inclusive 1 or more partons) are shown in Figures 75, 76 77. Finally, comparisons to MC@NLO are shown in Figures 78, 79 80. The agreement in the $t\bar{t}$ system p_T is better in Herwig than in Pythia, though it is not great for any of the comparisons. The b-jet p_T distrbution also seems poorly modeled.

Table 15: Cross-checks on the data

Fit type	Comb	$M_{top}(GeV/c^2)$ LJ 1tag n_s	$M_{top}(GeV/c^2)$ LJ 2tag n_s	Δ_{JES} (σ_c) LJ 1tag n_b	Δ_{JES} (σ_c) LJ 2tag n_b
		DIL 0tag n_s	DIL tagged n_s	DIL 0tag n_b	DIL tagged n_b
	LJ-only	$M_{top}(GeV/c^2)$ 1tag n_s	$M_{top}(GeV/c^2)$ 2tag n_s	Δ_{JES} (σ_c) 1tag n_b	Δ_{JES} (σ_c) 2tag n_b
	DIL-only	$M_{top}(GeV/c^2)$ 0tag n_s	tagged n_s	0tag n_b	tagged n_b
Nominal	Combo	171.9 ± 1.7		-0.12 ± 0.34	
		$184.1\ ^{+17.7}_{-17.1}$	$96.4\ ^{+10.4}_{-9.7}$	$47.4\ ^{+10.2}_{-10.0}$	3.4 ± 1.9
		$43.8\ ^{+10.4}_{-9.8}$	$56.9\ ^{+8.2}_{-7.5}$	$41.5\ ^{+6.5}_{-6.4}$	3.9 ± 1.0
	LJ	171.8 ± 1.8		-0.09 ± 0.36	
		$184.0\ ^{+17.8}_{-17.1}$	$96.4\ ^{+10.4}_{-9.7}$	$47.5\ ^{+10.2}_{-10.1}$	3.4 ± 1.9
		-	-	-	-
	DIL	$171.6\ ^{+3.5}_{-3.3}$		-	
		-	-	-	-
		$43.7\ ^{+10.4}_{-9.8}$	$56.9\ ^{+8.2}_{-7.5}$	$41.6\ ^{+6.5}_{-6.4}$	3.9 ± 1.0
No JES prior	Combo	171.9 ± 1.7		$-0.14\ ^{+0.36}_{-0.37}$	
		$184.1\ ^{+17.7}_{-17.1}$	$96.4\ ^{+10.4}_{-9.7}$	$47.4\ ^{+10.2}_{-10.0}$	3.4 ± 1.9
		$43.8\ ^{+10.4}_{-9.8}$	$56.9\ ^{+8.2}_{-7.5}$	$41.5\ ^{+6.5}_{-6.4}$	3.9 ± 1.0
	LJ	171.8 ± 1.9		$-0.11\ ^{+0.39}_{-0.38}$	
		$184.1\ ^{+17.8}_{-17.1}$	$96.4\ ^{+10.4}_{-9.7}$	$47.5\ ^{+10.2}_{-10.1}$	3.4 ± 1.9
		-	-	-	-
No bkgd prior	Combo	171.9 ± 1.7		$-0.11\ ^{+0.35}_{-0.34}$	
		$176.1\ ^{+21.5}_{-20.7}$	$99.0\ ^{+10.3}_{-9.6}$	$57.0\ ^{+18.6}_{-17.5}$	$0.0\ ^{+2.2}_{--0.0}$
		$54.8\ ^{+15.8}_{-15.2}$	54.3 ± 12.2	$28.2\ ^{+15.2}_{-14.0}$	$6.7\ ^{+11.1}_{--0.0}$
	LJ	171.8 ± 1.8		-0.06 ± 0.36	
		$175.7\ ^{+21.6}_{-20.7}$	$99.0\ ^{+10.3}_{-9.6}$	$57.3\ ^{+18.6}_{-17.6}$	$0.0\ ^{+2.2}_{--0.0}$
		-	-	-	-
	DIL	171.5 ± 3.4		-	
		-	-	-	-
		$54.6\ ^{+15.8}_{-15.2}$	54.2 ± 12.3	$28.4\ ^{+15.3}_{-14.0}$	$6.8\ ^{+11.2}_{--0.0}$
1-tag LJ	LJ	$169.1\ ^{+3.1}_{-2.6}$		$-0.17\ ^{+0.48}_{-0.57}$	
		$187.6\ ^{+17.9}_{-17.2}$	-	44.8 ± 10.3	-
		-	-	-	-
2-tag LJ	LJ	$173.6\ ^{+2.6}_{-2.3}$		$0.20\ ^{+0.47}_{-0.50}$	
		-	$96.3\ ^{+10.4}_{-9.7}$	-	3.5 ± 1.9
		-	-	-	-
0-tag DIL	DIL	$170.1\ ^{+6.4}_{-7.6}$		-	
		-	-	-	-
		$43.7\ ^{+10.5}_{-9.8}$	-	$41.6\ ^{+6.5}_{-6.4}$	-
Tagged DIL	DIL	$172.2\ ^{+4.4}_{-4.0}$		-	
		-	-	-	-
		-	$57.0\ ^{+8.2}_{-7.5}$	-	3.9 ± 1.0

Table 16: More cross-checks on the data

Fit type		M_{top}(GeV/c^2)		Δ_{JES} (σ_c)	
	Comb	LJ 1tag n_s	LJ 2tag n_s	LJ 1tag n_b	LJ 2tag n_b
		DIL 0tag n_s	DIL tagged n_s	DIL 0tag n_b	DIL tagged n_b
	LJ-only	M_{top}(GeV/c^2)		Δ_{JES} (σ_c)	
		1tag n_s	2tag n_s	1tag n_b	2tag n_b
	DIL-only	M_{top}(GeV/c^2)			
		0tag n_s	tagged n_s	0tag n_b	tagged n_b
First 1 fb^{-1}	Combo	$171.7\ ^{+2.3}_{-2.4}$		$0.45\ ^{+0.55}_{-0.50}$	
		$90.8\ ^{+15.6}_{-14.8}$	$48.0\ ^{+7.3}_{-6.6}$	$41.2\ ^{+13.9}_{-13.0}$	$0.0\ ^{+1.7}_{--0.0}$
		$32.8\ ^{+11.4}_{-10.9}$	$17.6\ ^{+8.1}_{-7.8}$	$9.2\ ^{+10.8}_{--0.0}$	$8.4\ ^{+8.1}_{-6.4}$
	LJ	$172.2\ ^{+2.5}_{-2.4}$		$0.59\ ^{+0.52}_{-0.55}$	
		$89.7\ ^{+15.5}_{-14.7}$	$48.0\ ^{+7.3}_{-6.6}$	$42.3\ ^{+13.9}_{-13.0}$	$0.0\ ^{+1.7}_{--0.0}$
		-	-	-	-
	DIL	166.1 ± 5.0		-	
		-	-	-	-
		$34.5\ ^{+10.6}_{-10.2}$	$16.9\ ^{+7.8}_{-7.7}$	$7.5\ ^{+9.8}_{--0.0}$	$9.1\ ^{+8.1}_{-6.3}$
Last 0.9 fb^{-1}	Combo	171.7 ± 2.7		$-0.70\ ^{+0.53}_{-0.59}$	
		$89.1\ ^{+14.9}_{-14.2}$	$51.0\ ^{+7.5}_{-6.8}$	$11.9\ ^{+12.2}_{-11.1}$	$0.0\ ^{+2.7}_{--0.0}$
		$20.3\ ^{+11.2}_{-10.4}$	$35.0\ ^{+6.3}_{-6.9}$	$20.7\ ^{+11.4}_{-10.3}$	$0.0\ ^{+5.5}_{--0.0}$
	LJ	$170.2\ ^{+3.1}_{-3.0}$		$-0.61\ ^{+0.54}_{-0.64}$	
		$90.5\ ^{+15.1}_{-14.3}$	$51.0\ ^{+7.5}_{-6.8}$	$10.5\ ^{+12.2}_{--0.0}$	$0.0\ ^{+2.6}_{--0.0}$
		-	-	-	-
	DIL	$175.2\ ^{+5.3}_{-4.7}$		-	
		-	-	-	-
		$22.1\ ^{+11.1}_{-10.5}$	$35.0\ ^{+6.3}_{-6.4}$	$18.9\ ^{+11.3}_{-10.0}$	$0.0\ ^{+4.9}_{--0.0}$
0d data	Combo	$174.0\ ^{+3.4}_{-3.3}$		$-0.24\ ^{+0.65}_{-0.80}$	
		$30.8\ ^{+9.5}_{-8.6}$	$14.0\ ^{+4.1}_{-3.4}$	$15.2\ ^{+8.6}_{-7.7}$	$0.0\ ^{+1.2}_{--0.0}$
		$11.2\ ^{+7.4}_{-7.6}$	$10.6\ ^{+5.4}_{-5.1}$	$3.8\ ^{+8.1}_{--0.0}$	$3.4\ ^{+5.3}_{--0.0}$
	LJ	$174.6\ ^{+3.7}_{-3.5}$		$-0.18\ ^{+0.68}_{-0.82}$	
		$30.6\ ^{+9.4}_{-8.6}$	$14.0\ ^{+4.1}_{-3.4}$	$15.4\ ^{+8.6}_{-7.6}$	$0.0\ ^{+1.3}_{--0.0}$
		-	-	-	-
	DIL	$168.4\ ^{+7.5}_{-7.8}$		-	
		-	-	-	-
		$11.9\ ^{+6.9}_{-7.5}$	$10.6\ ^{+5.3}_{-5.2}$	$3.1\ ^{+7.9}_{--0.0}$	$3.4\ ^{+5.4}_{--0.0}$
0h data	Combo	$172.0\ ^{+3.9}_{-3.6}$		$0.26\ ^{+0.68}_{-0.64}$	
		$29.7\ ^{+9.7}_{-8.8}$	$21.0\ ^{+4.9}_{-4.3}$	$21.3\ ^{+9.2}_{-8.4}$	$0.0\ ^{+1.8}_{--0.0}$
		$12.3\ ^{+6.6}_{-6.0}$	$5.7\ ^{+6.0}_{--0.0}$	$4.7\ ^{+6.4}_{--0.0}$	$4.3\ ^{+6.6}_{--0.0}$
	LJ	$173.0\ ^{+4.2}_{-3.6}$		$0.30\ ^{+0.70}_{-0.68}$	
		$29.0\ ^{+9.7}_{-8.8}$	$21.0\ ^{+4.9}_{-4.3}$	$22.0\ ^{+9.3}_{-8.4}$	$0.0\ ^{+1.8}_{--0.0}$
		-	-	-	-
	DIL	164.5 ± 7.7		-	
		-	-	-	-
		$11.8\ ^{+6.1}_{-5.5}$	$6.0\ ^{+5.2}_{-5.0}$	$5.2\ ^{+5.8}_{-4.6}$	$4.0\ ^{+5.7}_{--0.0}$

Table 17: Even more cross-checks on the data

Fit type		M_{top}(GeV/c^2)		Δ_{JES} (σ_c)	
	Comb	LJ 1tag n_s	LJ 2tag n_s	LJ 1tag n_b	LJ 2tag n_b
		DIL 0tag n_s	DIL tagged n_s	DIL 0tag n_b	DIL tagged n_b
	LJ-only	M_{top}(GeV/c^2)		Δ_{JES} (σ_c)	
		1tag n_s	2tag n_s	1tag n_b	2tag n_b
	DIL-only	M_{top}(GeV/c^2)			
		0tag n_s	tagged n_s	0tag n_b	tagged n_b
0i1 data	Combo	$169.8\ ^{+4.3}_{-3.6}$		$0.99\ ^{+0.68}_{-0.73}$	
		$30.7\ ^{+8.4}_{-7.6}$	$13.0\ ^{+3.9}_{-3.3}$	$4.3\ ^{+6.7}_{--0.0}$	$0.0\ ^{+0.0}_{--0.0}$
		$9.9\ ^{+3.6}_{-5.6}$	$1.0\ ^{+2.4}_{--0.0}$	$0.1\ ^{+0.0}_{--0.0}$	$1.0\ ^{+2.4}_{--0.0}$
	LJ	$171.1\ ^{+4.4}_{-4.2}$		$1.05\ ^{+0.69}_{-0.72}$	
		$30.3\ ^{+8.4}_{-7.6}$	$13.0\ ^{+3.9}_{-3.3}$	$4.7\ ^{+6.7}_{--0.0}$	$0.0\ ^{+1.5}_{--0.0}$
		-	-	-	-
	DIL	$FAIL\ ^{+-}_{--}$		-	
		-	-	-	-
		$0.0\ ^{+0.5}_{--0.0}$	$0.0\ ^{+0.5}_{--0.0}$	$10.0\ ^{+3.5}_{-2.8}$	$2.0\ ^{+1.8}_{-1.1}$
0i2 data	Combo	171.0 ± 3.3		$-0.64\ ^{+0.56}_{-0.65}$	
		$55.3\ ^{+11.7}_{-10.8}$	29.0 ± 5.7	$6.7\ ^{+9.3}_{--0.0}$	$0.0\ ^{+4.1}_{--0.0}$
		$3.9\ ^{+7.1}_{--0.0}$	$17.4\ ^{+5.2}_{-6.6}$	$16.1\ ^{+7.7}_{-7.0}$	$0.6\ ^{+6.3}_{--0.0}$
	LJ	171.1 ± 3.4		$-0.60\ ^{+0.55}_{-0.65}$	
		$55.0\ ^{+11.7}_{-10.8}$	$29.0\ ^{+5.7}_{-5.8}$	$7.0\ ^{+9.3}_{--0.0}$	$0.0\ ^{+4.2}_{--0.0}$
		-	-	-	-
	DIL	$166.2\ ^{+9.2}_{-9.7}$		-	
		-	-	-	-
		$3.0\ ^{+7.8}_{--0.0}$	$17.3\ ^{+5.2}_{-6.5}$	$17.0\ ^{+7.3}_{-7.7}$	$0.7\ ^{+6.1}_{--0.0}$
0j1 data	Combo	$165.9\ ^{+4.7}_{-4.8}$		$-0.32\ ^{+0.75}_{-0.78}$	
		$25.0\ ^{+5.3}_{-4.8}$	$14.0\ ^{+4.1}_{-3.4}$	$0.0\ ^{+2.9}_{--0.0}$	$0.0\ ^{+1.5}_{--0.0}$
		$5.8\ ^{+7.4}_{--0.0}$	$5.8\ ^{+5.1}_{-5.5}$	$5.2\ ^{+7.1}_{--0.0}$	$2.2\ ^{+6.1}_{--0.0}$
	LJ	$164.9\ ^{+4.6}_{-4.4}$		$-0.23\ ^{+0.74}_{-0.77}$	
		$25.0\ ^{+5.3}_{-4.8}$	$14.0\ ^{+4.1}_{-3.4}$	$0.0\ ^{+2.9}_{--0.0}$	$0.0\ ^{+1.5}_{--0.0}$
		-	-	-	-
	DIL	$172.0\ ^{+24.2}_{-14.0}$		-	
		-	-	-	-
		$5.7\ ^{+7.5}_{--0.0}$	$8.0\ ^{+3.2}_{-6.7}$	$5.3\ ^{+6.9}_{--0.0}$	$0.0\ ^{+0.0}_{--0.0}$

Table 18: Even more cross-checks on the data, one more time

Fit type		M_{top}(GeV/c^2)		Δ_{JES} (σc)	
	Comb	LJ 1tag n_s	LJ 2tag n_s	LJ 1tag n_b	LJ 2tag n_b
		DIL 0tag n_s	DIL tagged n_s	DIL 0tag n_b	DIL tagged n_b
	LJ-only	M_{top}(GeV/c^2)		Δ_{JES} (σc)	
		1tag n_s	2tag n_s	1tag n_b	2tag n_b
	DIL-only	M_{top}(GeV/c^2)			
		0tag n_s	tagged n_s	0tag n_b	tagged n_b
0j2 data	Combo	$178.6\ ^{+7.5}_{-6.3}$		$-0.14\ ^{+0.96}_{-1.12}$	
		$4.2\ ^{+5.6}_{--0.0}$	$8.0\ ^{+3.2}_{-2.5}$	$9.8\ ^{+6.2}_{-5.2}$	$0.0\ ^{+1.5}_{--0.0}$
		$10.0\ ^{+3.5}_{-3.6}$	$9.0\ ^{+3.3}_{-2.7}$	$0.0\ ^{+3.2}_{--0.0}$	$0.0\ ^{+1.4}_{--0.0}$
	LJ	$173.6\ ^{+10.3}_{-7.8}$		$-0.01\ ^{+1.06}_{-1.01}$	
		$5.0\ ^{+5.7}_{-4.9}$	$8.0\ ^{+3.2}_{-2.5}$	$9.0\ ^{+6.2}_{-5.1}$	$0.0\ ^{+1.5}_{--0.0}$
		-	-	-	-
	DIL	$180.7\ ^{+7.0}_{-6.4}$		-	
		-	-	-	-
		$10.0\ ^{+3.5}_{-3.7}$	$9.0\ ^{+3.3}_{-2.7}$	$0.0\ ^{+3.3}_{--0.0}$	$0.0\ ^{+1.4}_{--0.0}$
data thru p11	Combo	171.5 ± 1.7		-0.10 ± 0.34	
		$170.8\ ^{+21.0}_{-20.2}$	$91.0\ ^{+9.9}_{-9.2}$	$48.2\ ^{+17.8}_{-16.8}$	$0.0\ ^{+2.3}_{--0.0}$
		$43.6\ ^{+14.8}_{-14.1}$	41.1 ± 11.7	$29.4\ ^{+14.5}_{-13.3}$	$10.9\ ^{+11.3}_{-9.3}$
	LJ	171.6 ± 1.8		$-0.05\ ^{+0.35}_{-0.36}$	
		$169.8\ ^{+21.0}_{-20.1}$	$91.0\ ^{+9.9}_{-9.2}$	$49.2\ ^{+17.9}_{-16.9}$	$0.0\ ^{+2.3}_{--0.0}$
		-	-	-	-
	DIL	$168.7\ ^{+4.0}_{-4.4}$		-	
		-	-	-	-
		$43.5\ ^{+14.7}_{-13.9}$	$40.8\ ^{+11.6}_{-11.4}$	$29.5\ ^{+14.4}_{-13.2}$	$11.2\ ^{+11.1}_{-9.1}$

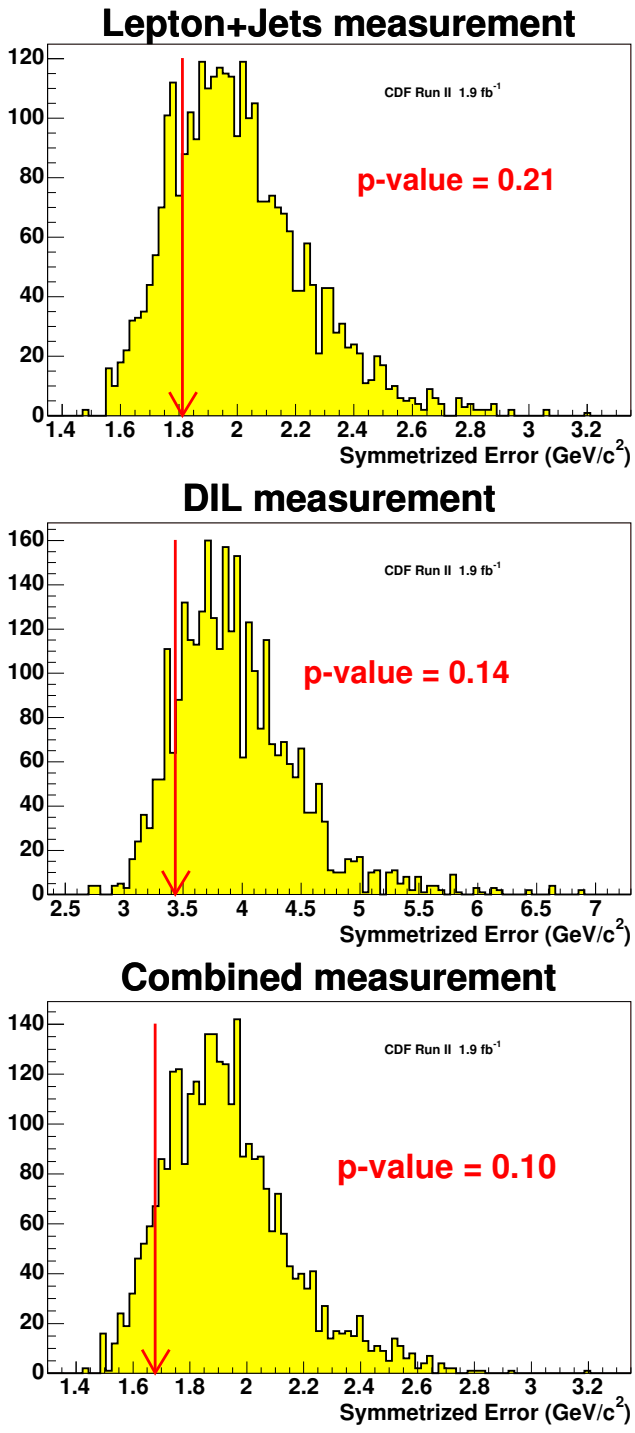

Figure 62: Expected errors and probability to get values equal to or smaller than the measured errors for L+J-only PEs (top), DIL-only PEs (middle) and combined PEs (bottom).

Table 19: Yet Even more cross-checks on the Lepton+Jets data

Fit Type	LJ-only	M_{top}(GeV/c^2) 1tag n_s	M_{top}(GeV/c^2) 2tag n_s	Δ_{JES} (σc) 1tag n_b	Δ_{JES} (σc) 2tag n_b
ele only, no bgcorr	LJ-only	$172.22\ ^{+2.66}_{-2.75}$ 95.1	54.0	$-0.09\ ^{+0.51}_{-0.51}$ 35.9	0.0
μ only, no bgcorr	LJ-only	$171.32\ ^{+2.38}_{-2.26}$ 81.0	45.0	$-0.04\ ^{+0.46}_{-0.47}$ 21.0	0.0
(-) lepton, no bgcorr	LJ-only	$169.68\ ^{+2.51}_{-3.31}$ 106.4	51.0	$0.19\ ^{+0.72}_{-0.45}$ 25.6	0.0
(-) lepton, no bgcorr, no jcorr	LJ-only	$168.05\ ^{+4.01}_{-2.29}$ 106.5	51.0	$0.59\ ^{+0.52}_{-0.85}$ 25.5	0.0
(+) lepton, no bgcorr	LJ-only	$174.95\ ^{+3.25}_{-3.07}$ 106.4	51.0	$-0.48\ ^{+0.62}_{-0.62}$ 25.6	0.0
(+) lepton, no bgcorr, no jcorr	LJ-only	$176.95\ ^{+3.79}_{-3.57}$ 70.2	48.0	$-0.77\ ^{+0.79}_{-0.82}$ 30.8	0.0
(-) lepton, no bgcorr 1-tag only	LJ-only	$169.76\ ^{+4.24}_{-3.38}$ 108.9		$0.19\ ^{+0.79}_{-0.70}$ 23.1	
(-) lepton, no bgcorr 2-tag only	LJ-only	$171.07\ ^{+3.16}_{-3.24}$	51.0	$0.32\ ^{+0.61}_{-0.55}$	0.0
(+) lepton, no bgcorr 1-tag only	LJ-only	$170.09\ ^{+4.66}_{-4.24}$ 75.1		$-0.46\ ^{+0.72}_{-0.82}$ 25.9	
(+) lepton, no bgcorr 2-tag only	LJ-only	$177.42\ ^{+3.99}_{-4.39}$	48.0	$-0.26\ ^{+0.83}_{-0.71}$	0.0

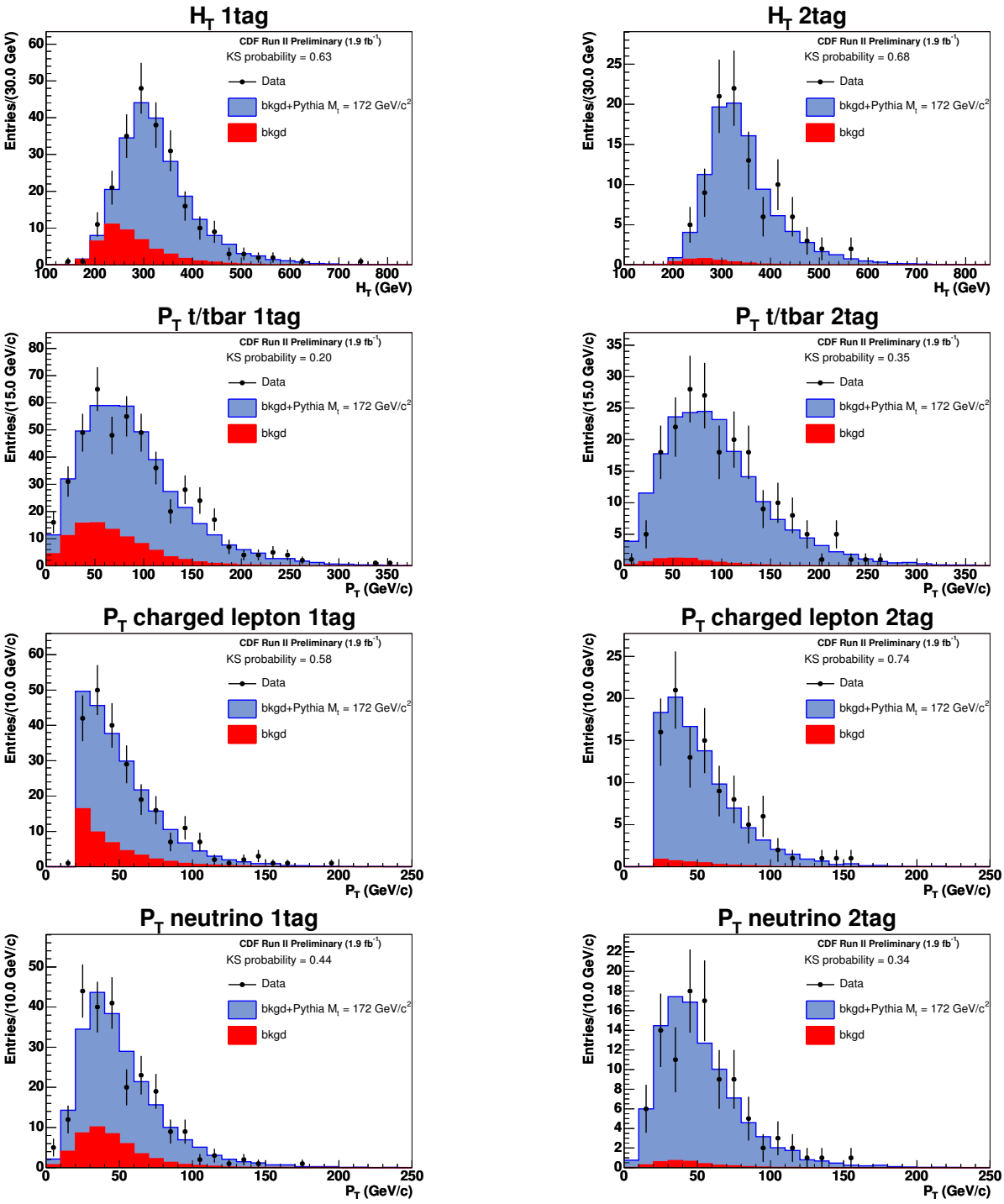

Figure 63: Distributions for L+J fitter output (1), Pythia M_{top}=172 GeV/c^2

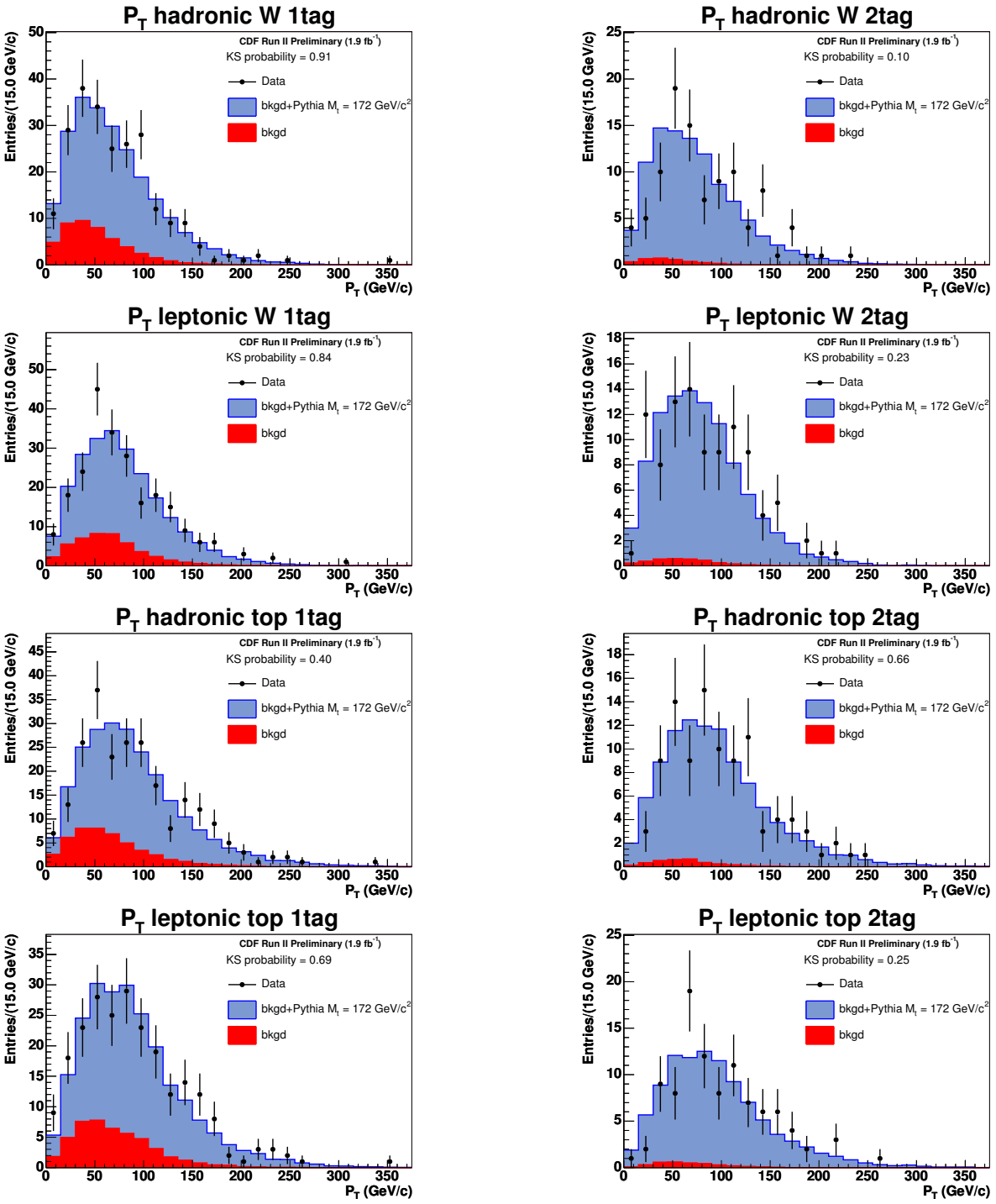

Figure 64: Distributions for L+J fitter output (2), Pythia M_{top}=172 GeV/c^2

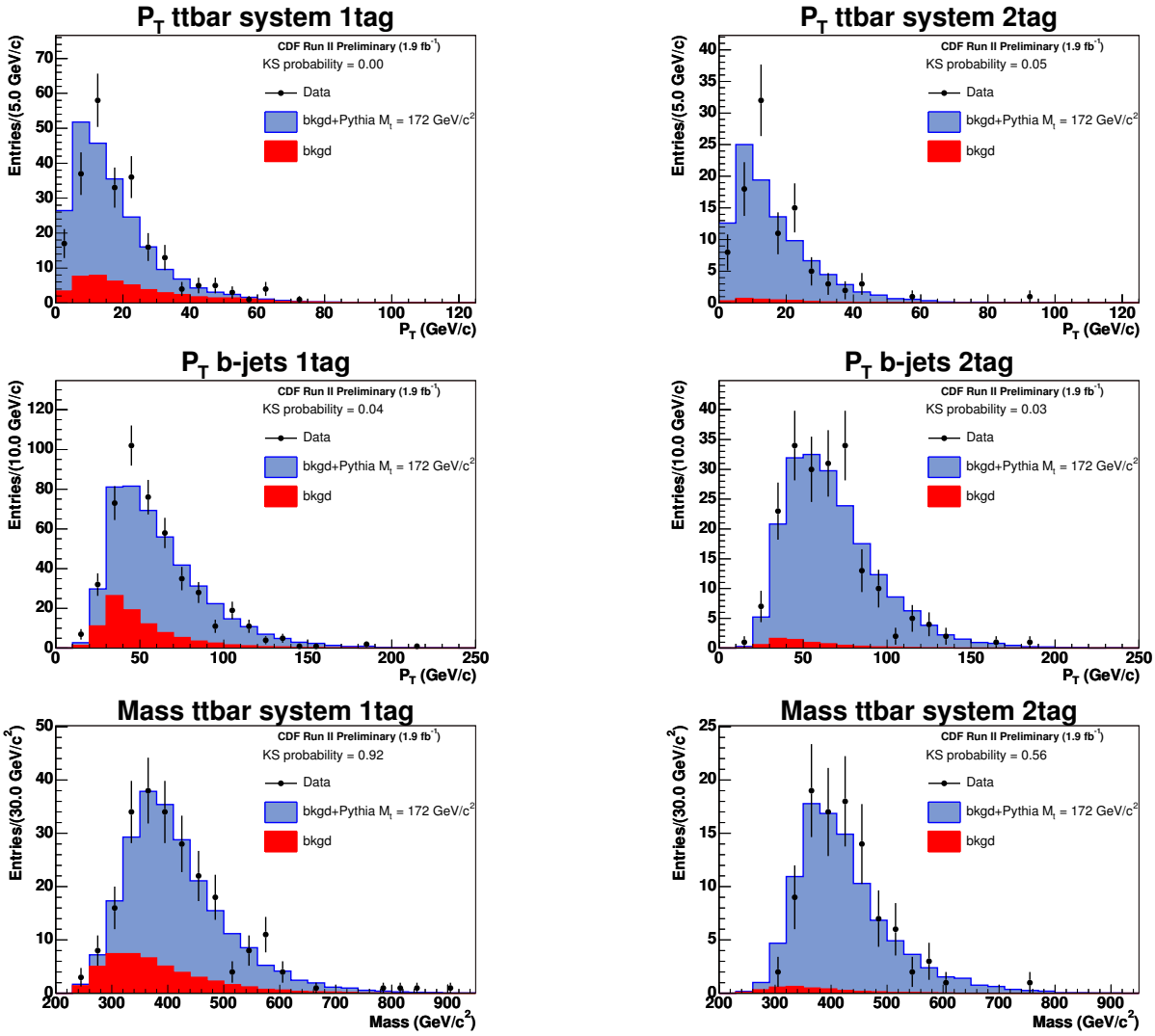

Figure 65: Distributions for L+J fitter output (3), Pythia M_{top}=172 GeV/c^2

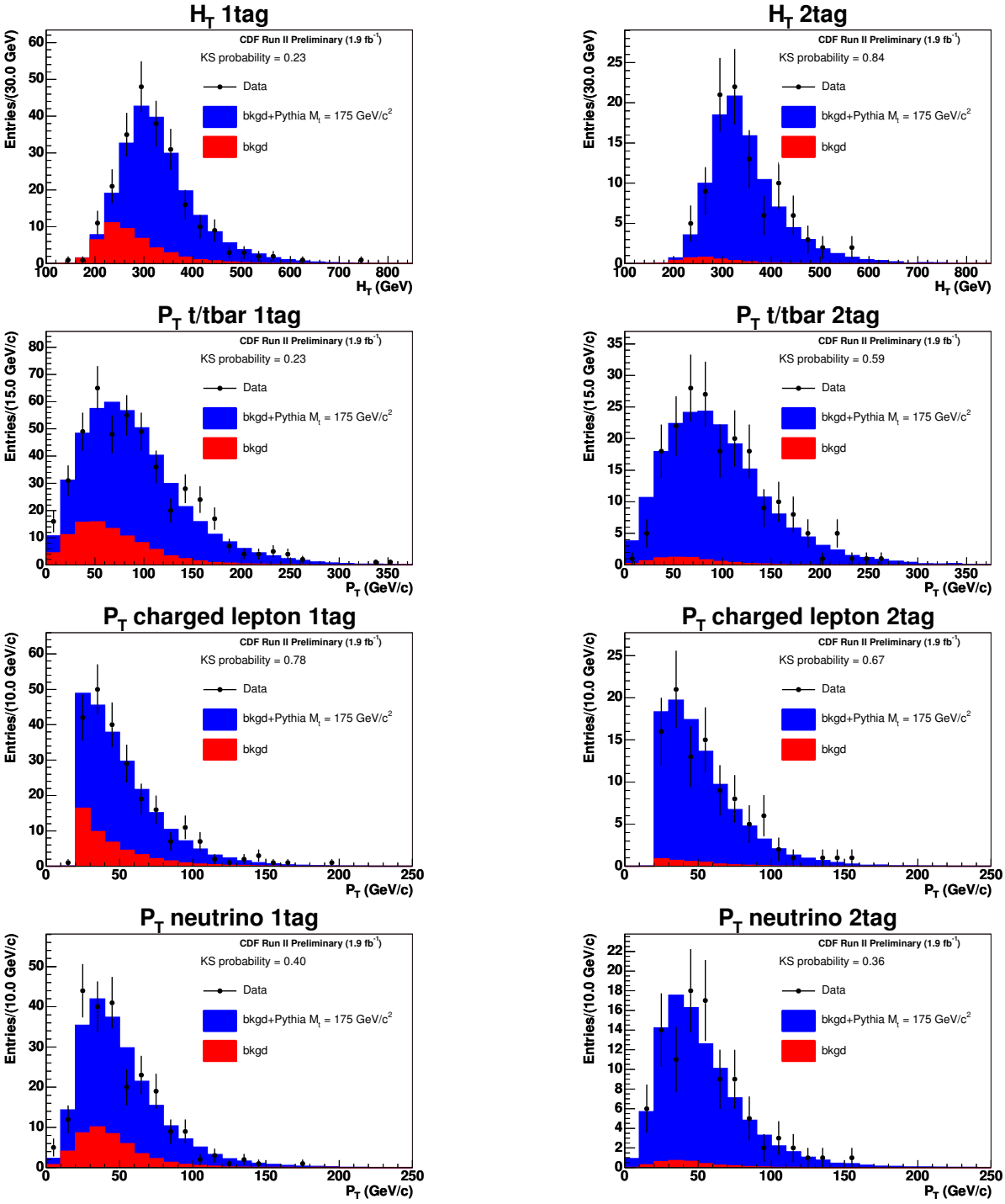

Figure 66: Distributions for L+J fitter output (1), Pythia M_{top}=175 GeV/c^2

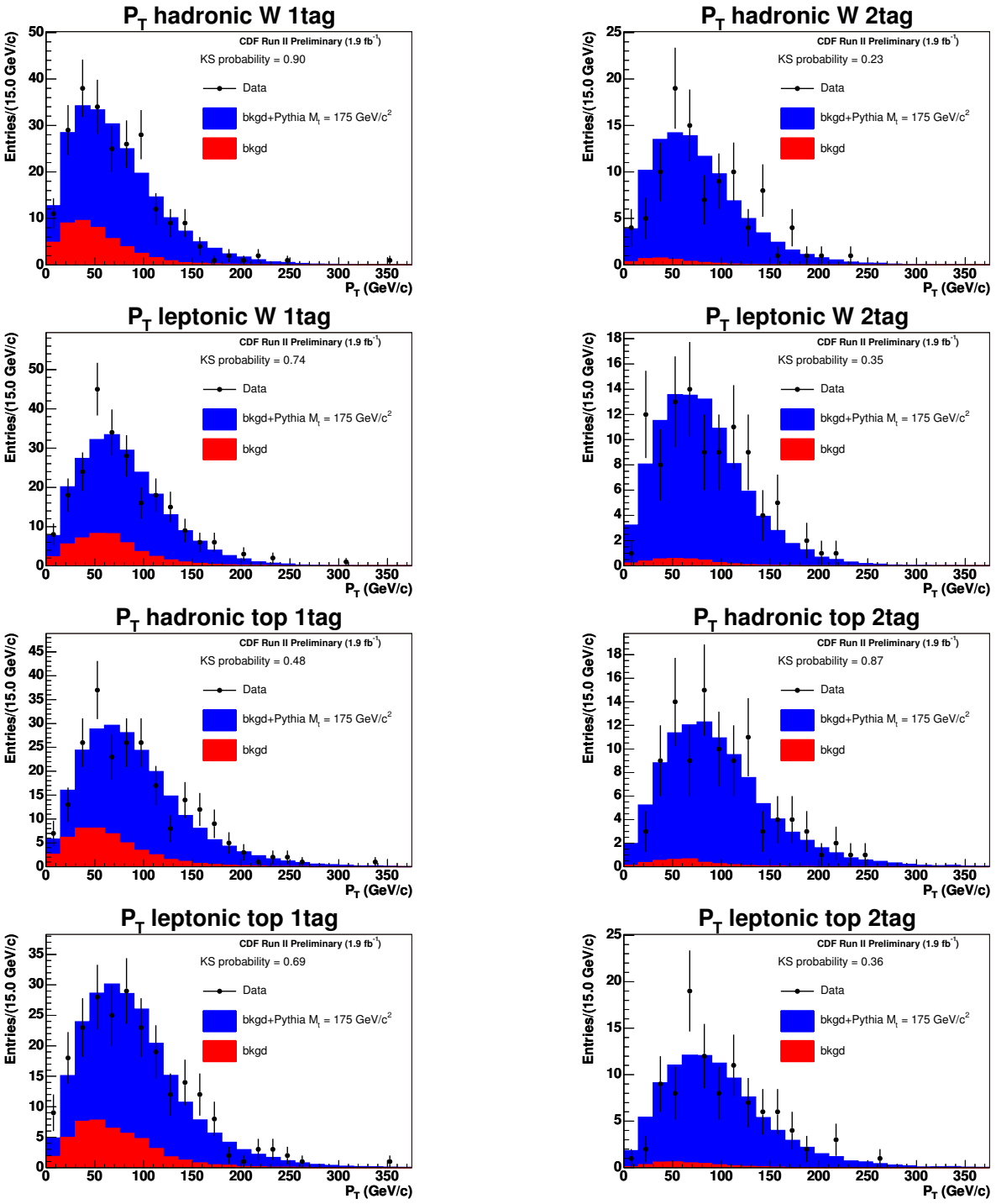

Figure 67: Distributions for L+J fitter output (2), Pythia M_{top}=175 GeV/c^2

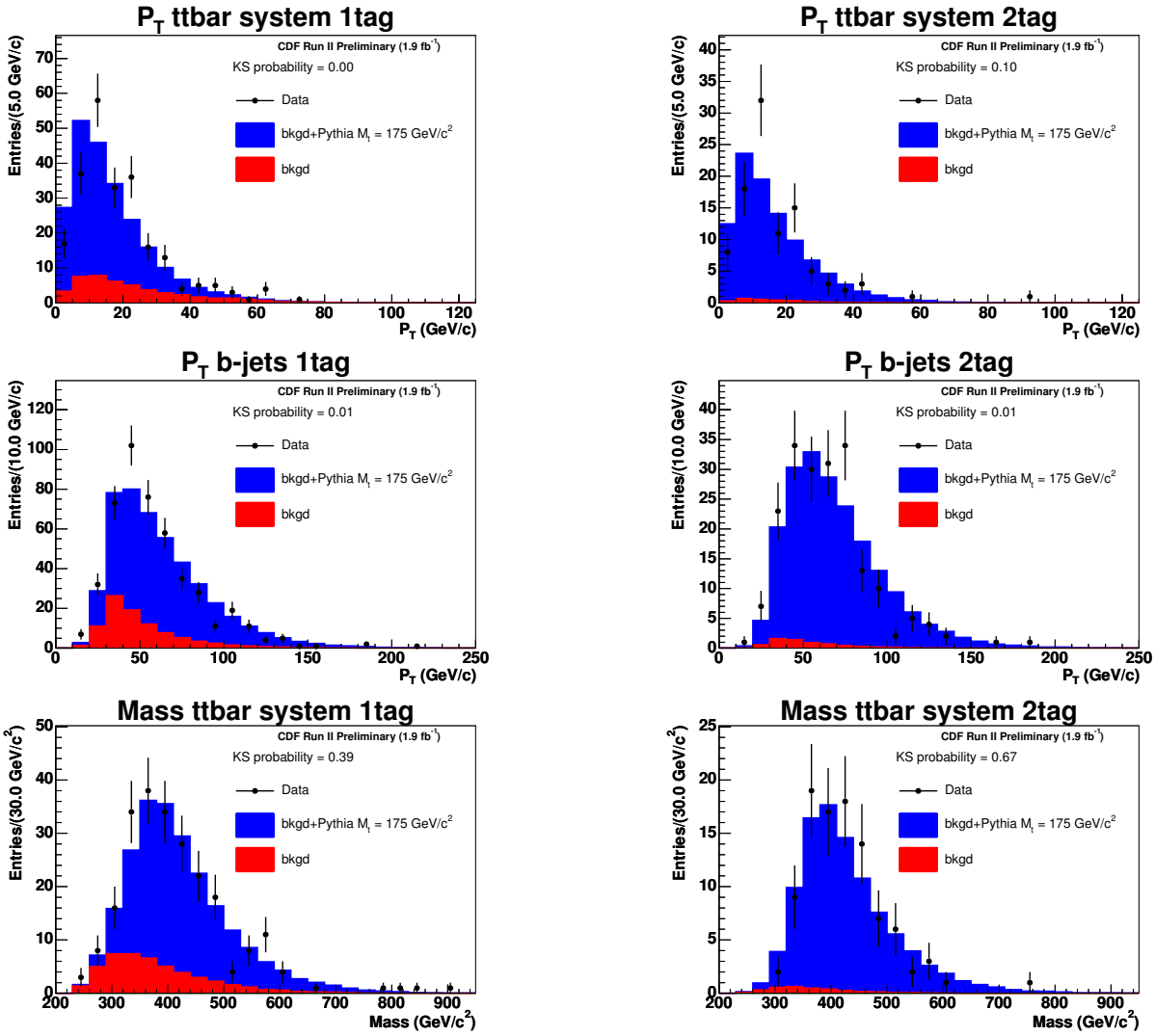

Figure 68: Distributions for L+J fitter output (3), Pythia M_{top}=175 GeV/c^2

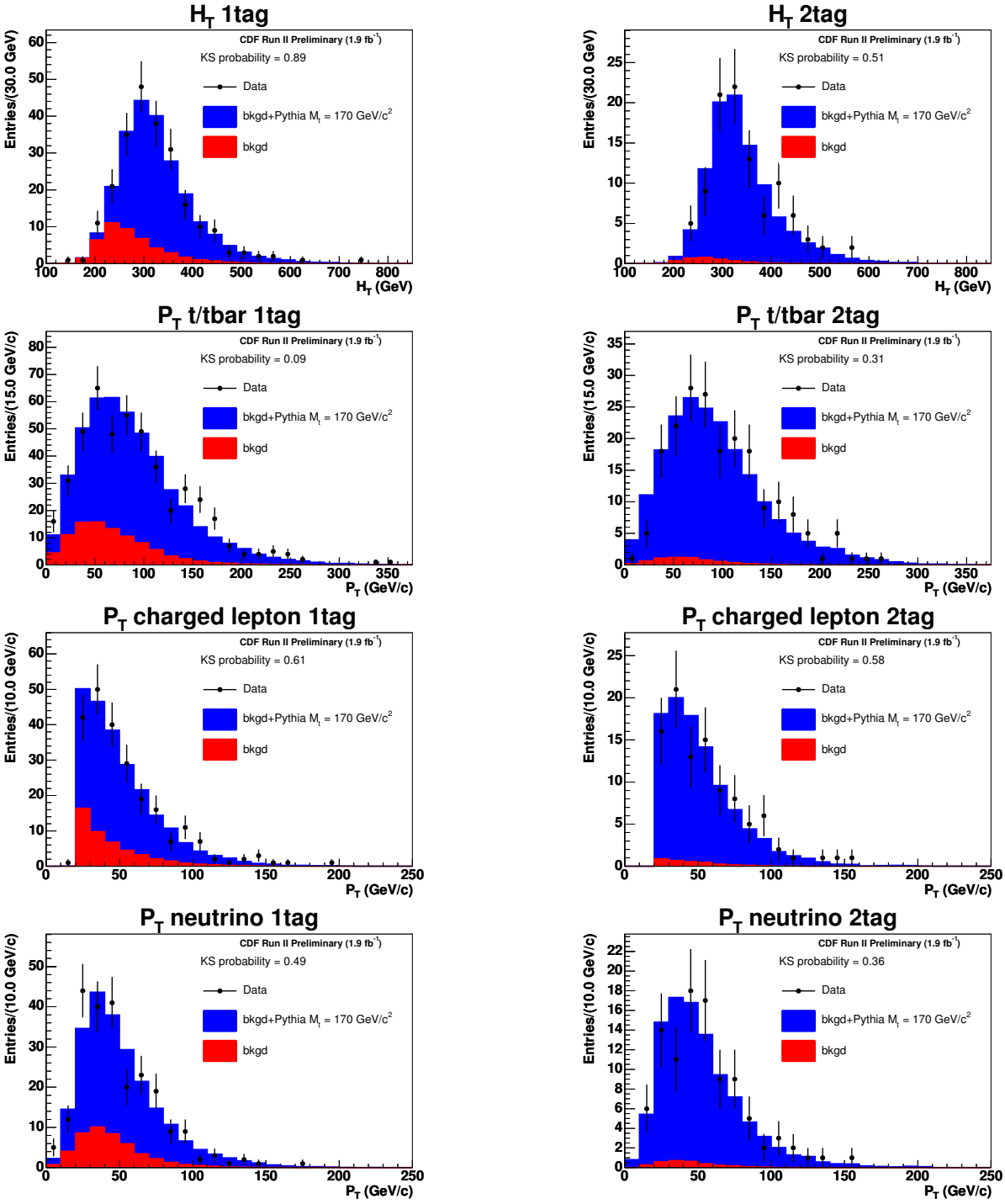

Figure 69: Distributions for L+J fitter output (1), Pythia M_{top}=170 GeV/c^2

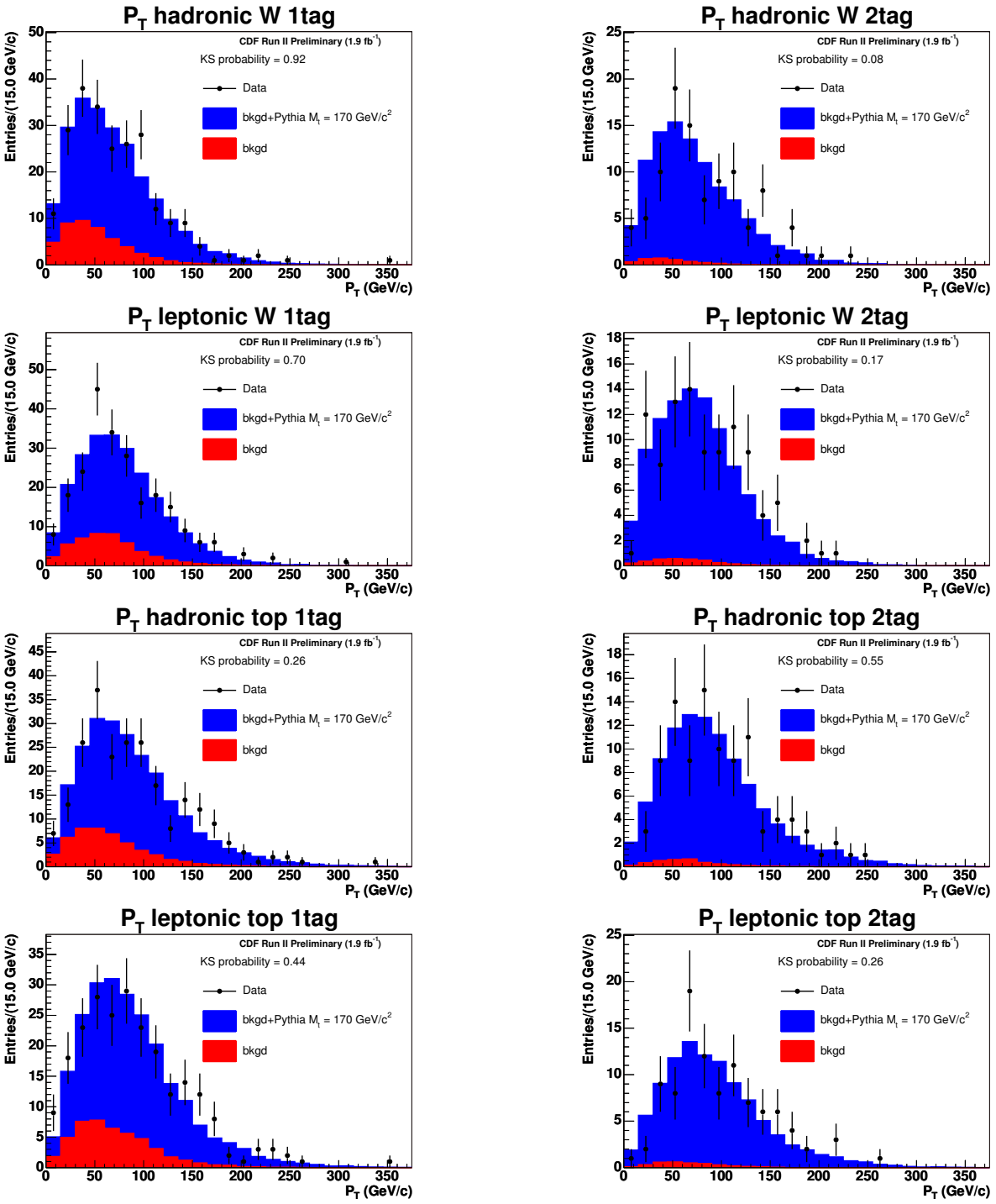

Figure 70: Distributions for L+J fitter output (2), Pythia M_{top}=170 GeV/c^2

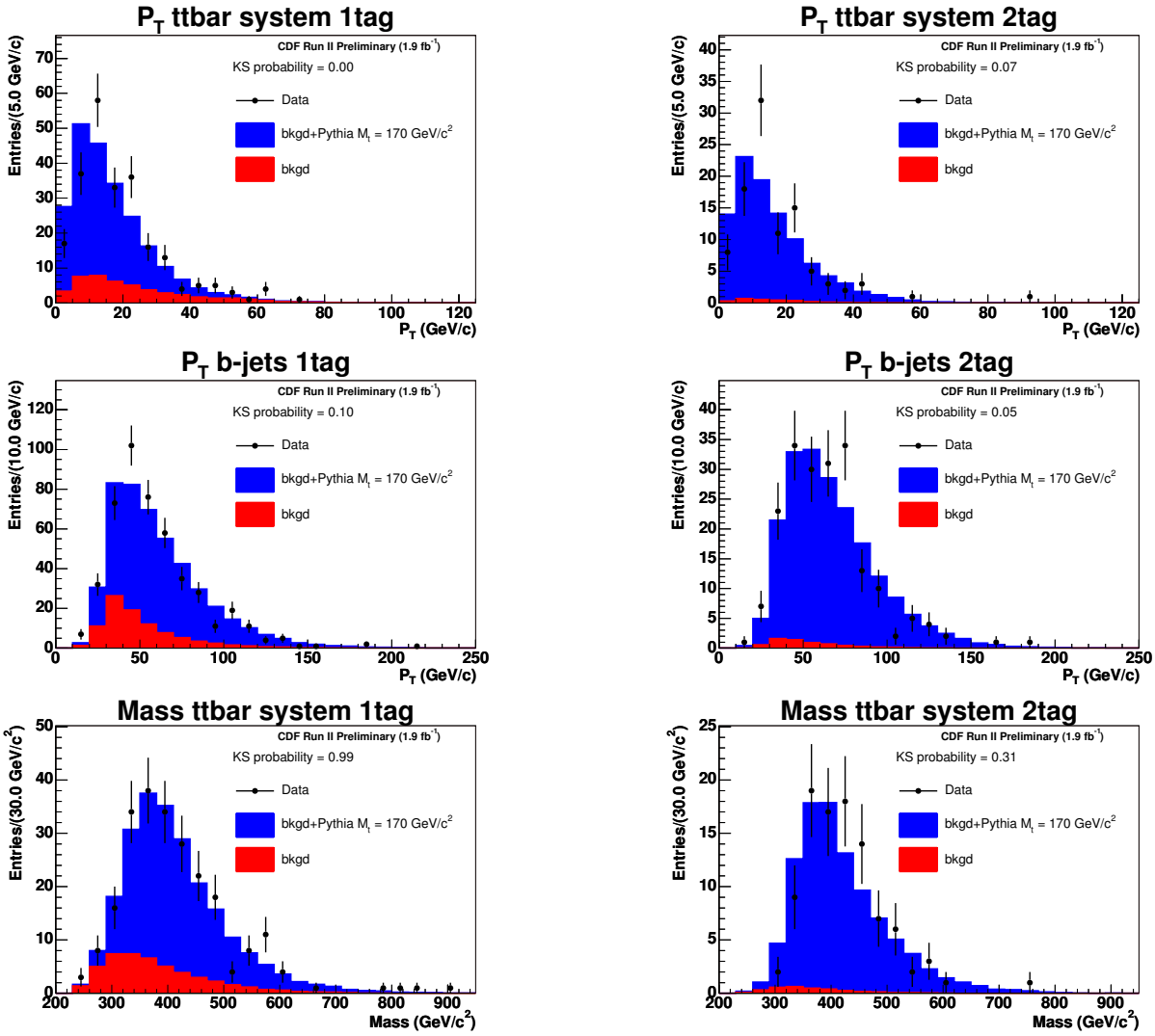

Figure 71: Distributions for L+J fitter output (3), Pythia M_{top}=170 GeV/c^2

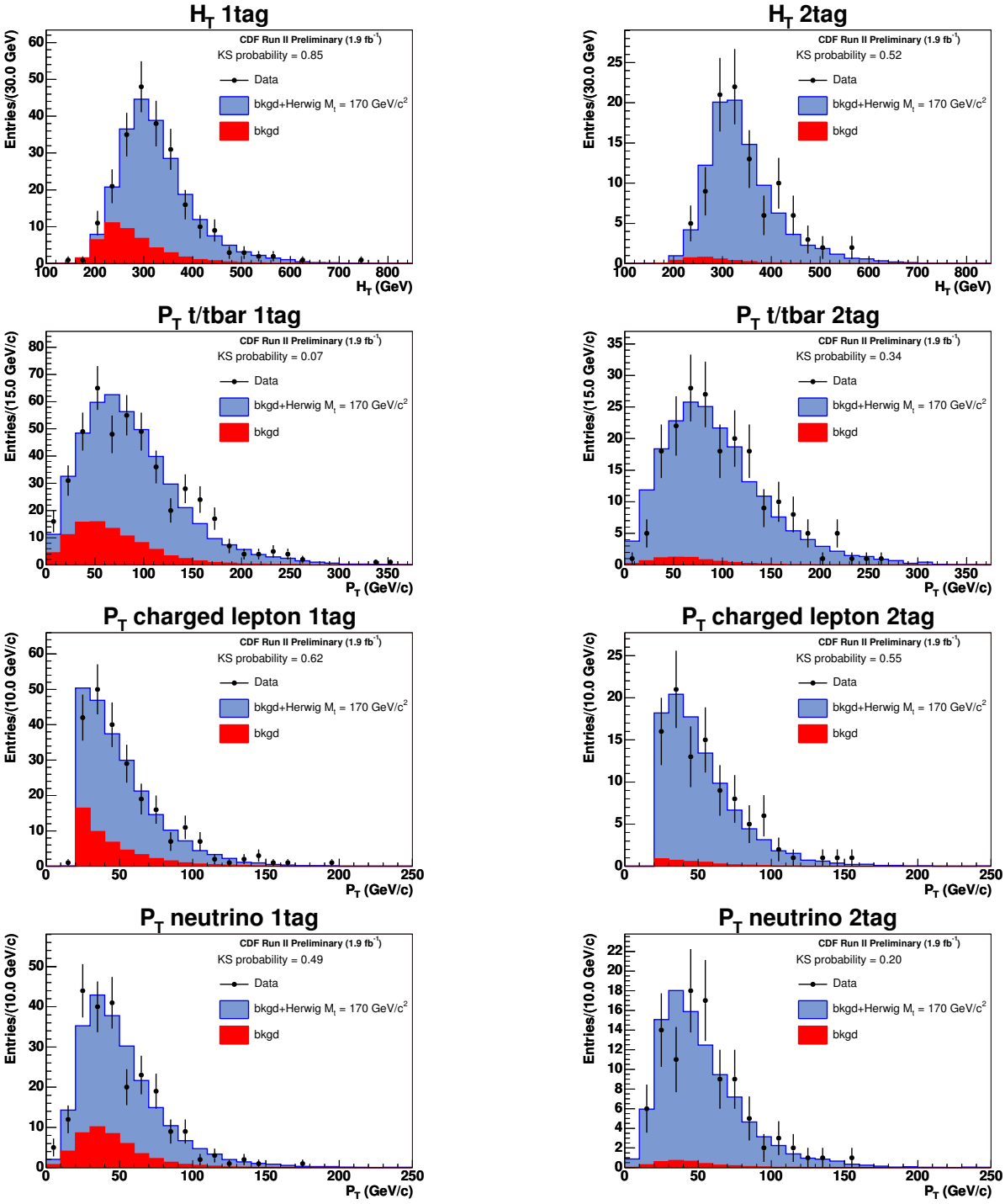

Figure 72: Distributions for L+J fitter output (1), Herwig M_{top}=170 GeV/c^2

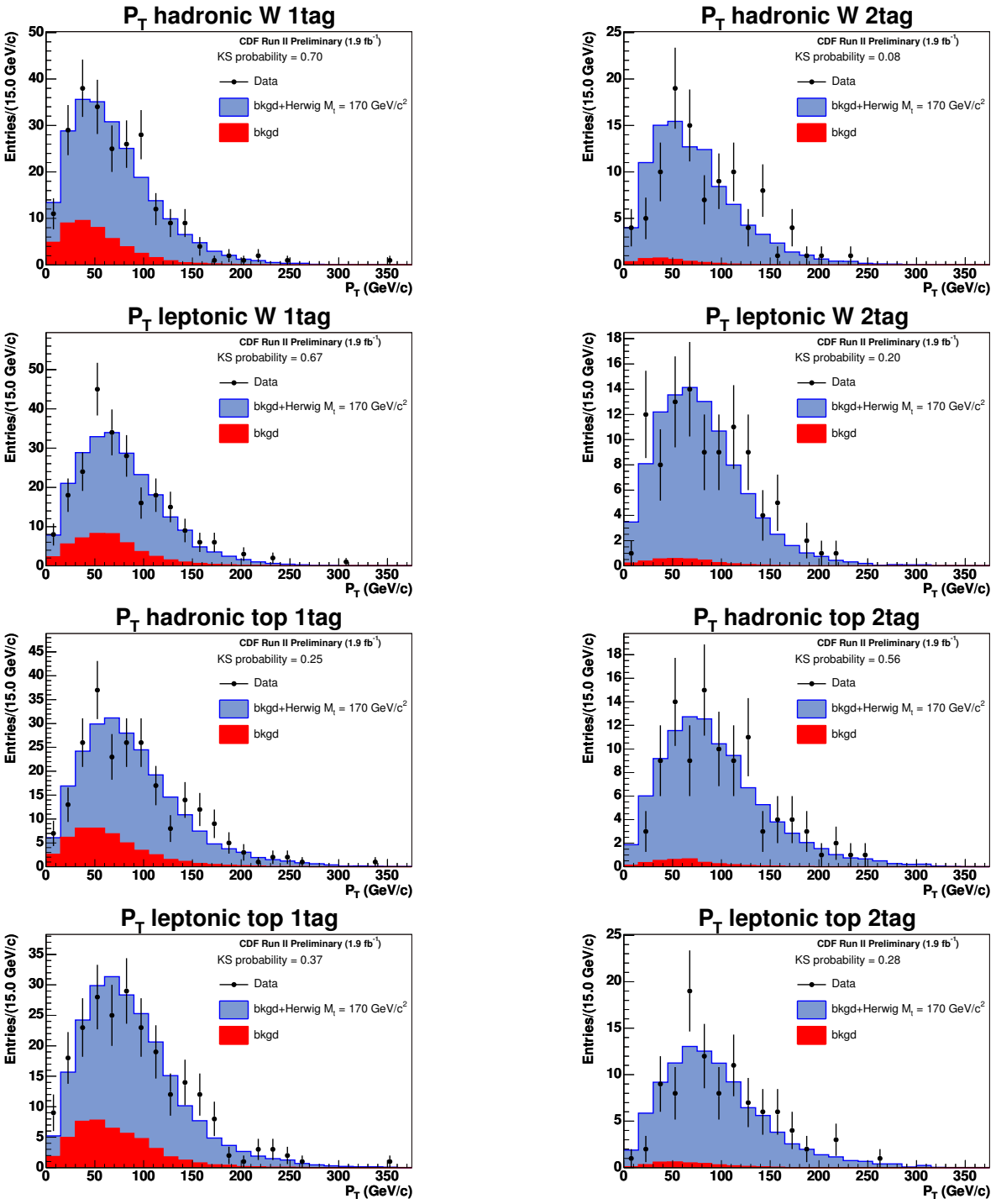

Figure 73: Distributions for L+J fitter output (2), Herwig M_{top}=170 GeV/c^2

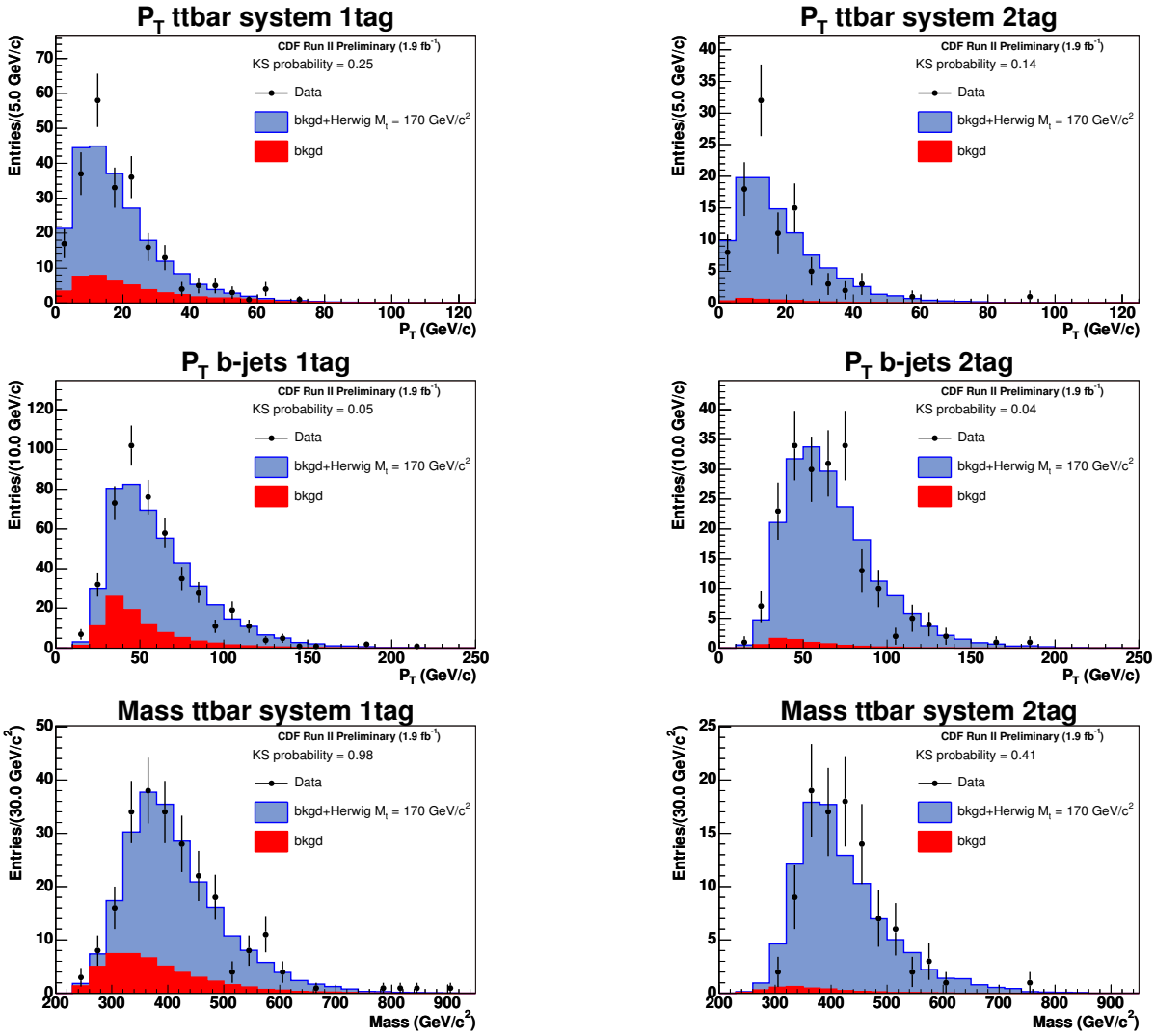

Figure 74: Distributions for L+J fitter output (3), Herwig M_{top}=170 GeV/c^2

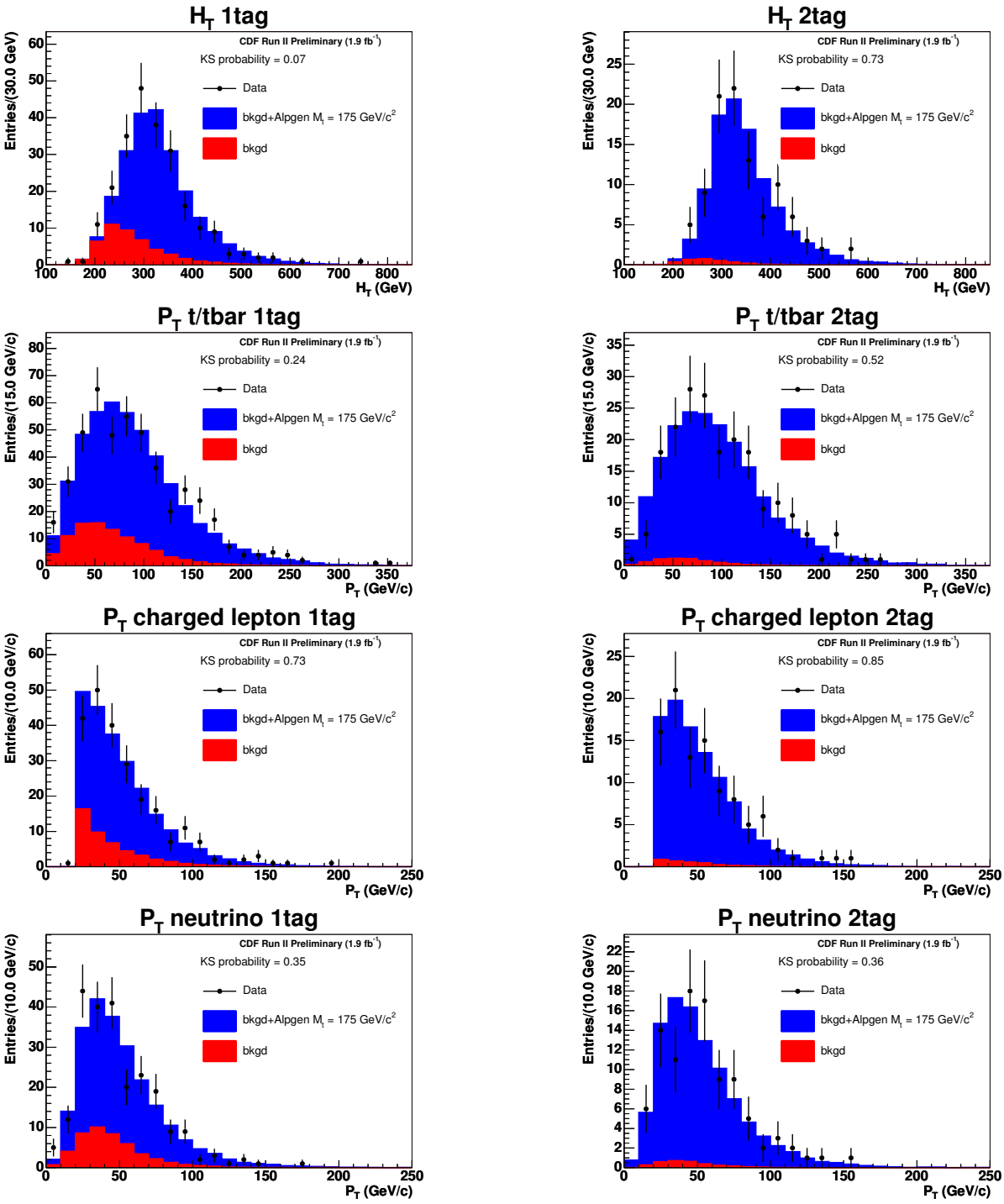

Figure 75: Distributions for L+J fitter output (1), Alpgen M_{top}=175 GeV/c^2

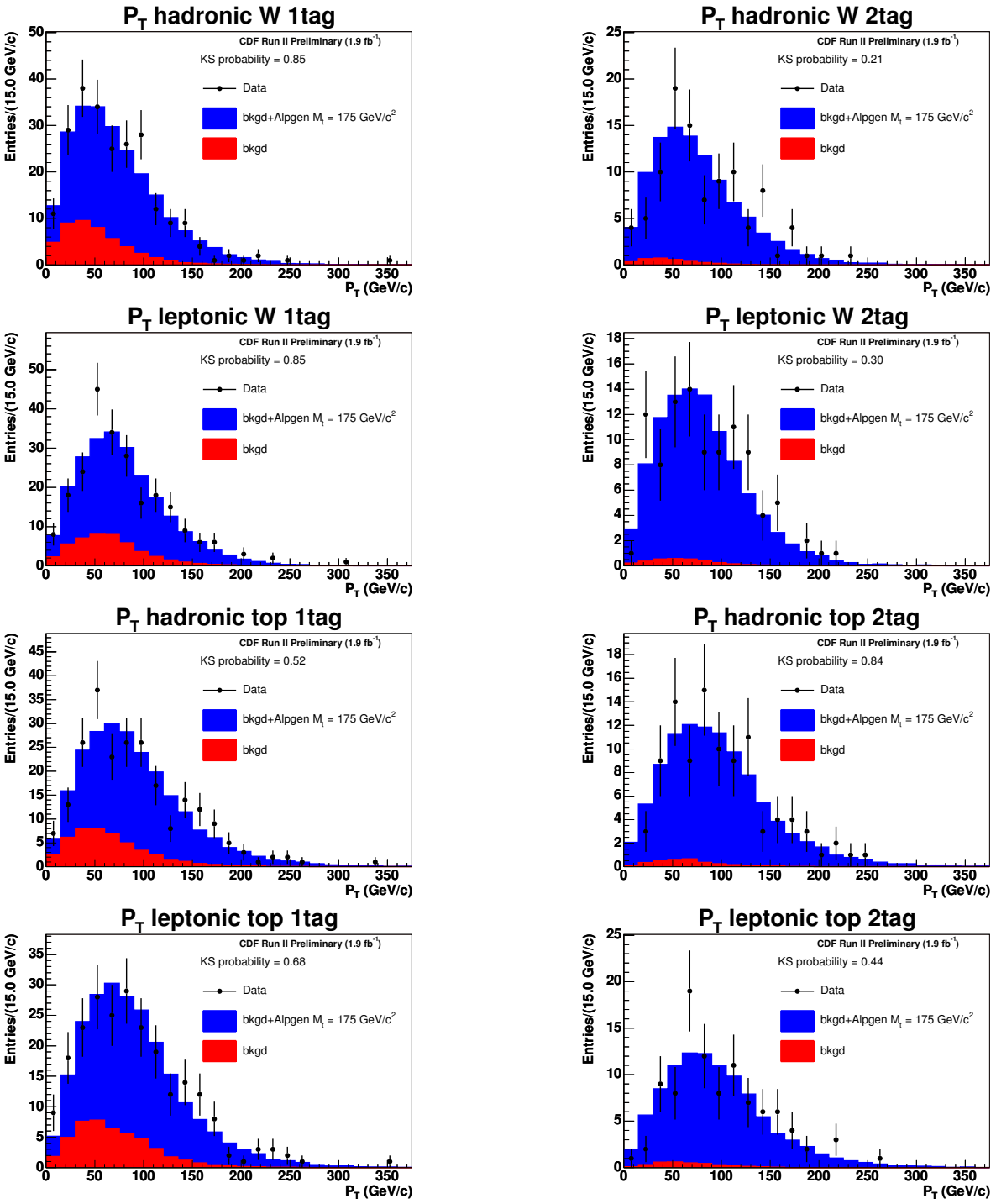

Figure 76: Distributions for L+J fitter output (2), Alpgen M_{top}=175 GeV/c^2

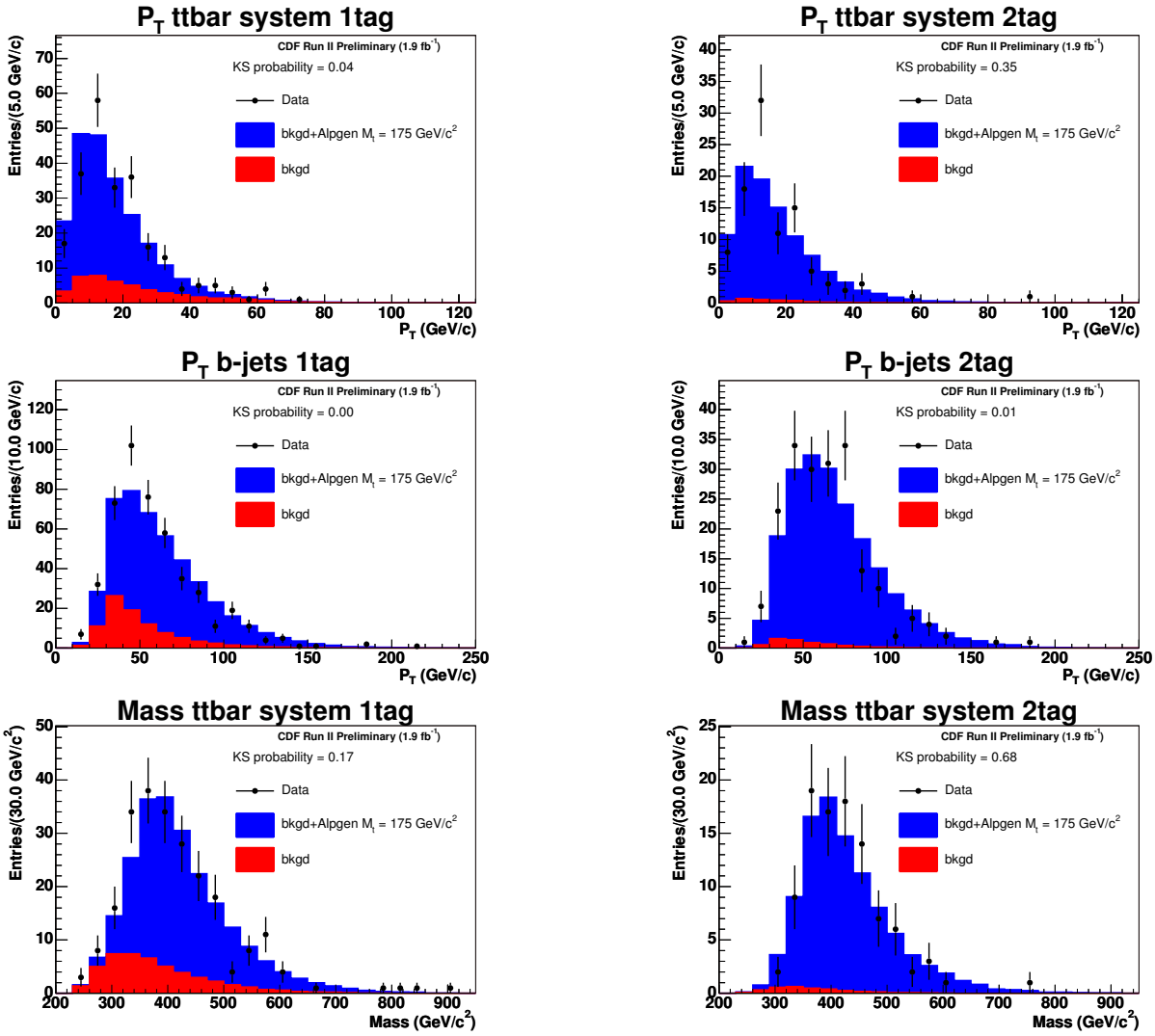

Figure 77: Distributions for L+J fitter output (3), Alpgen M_{top}=175 GeV/c^2

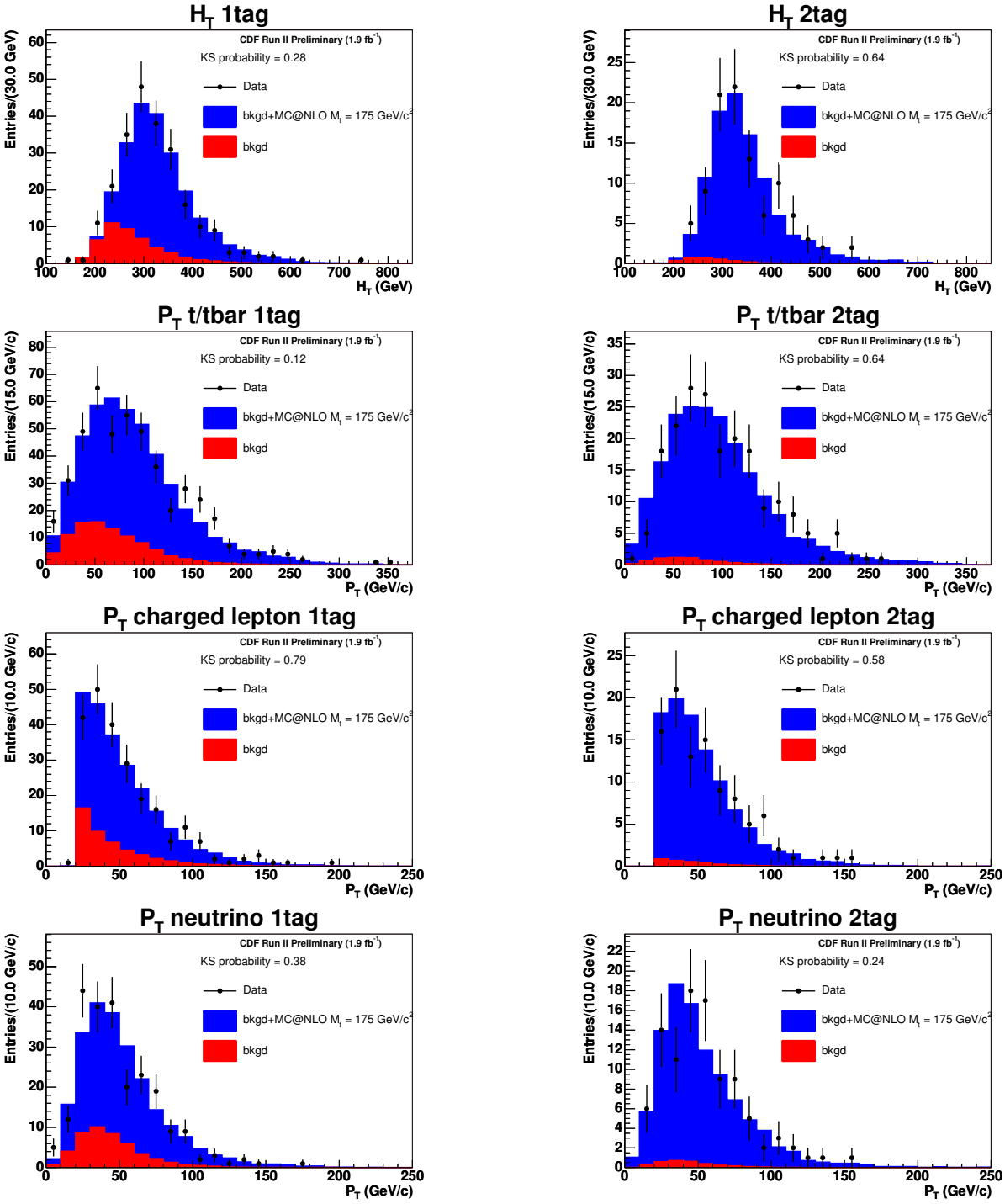

Figure 78: Distributions for L+J fitter output (1), MC@NLO M_{top}=175 GeV/c^2

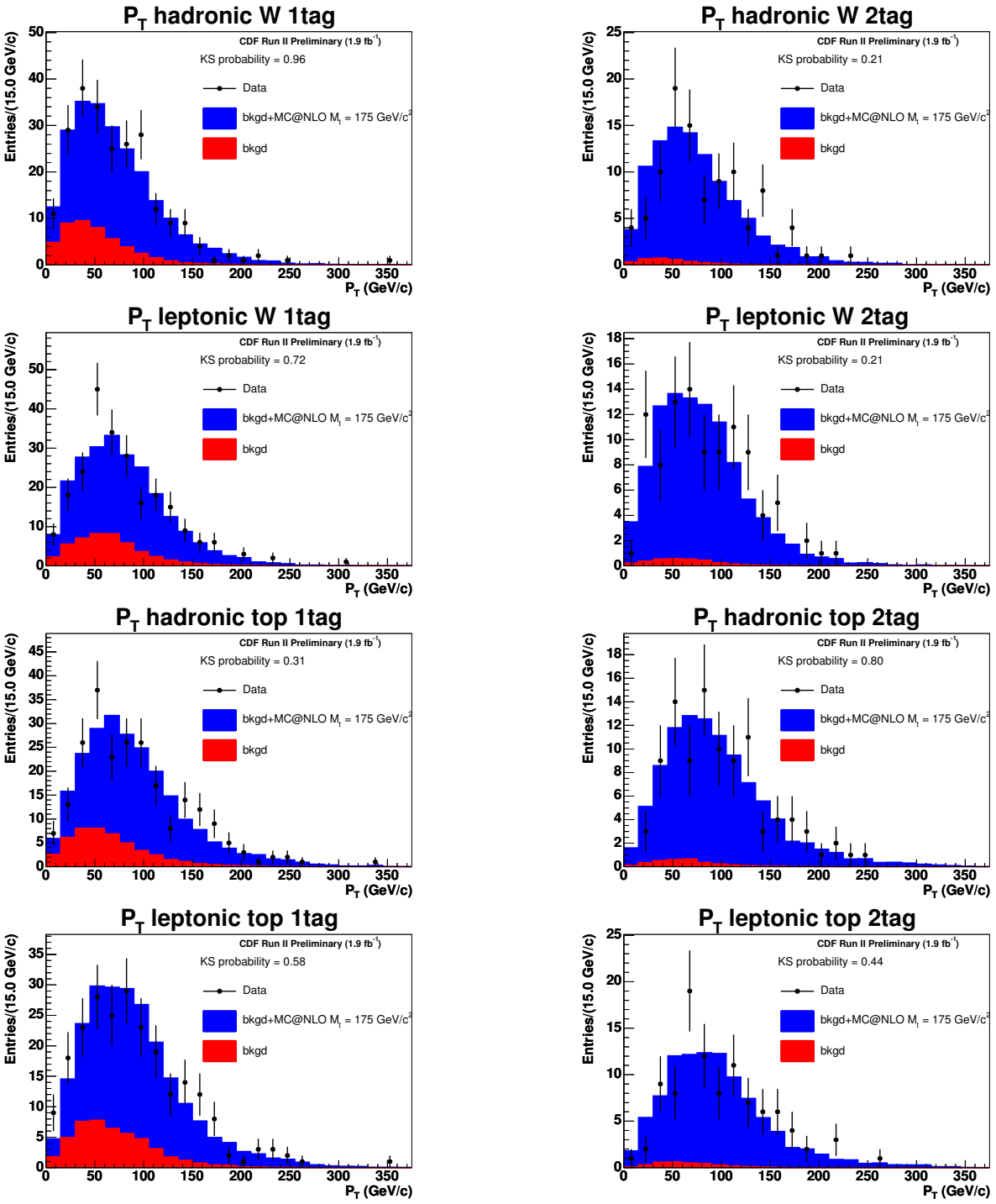

Figure 79: Distributions for L+J fitter output (2), MC@NLO M_{top}=175 GeV/c^2

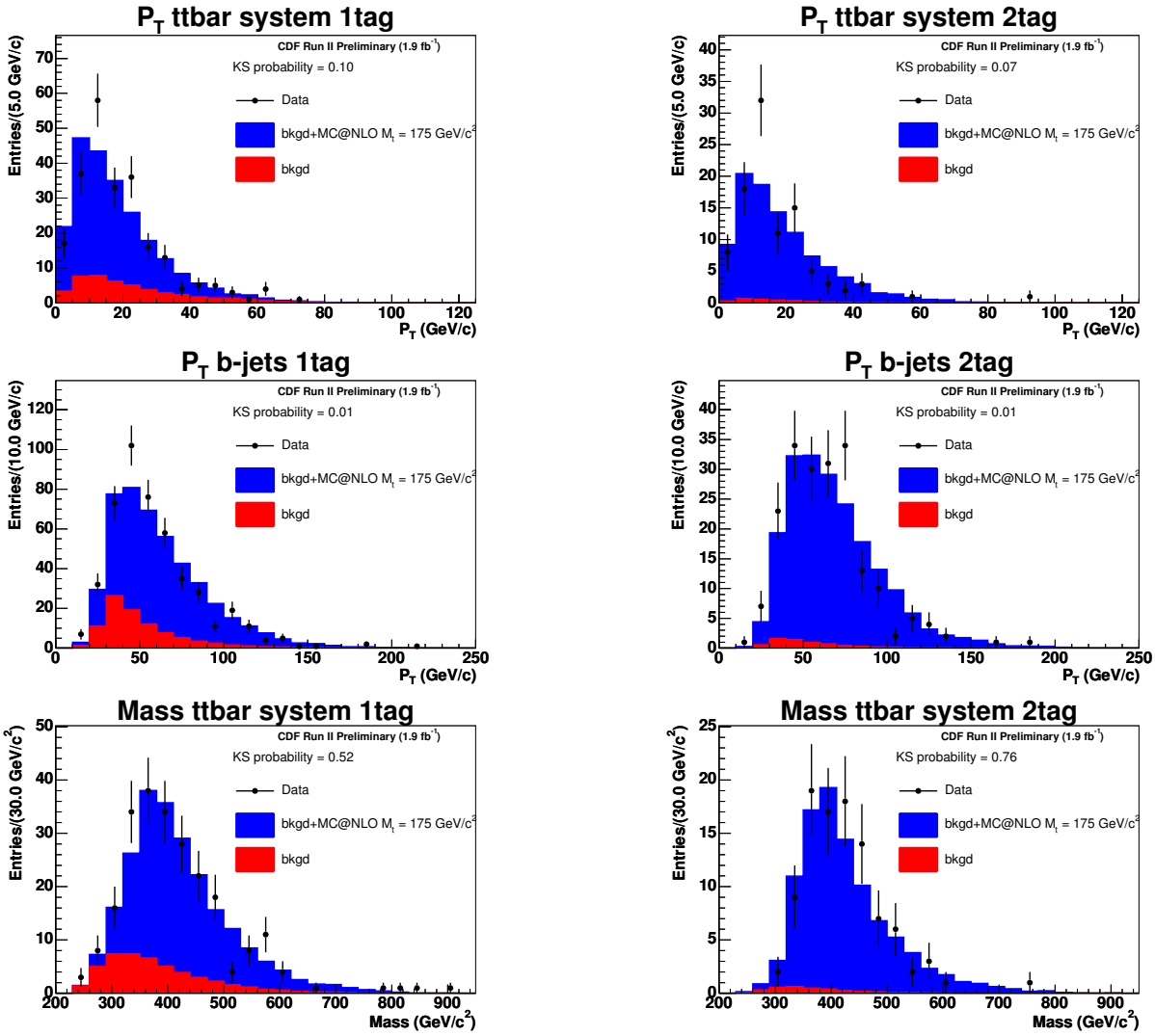

Figure 80: Distributions for L+J fitter output (3), MC@NLO M_{top}=175 GeV/c^2

Figure 81 and 82 show the 1d templates in Lepton+Jets data with best fit 1d shapes overlaid on top. The dilepton data is shown in Figures 83 and 84.

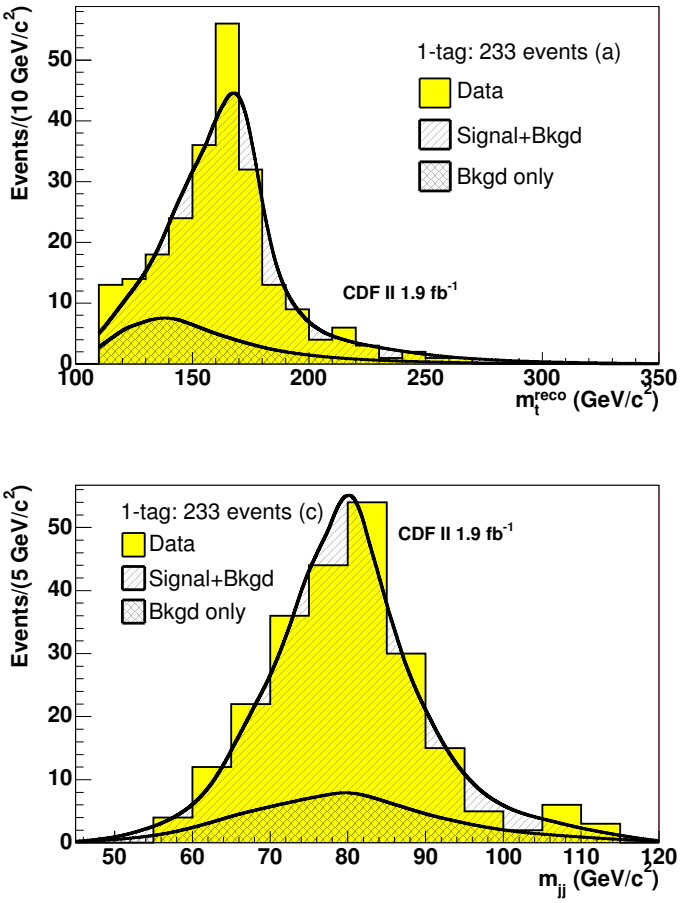

Figure 81: One-dimensional 1tag LJ data templates with PDFs from M_{top}= 172.0 GeV/c^2 and full background models overlaid. The expected number of events is set to the value from the combined, constrained L+J fit.

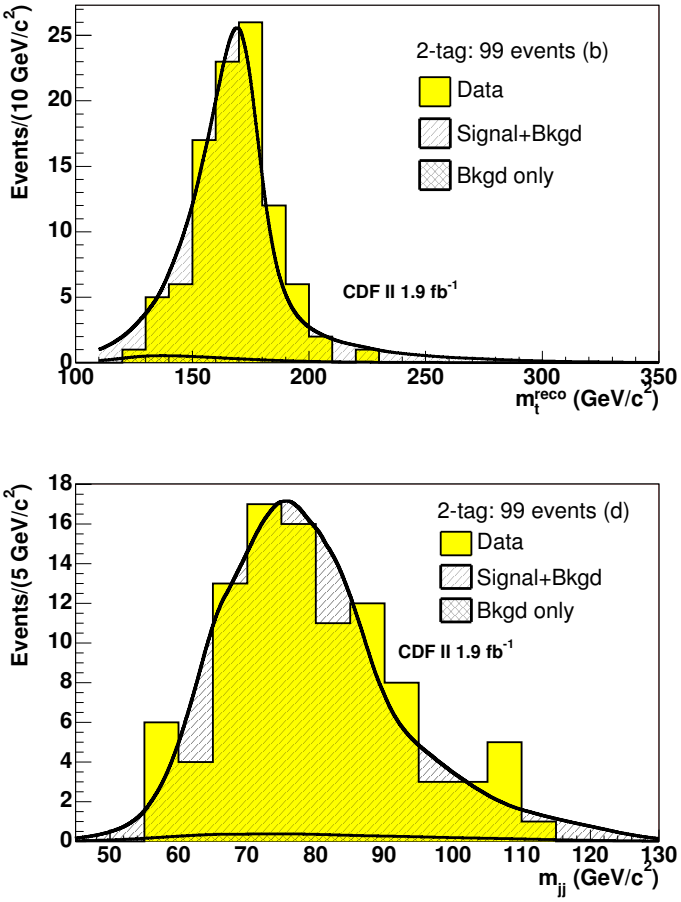

Figure 82: One-dimensional 2tag LJ data templates with PDFs from M_{top}= 172.0 GeV/c^2 and full background models overlaid. The expected number of events is set to the value from the combined, constrained L+J fit.

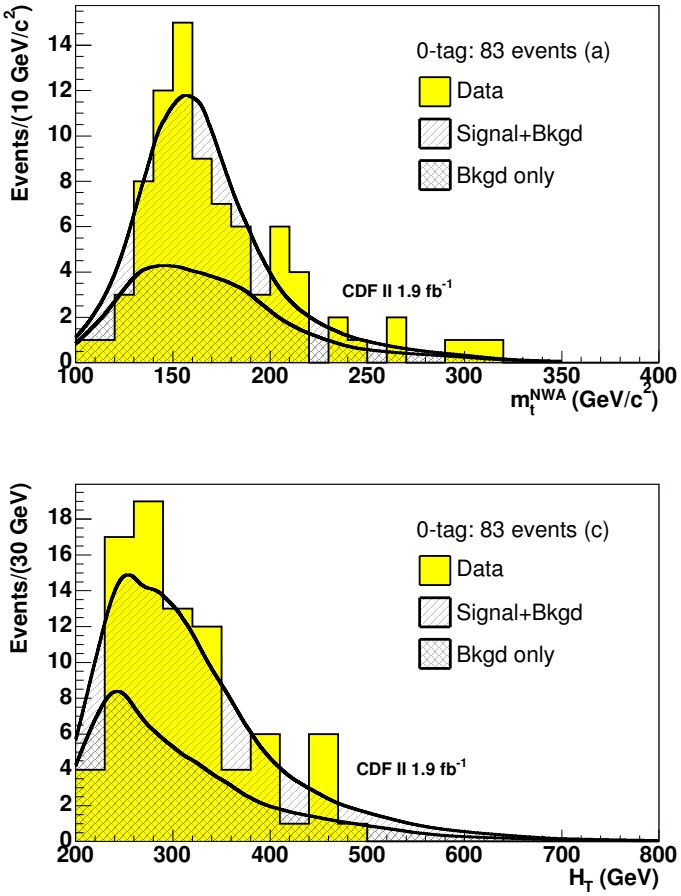

Figure 83: One-dimensional 0tag DIL data templates with PDFs from M_{top}= 172.0 GeV/c^2 and full background models overlaid. The expected number of events is set to the value from the combined, constrained DIL fit.

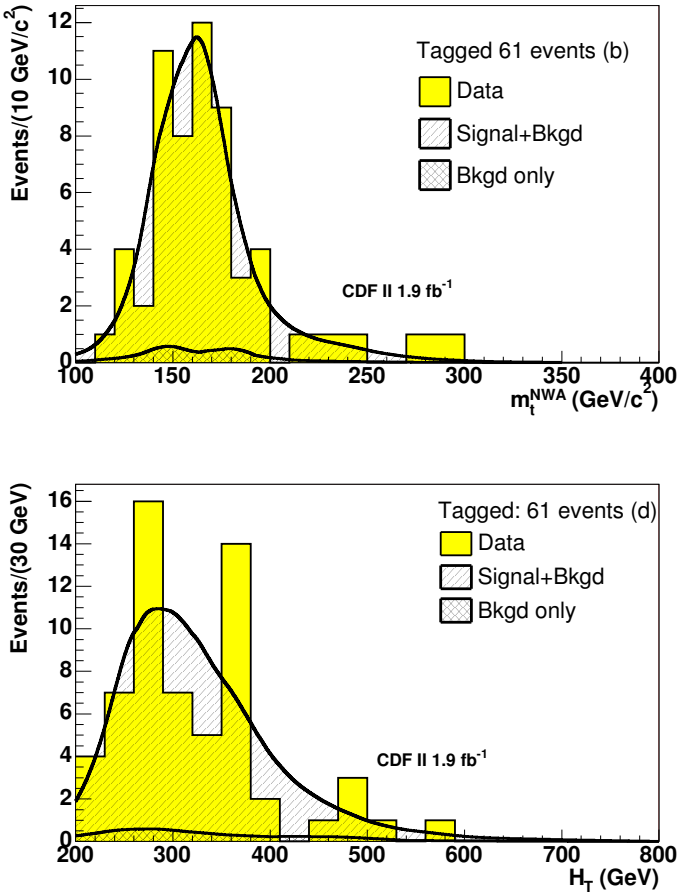

Figure 84: One-dimensional tagged DIL data templates with PDFs from M_{top}= 172.0 GeV/c^2 and full background models overlaid. The expected number of events is set to the value from the combined, constrained DIL fit.

23 Conclusions

We present the first measurement of the top quark mass from CDF to combine likelihoods across different decay channels. Using 1.9 fb^{-1} of data, we measure:

$$M_{top} = 171.9 \pm 1.7 \text{ (stat. + JES)} \pm 1.1 \text{ (syst.) GeV}/c^2 = 171.9 \pm 2.0 \text{ GeV}/c^2 \text{ (combined)}$$

$$M_{top} = 171.8 \pm 1.9 \text{ (stat. + JES)} \pm 1.1 \text{ (syst.) GeV}/c^2 = 171.8 \pm 2.2 \text{ GeV}/c^2 \text{ (LJ-only)}$$

$$M_{top} = 171.2 \, ^{+3.6}_{-3.4} \text{ (stat.)} \pm 3.8 \text{ (syst.) GeV}/c^2 = 171.2 \, ^{+5.3}_{-5.1} \text{ GeV}/c^2 \text{ (Dilepton-only)}$$

The Jet Energy Scale measurements are:

$$\Delta_{JES} = -0.17 \pm 0.35 \text{ (stat. + } M_{top} \text{ only) } \sigma_C \text{ (combined)}$$

$$\Delta_{JES} = -0.13 \pm 0.37 \text{ (stat. + } M_{top} \text{ only) } \sigma_C \text{ (LJ-only)}$$

The statistical errors are scaled by the pull width for all the measurements. The M_{top}result in the dilepton channel and the Δ_{JES} measurements are corrected for the luminosity profile effects.

24 Acknowledgements

The authors would like to thank Paul Lujan and Kevin Lannon for helping us track down the subtle differences in MET between our event selection and the top group's Lepton+Jets selection. Many thanks also to Alexander Varganov and Naoki Kimura for discussion of DIL event selection and fake estimates.

References

[1] CDF Note 7139

[2] CDF Note 7532

[3] CDF Note 7533

[4] CDF Note 8074

[5] CDF Note 8190

[6] CDF Note 8761

[7] CDF Note 8824

[8] CDF Note 8904

[9] CDF Note 8909

[10] A. Varganov's talk Jan 10 2008 Top Group

[11] CDF Note 8917

[12] CDF Note 9081

[13] CDF Note 9110

[14] CDF Note 7548

[15] CDF Note 8692

[16] CDF Note 8919

[17] CDF Note 8901

[18] CDF Note 8635

[19] CDF Note 9247

[20] CDF Note 9353 5 5 5 5 5 5, 8 5 9, 10 5 10 5, 20 57 5 5 5 6, 10, 36 5 6 7, 35 8, 73

[21] Bradley Efron (1979). "Bootstrap methods: Another look at the jackknife", The Annals of Statistics, 7, 1-26.

[22] Bradley Efron and Robert J. Tibshirani, An Introduction to the Boostrap. Monographs on Statistics and Applied Probability, 57 (Chapman and Hall, 1993).

[23] C. Loader "Local Regression and Likelihood"

[24] http://www.locfit.info 27 27